Monthly Notices of the ROYAL ASTRONOMICAL SOCIETY
MNRAS Advance Access published December 17, 2012
MNRAS (2012) doi:10.1093/mnras/sts298

Current flow and pair creation at low altitude in rotation-powered pulsars' force-free magnetospheres: space charge limited flow

A. N. Timokhin[1,2,3]★ and J. Arons[2,4]

[1]*Astrophysics Science Division, NASA Goddard Space Flight Center, Greenbelt, MD 20771, USA*
[2]*Theoretical Astrophysics Center, University of California at Berkeley, Berkeley, CA 94720, USA*
[3]*Moscow State University, Sternberg Astronomical Institute, Universitetskij Pr. 13, 119991 Moscow, Russia*
[4]*Astronomy Department, Physics Department, and Space Sciences Laboratory, University of California at Berkeley, Berkeley, CA 94720, USA*

Accepted 2012 October 28. Received 2012 September 7; in original form 2012 June 21

ABSTRACT

We report the results of an investigation of particle acceleration and electron–positron plasma generation at low altitude in the polar magnetic flux tubes of rotation-powered pulsars, when the stellar surface is free to emit whatever charges and currents are demanded by the force-free magnetosphere. We apply a new 1D hybrid plasma simulation code to the dynamical problem, using Particle-in-Cell methods for the dynamics of the charged particles, including a determination of the collective electrostatic fluctuations in the plasma, combined with a Monte Carlo treatment of the high-energy gamma-rays that mediate the formation of the electron–positron pairs. We assume the electric current flowing through the pair creation zone is fixed by the much higher inductance magnetosphere, and adopt the results of force-free magnetosphere models to provide the currents which must be carried by the accelerator. The models are spatially one dimensional, and designed to explore the physics, although of practical relevance to young, high-voltage pulsars.

We observe novel behaviour (a) When the current density j is less than the Goldreich–Julian value ($0 < j/j_{\rm GJ} < 1$), space charge limited acceleration of the current carrying beam is mild, with the full Goldreich–Julian charge density comprising the charge densities of the beam and a cloud of electrically trapped particles with the same sign of charge as the beam. The voltage drops are of the order of mc^2/e, and pair creation is absent. (b) When the current density exceeds the Goldreich–Julian value ($j/j_{\rm GJ} > 1$), the system develops high voltage drops (TV or greater), causing emission of curvature gamma-rays and intense bursts of pair creation. The bursts exhibit limit cycle behaviour, with characteristic time-scales somewhat longer than the relativistic fly-by time over distances comparable to the polar cap diameter (microseconds). (c) In return current regions, where $j/j_{\rm GJ} < 0$, the system develops similar bursts of pair creation. These discharges are similar to those encountered in previous calculations by Timokhin of pair creation when the surface has a high work function and cannot freely emit charge. In cases (b) and (c), the intermittently generated pairs allow the system to simultaneously carry the magnetospherically prescribed currents and adjust the charge density and average electric field to force-free conditions. We also elucidate the conditions for pair creating beam flow to be steady (stationary with small fluctuations in the rotating frame), finding that such steady flows can occupy only a small fraction of the current density parameter space exhibited by the force-free magnetospheric model. The generic polar flow dynamics and pair creation are strongly time dependent. The model has an essential difference from almost all previous quantitative studies, in that we sought the accelerating voltage (with pair creation, when the voltage drops are sufficiently large; without, when they are small) as a function of the applied current.

★ E-mail: andrey.timokhin@nasa.gov

The 1D results described here characterize the dependence of acceleration and pair creation on the magnitude and sign of current. The dependence on the spatial distribution of the current is a multi-dimensional problem, possibly exhibiting more chaotic behaviour. We briefly outline possible relations of the electric field fluctuations observed in the polar flows (both with and without pair creation discharges) to direct emission of radio waves, as well as revive the possible relation of the observed limit cycle behaviour to microstructure in the radio emission. Actually modelling these effects requires the multi-dimensional treatment, to be reported in a later paper.

Key words: acceleration of particles – plasmas – stars: magnetic field – stars: neutron – pulsars: general.

1 INTRODUCTION

Young pulsar wind nebulae (PWNe) show that rotation-powered pulsars (RPPs) have dense magnetospheres, at least with regard to those regions that feed the plasma outflow (e.g. Bucciantini, Arons & Amato 2011). Electron–positron pair creation in the open field line region that connects to the external world is the only known candidate for the origin of such outflows, with acceleration and convertible gamma-ray emission occurring either at low altitude (Sturrock 1971) or in the outer magnetosphere (Cheng, Ho & Ruderman 1986). High-density flows that can feed all the open field lines can exist only in the low-altitude polar cap region (for a general discussion, see Arons 2009).

Theoretical studies of charged particle flow from the magnetic polar regions of RPPs began with the observation by Goldreich & Julian (1969) that an isolated magnetic rotator in vacuum must have a charged magnetosphere almost corotating with the star. Since RPPs are strongly gravitationally bound and cool objects (thermal scale height in any atmosphere orders of magnitude less than the stellar radius) and have no external source of plasma supply (so far as we know), the only plasma source is an extraction of charged particles from the stellar surface, leading to a conjectured magnetosphere whose plasma is fully charge separated, in contrast to all other known astrophysical systems, whose plasmas are charged but quasi-neutral. Goldreich & Julian (1969) speculated that on polar field lines – those that extend beyond the light cylinder located at cylindrical radius $R_{\rm LC} = cP/2\pi \simeq 48\,000\,P$ km, P = rotation period in seconds – a charge-separated outflow would form. They argued that the energy/particle in the outflow would be no more than the gravitational escape energy $GM_*/R_* \sim 0.3mc^2(M_*/1.4M_\odot)(10\,{\rm km}/R_*)$; M_* and R_* are star's mass and radius correspondingly – the particles leave at non-relativistic energies in spite of the fact that the electric potential drop *across* the polar field lines is equal to the full potential of an open rotating magnetosphere with a dipole magnetic field $\Phi_{\rm m} = \sqrt{W_{\rm R}/c} \approx 10\,(\dot{P}/10^{-15})^{1/2}P^{-3/2}$ TV, $W_{\rm R}$ = rotational energy loss rate, with $\dot{P} = {\rm d}P/{\rm d}t$. $\Phi_{\rm m}$ vastly exceeds the rest energy and gravitational energy of the particles, either electrons or protons (or He or other ions populating the star's crust and atmosphere). The super strong magnetic field suppresses free acceleration of the particles in the transverse electric field, whose primary ('zeroth order') consequence is the corotation of the field lines with the magnetic field embedded in the neutron star (NS), with the field line motion measured by the $\boldsymbol{E} \times \boldsymbol{B}$ drift of charged particles across the magnetic field (which occurs even when the particles have zero Larmor gyration). The particle loss rate in the conjectured charge-separated scenario is $\dot{N}_{\rm R} = c\Phi_{\rm m}/e \approx 2 \times 10^{30}\,(\dot{P}/10^{-15})^{1/2}P^{-3/2}$ s^{-1}, orders of magnitude less than that inferred from the injection of plasma into the young PWNe. The electrodynamics of the magnetosphere differ drastically, depending on whether the particle loss rate falls short of or exceeds $\dot{N}_{\rm R}$. For the young PWNe, the particle injection rate exceeds $\dot{N}_{\rm R}$ (by a lot). In that case, the magnetosphere's basic state should be one in which $\boldsymbol{E} \cdot \boldsymbol{B} = 0$, with no parallel acceleration sufficient to generate convertible gamma-rays occurring under the pulsar's rotational control.

The discovery of gamma-ray pulsars in the 1970s, and their proliferation into a population with more than 100 such stars in the most recent published *Fermi* pulsar catalogue (Abdo et al. 2010), has shown that parallel acceleration to GeV gamma-ray emitting energies (indeed, multi-hundred GeV, in the Crab pulsar; Aliu et al. 2011) must occur somewhere, with energy efficiency exceeding a few tenths of a per cent, as measured by $L_\gamma/W_{\rm R}$, L_γ = gamma-ray luminosity. If the acceleration is limited by radiation reaction, as is true in many models, L_γ is a good proxy for the energy put into parallel acceleration. $L_\gamma/W_{\rm R}$ can approach as much as 50 per cent at smaller spin down luminosities. Just how some fraction of the total potential drop gets released in acceleration along B, gamma-ray emission and pair creation has been mysterious since the beginning of pulsar research, made relevant to the real world by the gamma-ray discoveries. Since the polar cap source is the only one capable of feeding the whole (open) magnetosphere, its understanding remains of central interest to modelling pulsar magnetospheres, even though the spectral and beaming characteristics of the pulsed gamma-rays are better modelled by accelerators in the outer magnetosphere.

Free particle outflow from the NS surface is a common assumption in most of the current pulsar models (see Section 2). The polar cap accelerator problem has been studied under that assumption before (e.g. Michel 1974; Fawley, Arons & Scharlemann 1977; Mestel et al. 1985; Shibata 1997; Beloborodov 2008). Michel (1974) and Fawley et al. (1977) obtained solutions for the non-neutral space charge limited charged particle flow for the current density almost equal to the GJ current density. All these models assume strictly steady flow in the corotating frame on *all* time-scales. In these models, the charge density of the current carrying beam supplies almost all of the charge density needed to short out the parallel component of the electric field, while leaving a residuum $E_\parallel$ sufficient to accelerate the beam – relativistic energies in a temporally steady flow are found if the current density $j_\parallel = -(B/P)\cos\chi +$ small corrections $\cong j_{\rm GJ}$; $\chi = \angle(\boldsymbol{\mu}, \boldsymbol{\Omega})$, the pulsar inclination angle. Mestel et al. (1985) showed that the velocity of the beam is monotonically increasing with altitude to relativistic speeds only if the current density is larger than $j_{\rm GJ}$. If the current density is smaller than $j_{\rm GJ}$ the temporally steady velocity of the beam (assumed to have no momentum dispersion) oscillates spatially, i.e. particles accelerate and decelerate to a complete halt as they move outwards into the magnetosphere. Beloborodov (2008) rediscovered Mestel et al.'s solution and suggested that in the region of the polar cap where $j_\parallel < j_{\rm GJ}$ particles will not be accelerated up to high energies as

the beam velocity oscillates, but along the magnetic field lines with $j_\parallel/j_{\rm GJ} > 0$ or $j_\parallel/j_{\rm GJ} < 0$ particle acceleration will be efficient and will lead to pair formation. The quantitative model which we describe in this paper lends some support to Beloborodov's speculations, although it does not agree with them in detail.

In this paper we describe our study of the physics of the polar cap accelerator in the space charge limited flow regime starting from first principles – assuming free particle outflow from the surface of a NS we compute the electric field, particle acceleration, gamma-ray emission, propagation and pair creation simultaneously. It extends the study of current flow and pair cascades in NS magnetospheres using the theoretical formulation and self-consistent numerical techniques introduced in Timokhin (2010).

The plan of the paper is as follows. In Section 2, we review the properties of the current flow imposed by the magnetosphere, in the force-free model, pointing out that the current density is the main parameter which regulates the efficiency of particle acceleration. In Section 3 we review the properties of stationary solutions for the charge-separated space charge limited flow problem. In Section 4 we briefly describe our numerical model. In Section 5 we describe the results of numerical modelling for the case of sub-GJ current density, the regime when particle acceleration is inefficient and no pair creation is possible. In Section 6 we consider flow regimes with efficient pair creation. In Section 6.4 we pay special attention to the stationary flow regime, which up to now was assumed in (most) works on pulsar polar cap accelerators, and describe why it has limited relevance to the force-free model of the pulsar magnetosphere. We discuss the implications of our results for the physics of RPPs in Section 7 and summarize our conclusions in Section 8.

2 CURRENT DENSITY IN THE POLAR CAP

Nebular observations of plasma supply by RPPs suggest the open field line regions are 'magnetohydrodynamic (MHD)-like', i.e. having $E_\parallel = 0$ except in special zones (such as the polar cap), which are, in effect, boundary layers. There is essentially no observational information on the properties of the closed magnetosphere, thus the simplest hypothesis is to follow Goldreich & Julian (1969) and assume the magnetosphere is (almost everywhere) filled with plasma that shorts out $E_\parallel$. The magnetosphere has open and closed magnetic field line zones. In the open zone plasma flows away into the pulsar wind; currents and their associated electromagnetic inertia keep the magnetic field open, so sustaining the flow. The plasma flows all the way from the base of the open field line zone in the polar cap of the pulsar where it is either extracted from the NS surface or generated by electron–positron cascades (or both). The distribution of the current density across the open field line zone, and therefore across the polar cap, is determined by the global magnetospheric structure. Stability of the pulsar mean profiles and sharpness of the peaks in the spectra of gamma-ray pulsars strongly suggest that on scales comparable to the light cylinder, the magnetosphere is stationary in the frame corotating with the NS with smooth and continuous plasma outflow. However, the stationary corotating magnetosphere hypothesis demands stationarity only in a statistical sense; fast local fluctuations which average to a stationary state (and even more broadly, global variations) can be included within this picture, so long as they do not smear the beaming profiles.

The polar cap acceleration and possible pair cascade zone – the main place where electron–positron plasma that feeds the wind can be produced – are much smaller than the characteristic scale $R_{\rm LC}$ of the magnetosphere. Therefore its inductance is negligible compared with that of the magnetosphere, and the polar current flow within the polar cap region must have an average equal to that set by the magnetosphere's global structure.

In this paper we solve a *local* problem of how the polar cap cascade zone adjusts itself to the current density required by the magnetosphere. On the dynamical time-scales typical for the cascade zone (microseconds) the magnetospherically required current density is stationary because it could change only on magnetospheric time-scales (tens of milliseconds up to several seconds). The idea that the acceleration zone has a magnetospherically determined current appears in the electrodynamics through the magnetic induction equation

$$\frac{\partial E_\parallel}{\partial t} = -4\pi j_\parallel + c(\nabla \times \boldsymbol{B})_\parallel \approx -4\pi(j_\parallel - j_{\rm m}), \tag{1}$$

with

$$j_{\rm m} = \frac{c}{4\pi}(\nabla \times \boldsymbol{B}_{\rm magnetosphere})_\parallel \tag{2}$$

being the current that sustains the twist to the field lines. In this paper we neglect the induced variations in the magnetic field that accompany variable $E_\parallel$ – because of the very strong background magnetic field (which in the region of interest has $\nabla \times \boldsymbol{B} = 0$), these have little dynamical effect on the acceleration and cascade dynamics [see Appendix A for the derivation of equation (1)].

We study the behaviour of the cascade zone under different current loads, sampling the range of possibilities illustrated in Fig. 1. The model has an essential difference from previous studies, in that we seek the accelerating voltage (with pair creation when the voltage drops are sufficiently large, without when they are small) as a function of the applied current. Previous work has almost entirely focused on the opposite direction, seeking the current that emerges from the accelerator when the voltage is fixed, either by the geometry or by the poisoning of the accelerator by pair creation. In addition, we allow the system to be fully time dependent. These generalizations lead to qualitatively different results from what has appeared before. Our model is one-dimensional, with spatial axis along magnetic field lines; from here on we drop subscript $\parallel$ from all quantities.

The characteristic charge density, the Goldreich-Julian charge density,

$$\eta_{\rm GJ} = -\frac{\boldsymbol{\Omega} \cdot \boldsymbol{B}}{2\pi c} \tag{3}$$

sets the characteristic current density

$$j_{\rm GJ} = \eta_{\rm GJ} c\,. \tag{4}$$

Following Fawley et al. (1977) and Arons & Scharlemann (1979), we also assume that if the star lacks an atmosphere, the work function for charged particles to leave the NS surface is small enough that any number of charged particles can be extracted from the NS surface until the extracting electric field is screened. In the classical pulsar regime, the theory of charged particle binding to the crust suggests such free emission to be likely (Medin & Lai 2010). More relevantly, X-ray observations of heated polar caps (Bogdanov, Rybicki & Grindlay 2007, and references therein) suggest that these stars have atmospheres overlying the solid and ocean components of the crust, which guarantees free emission of charges. The opposite case, with complete suppression of particle emission from the surface, was studied in Timokhin (2010), a realization of the scenario conjectured by Ruderman & Sutherland (1975).

As we will show in the following sections there are three qualitatively different plasma flow types in the polar cap of pulsar depending on the ratio of the current density imposed by the magnetosphere

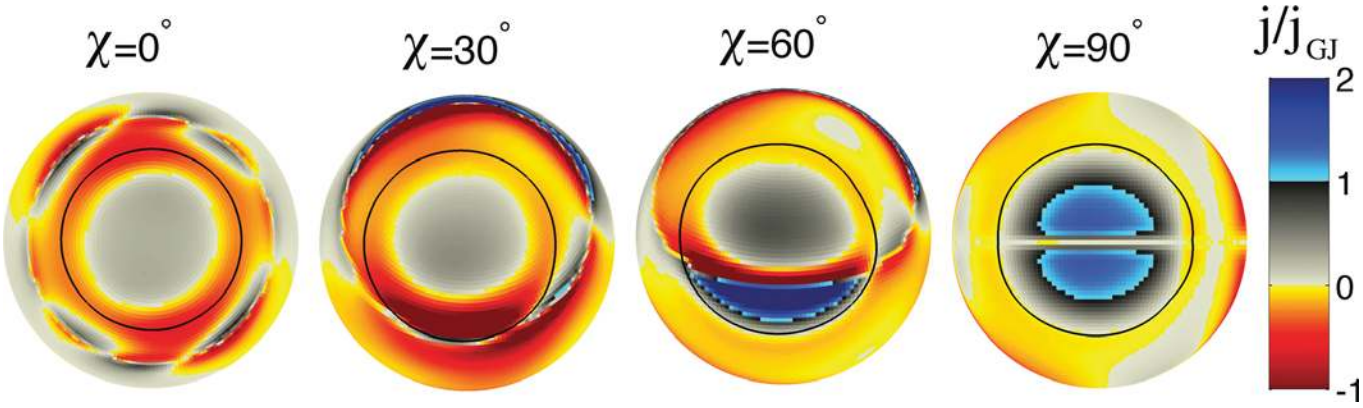

Figure 1. Field-aligned current density at the polar cap of the force-free rotator, with $j_\parallel$ measured in units of the Goldreich–Julian current density $j_{\rm GJ} \equiv -\boldsymbol{\Omega}\cdot\boldsymbol{B}/2\pi c$. The black circle is the rim of the polar cap – the footprints of the field lines that pass outside the light cylinder fall with that circle. The distributed current is shown. The current sheet component coincides with the polar cap boundary. This plot was made by Xuening Bai using results of force-free magnetosphere simulations presented in Bai & Spitkovsky (2010).

to the GJ current density: (i) $j_{\rm m}$ has the same sign and its absolute value is *smaller* than the GJ current density, $0 \le j_{\rm m}/j_{\rm GJ} < 1$, hereafter sub-GJ current density; (ii) $j_{\rm m}$ has the same sign and its absolute value is *larger* than the GJ current density, $j_{\rm m}/j_{\rm GJ} \ge 1$, hereafter super-GJ current density; (iii) $j_{\rm m}$ has the *opposite* sign to the GJ current density, $j_{\rm m}/j_{\rm GJ} < 0$, hereafter anti-GJ current density.

The advent of quantitative solutions for the structure of the force-free model (e.g. Contopoulos, Kazanas & Fendt 1999; Timokhin 2006; Spitkovsky 2006; Kalapotharakos & Contopoulos 2009; Bai & Spitkovsky 2010) has provided, for the first time, a theory of the current flow expected as a function of pulsar parameters (B, P, χ, when the magnetic field is a star-centred dipole). Earlier modelling of polar cap, slot gap and outer gap accelerators adopted the expectation that the current density is of the order of $j_{\rm GJ}$, and expressed the hope that the accelerator and pair creation physics do not sensitively depend on the precise value and spatial distribution of j. The results reported here show that the magnitude and sign of the current flow do lead to drastic differences in the open field line accelerator's behaviour in the three regimes (i)–(iii), even though the order of magnitude of the current is as expected. Fig. 1, showing $\tilde{\jmath} \equiv j/j_{\rm GJ}$, reveals that all three flow regimes occur in the force-free magnetosphere model. While $|\tilde{\jmath}\,|$ always has numerical values of the order of unity, it can be negative (return current) as well as lying in the separate regimes $0 < \tilde{\jmath} < 1$ and $\tilde{\jmath} > 1$. We show these separate regimes have different dynamical behaviour and different implications for pair creation.

We also show that once the constraints of the steady flow models for space charge limited flow are relaxed, the small departures of the GJ charge density from the simple estimate $-\Omega B\cos\chi/2\pi c$ created by geometric and general relativistic considerations (Arons & Scharlemann 1979; Muslimov & Tsygan 1992) that play an essential role in the steady flow models[1] have little significance when the flow is fully time dependent. Since we consider only the polar cap region, with altitudes not exceeding the width of the polar flux tube $r_{\rm pc} = R_*\sqrt{R_*/R_{\rm LC}} = 0.145P^{-1/2}$ km $\ll R_* = 10$ km, spatial variation of B is mostly unimportant. If we do not say so explicitly otherwise, throughout the paper we assume that the GJ charge density is constant, independent of the distance along B.

[1] If the GJ charge density were uniform and the beam is everywhere relativistic and time stationary, the unique model is no acceleration at all (Tademaru 1973; Fawley et al. 1977), a severe contradiction.

3 TIME-STATIONARY SPACE CHARGE LIMITED FLOW

Copious pair creation occurs when there is a sufficiently large accelerating potential difference along B when pairs are absent. Such potential drops, typically $\gtrsim 10^{12}$ V (Sturrock 1971), readily exist in the absence of current flow, that is, in a vacuum. Under pulsar conditions, if current does flow, pairs appear when the current flow co-exists with TV potential drops,[2] that is the current is a relativistic beam. Therefore, the starting place is the properties of time stationary, space charge limited, charge-separated flow. In this section we give an overview of these properties while detailed derivation of the equations used in this section is given in Appendix B together with some useful asymptotics. These review and extend a variety of results already in the literature.

For definiteness, we consider pulsars with an acute angle χ between $\boldsymbol{\Omega}$ and $\boldsymbol{B}$ ('acute' pulsars). These objects have $\eta_{\rm GJ} < 0$ at the polar cap, and require electron emission to supply $\eta_{\rm GJ}$.

Let us consider an electron beam starting with zero velocity at $x = 0$ and let the current density $j_{\rm m}$ imposed by the magnetosphere (equation (2)) be a fraction ξ of the GJ charge density

$$j_{\rm m} \equiv \xi\, j_{\rm GJ}\,. \tag{5}$$

In our case the GJ charge density is negative. In stationary flow the current density is constant in both space and time and is equal to the imposed current density $j \equiv j_{\rm m}$, thus $dE/dt = 0$ in equation (1). The stationary electric field $E_{\rm s}$ is then given by Gauss's law which in the frame corotating with the NS takes the form (e.g. Fawley et al. 1977, and references therein)

$$\frac{{\rm d}E_{\rm s}}{{\rm d}x} = 4\pi(\eta - \eta_{\rm GJ})\,. \tag{6}$$

The magnitude of the electric field increases with distance if the magnitude of the charge density η is larger than the GJ charge density and decreases otherwise.

[2] TV potential drops are required if curvature radiation from charges accelerated along a locally dipole magnetic field is the emission mechanism for the gamma-rays that convert to pairs. The required potential drops are smaller if the emission mechanism is inverse Compton scattering (either resonant or non-resonant) of softer photons from the surface (e.g. Hibschman & Arons 2001, and references therein).

The charge density at any given point of the flow is

$$\eta = j/v = \frac{j_{\rm m}}{c}\frac{\sqrt{p^2+1}}{p}\,, \tag{7}$$

where v is the flow velocity and $p \equiv \gamma v/c$ is the four-velocity = momentum in units of mc. p of a charge-separated stationary beam is given by the solution of the equation (B10)

$$\left(\frac{{\rm d}p}{{\rm d}s}\right)^2 = 2\,\frac{p^2+1}{p^2}\left(1+\xi\,p-\sqrt{p^2+1}\right), \tag{8}$$

where the distance s is measured in units of the Debye length $\lambda_{\rm D,\,GJ}$ of a cold electron plasma with GJ number density

$$\lambda_{\rm D,GJ} = c\left(\frac{4\pi\eta_{\rm GJ}e}{m}\right)^{-1/2} \simeq 2\,B_{12}^{-1/2}\,P^{1/2}\,{\rm cm}\,. \tag{9}$$

B_{12} is the pulsar magnetic field in 10^{12} G, and P is the pulsar period in seconds.

The numerical solutions of (8) for different imposed current densities are shown in Figs 2 and 3 for different values of ξ; these results confirm the work of Shibata (1997). For $0 < j_{\rm m}/j_{\rm GJ} < 1$ the steady flow oscillates spatially, with particle momenta oscillating in the interval $[0, p_{\rm max}]$, with

$$p_{\rm max} = \frac{2\xi}{1-\xi^2}. \tag{10}$$

${\rm d}p/{\rm d}s = 0$ at $p = p_{\rm max}$ and so is the RHS of equation (8). The value of $p_{\rm max}$ and the spatial period of oscillations s_0 increase with increasing ξ (see Figs 2 and 3). For $\xi \geq 1$ acceleration is monotonic with p increasing to infinity, with asymptotic behaviour

$$p = \sqrt{2}s + \frac{\xi-1}{2}s^2\,. \tag{11}$$

See Fig. 3 for $\xi = 1$, 1.1, 1.5.

The reason for such behaviour is as follows. The flow starts with zero initial velocity at $x = 0$ where the electric field is zero.

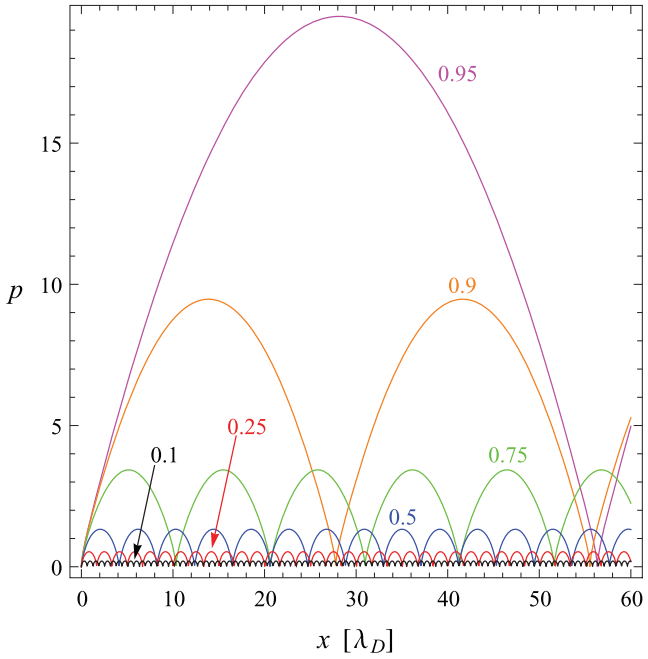

Figure 2. Phase space trajectories (four-velocity p versus distance normalized to $\lambda_{\rm D,\,GJ}$) for stationary space charge limited flow for current densities $j_{\rm m}/j_{\rm GJ} = 0.1, 0.25, 0.5, 0.75, 0.9, 0.95$.

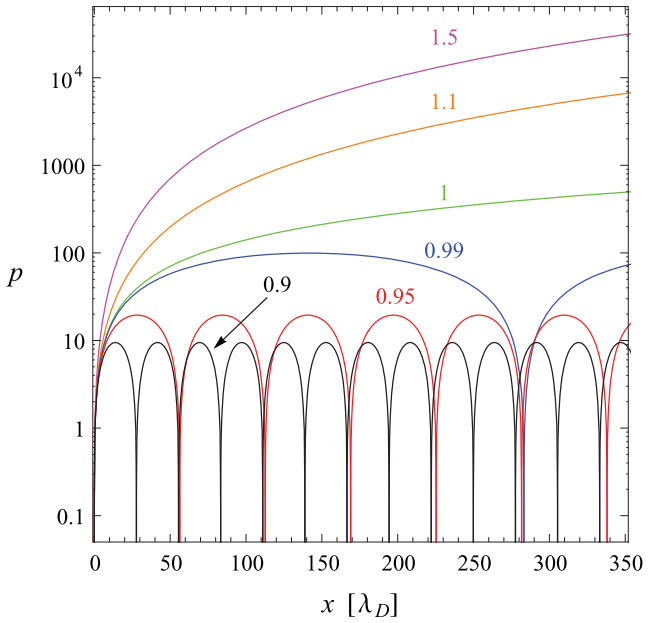

Figure 3. Phase space trajectories for stationary space charge limited flow for current densities $j_{\rm m}/j_{\rm GJ} = 0.9, 0.95, 0.99, 1, 1.1, 1.5$. Note that in contrast to Fig. 2 the vertical axis on this plot is logarithmic.

When the particle velocity is small the imposed current density is produced by high particle density moving slowly. In such places the absolute value of the beam charge density (cf. equation 7) is larger than that of the GJ charge density, $|\eta| > |\eta_{\rm GJ}|$ (see Fig. 4 where we plot the ratio $\eta/\eta_{\rm GJ}$ for flows with $\xi = 0.5$, 1, 1.5). The charge density is negative and according to equation (6) the electric field in this region is decreasing towards more negative values, thus accelerating electrons. If the imposed current density exceeds the GJ current density, $\xi > 1$, the absolute value of the beam charge density – whose maximum value is $|j_{\rm m}/c| = \xi\,|\eta_{\rm GJ}|$ – never becomes

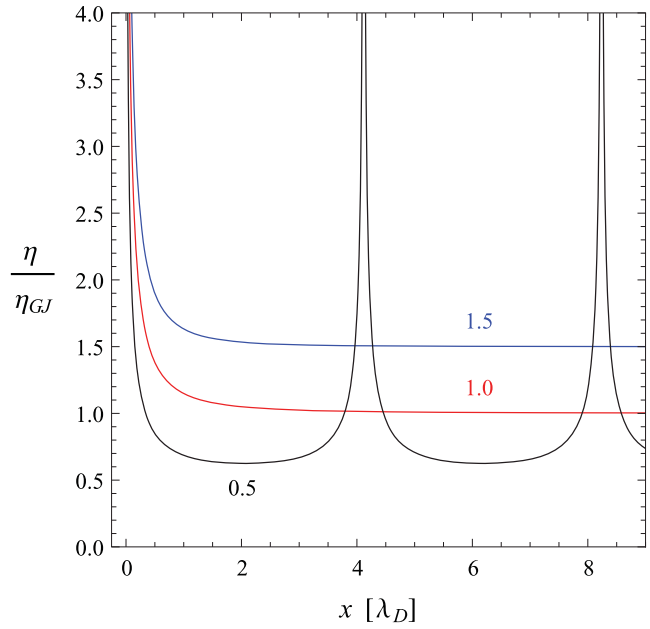

Figure 4. Charge density of stationary space charge limited flow normalized to the GJ charge density $\eta_{\rm GJ}$ as a function of distance x normalized to $\lambda_{\rm D}$ for current densities $j_{\rm m}/j_{\rm GJ} = 0.5$, 1.0, 1.5.

smaller than $|\eta_{\rm GJ}|$, hence, $dE_{\rm s}/dx < 0$ and acceleration continues up to infinity – the electric field and potential are monotonic. For $\xi < 1$, on the other hand, particles' velocities increase to values such that the imposed current density can be sustained by particle number density smaller than the GJ number density. Then $|\eta| < |\eta_{\rm GJ}|$ (see the line for $j_{\rm m} = 0.5 j_{\rm GJ}$ in Fig. 4), $dE_{\rm s}/dx > 0$ and the accelerating electric field weakens, changes sign and decelerates particles – in cold flow, the particles decelerate to zero velocity, and the cycle repeats.

The model of space charge limited flow outlined here provides a physical framework for the expected particle energetics. It is based on the approximation of one cold fluid and an assumption of complete stationarity of the flow. It can be extended to a two-fluid model to account for the presence of positrons and pair creation (as in Arons 1983). However, kinetic effects such as particle trapping cannot be included in a cold fluid approximation, although certain aspects *can* be modelled if momentum dispersion ('pressure') is included, with an assumed equation of state. A kinetic model incorporates momentum dispersion in the collisionless medium without having to make arbitrary assumptions about the equation of state. As we show in the following sections, particle trapping and pair creation profoundly affect the plasma dynamics, with momentum dispersion being essential to the dynamics behind the simultaneous adjustment of the charge density to the condition of low voltage drop along B, modelled as $\boldsymbol{E} \cdot \boldsymbol{B} = 0$ in the force-free global model, and the adjustment of the field aligned current j to the magnetospherically imposed $j_{\rm m}$.

The study of plasma kinetics in a general regime – without relying on stationarity or perturbation theory – is possible only by means of numerical simulations. In following sections we describe our study of plasma, both fully non-neutral and quasi-neutral when pair cascades form, with the help of a self-consistent hybrid numerical model incorporating both charged particles and photons.

4 NUMERICAL SETUP

We use the same one-dimensional hybrid Particle-In-Cell/Monte Carlo hybrid code described in Timokhin (2010) modified for the space charge limited flow regime. Below we briefly describe the main equations, notations and numerical algorithms; a detailed description can be found in Timokhin (2010, sections 2 and 3).

We solve the evolutionary equation for the electric field E

$$\frac{\partial E(x,t)}{\partial t} = -4\pi \left(j(x,t) - j_{\rm m} \right) , \tag{12}$$

where $j(x, t)$ is the actual current density and $j_{\rm m}$ is the current density imposed on the cascade zone by the magnetosphere. This equation is Ampere's law, equation (1). We are solving an initial value problem; thus an initial distribution of the electric field $E(x, t = 0)$ must be supplied. At the start of the simulation we construct the initial distribution of the electric field by solving the Gauss equation for the electric potential ϕ assuming some initial charge density distribution $\eta_{\rm start}$

$$\frac{{\rm d}^2\phi}{{\rm d}x^2} = -4\pi(\eta_{\rm start} - \eta_{\rm GJ}) \tag{13}$$

$$E = -\frac{{\rm d}\phi}{{\rm d}x}. \tag{14}$$

We proceed with the time integration of equation (12) using a charge conserving scheme (e.g. Birdsall & Langdon 1985; Villasenor & Buneman 1992), so the Gauss equation is satisfied at each successive time-step up to machine precision. The GJ charge density enters in equation (13) for the initial configuration of the electric field; this information is then 'carried on' in time by equation (12).

To model the space charge limited flow at every time-step we inject electrons and protons just outside the numerical domain used for the electric field calculation and let the system pull the necessary amount of particles into that domain. We *do not* set $E(x = 0, t)$ to zero as a boundary condition but rather allow the plasma in the system to enforce this condition as part of the simulated physics. A detailed description of our algorithm for reproducing the space charge limited flow condition at the NS surface is given in Appendix C. When pair creation cascades occur, we take into account only curvature radiation as the gamma-ray emission mechanism; pairs are created by single photon absorption in the strong magnetic field (e.g. Erber 1966).

We performed many numerical experiments starting from different initial conditions: (i) computational domain filled by plasma with charge density equal, less and higher than the GJ charge density as well as starting with vacuum; (ii) different initial potential drop over the domain; (iii) different length of the computation domain. In all cases without exception after initial relaxation on the time-scale of the order of the fly-by time of the domain the system settled down to a configuration which depends only on the imposed current density $j_{\rm m}$.

5 LOW ENERGY CHARGE SEPARATED, SUB-GJ FLOW: $0 < j_{\rm m}/j_{\rm GJ} < 1$

As it turns out, there is no pair formation for $0 < j_{\rm m}/j_{\rm GJ} < 1$ and the only characteristic spatial scale of the flow is the Debye length $\lambda_{\rm D,\,GJ}$. In this section we will discuss the properties of such flow using simulations in domains with the length L up to several hundreds of $\lambda_{\rm D,\,GJ}$, which is much less than the width of the polar cap. Using such a small domain we well resolve the characteristic spatial scale; increasing the domain length does not change the results.

According to the stationary solution from Section 3 there is no relativistic particle acceleration when $0 < j_{\rm m}/j_{\rm GJ} < 1$. The flow is spatially oscillatory and the maximum momentum of particles $p_{\rm max}$ is by far too small for emission of pair producing photons. It is unlikely that such oscillatory cold flow can exist – near the stagnation points it may be a subject to 'instability' with characteristics of the wave breaking to which non-linear waves in cold fluids with velocity stagnation are subject, which could destroy the spatial oscillation and create an effective resistor, across which a substantial fraction of the perpendicular (to B) voltage drop might appear. The available voltage drop across B is huge and in principle it might happen that the system ends up in a state with highly oscillatory electric field and bursts of pair formation as predicted in the two-fluid plasma model of Levinson et al. (2005). On the other hand, finite amplitude electrostatic waves containing similar stagnation points show wave breaking, with alteration of cold to hot flow with momentum dispersion no more than comparable to the flow velocities found in the originally constructed cold oscillation (Akhiezer & Polovin 1956; Tajima & Dawson 1979). That would create a warm but non-relativistic or mildly relativistic charge-separated outflow.

We find that in the sub-GJ regime, the non-neutral flow is indeed low-energetic, with particle energies orders of magnitude below the energy/particle required for pair production. However, the final state differs drastically from the oscillatory flow from the stationary solution shown in Figs 2 and 3. Even if at the beginning of the simulations particles follow trajectories of the stationary solution,

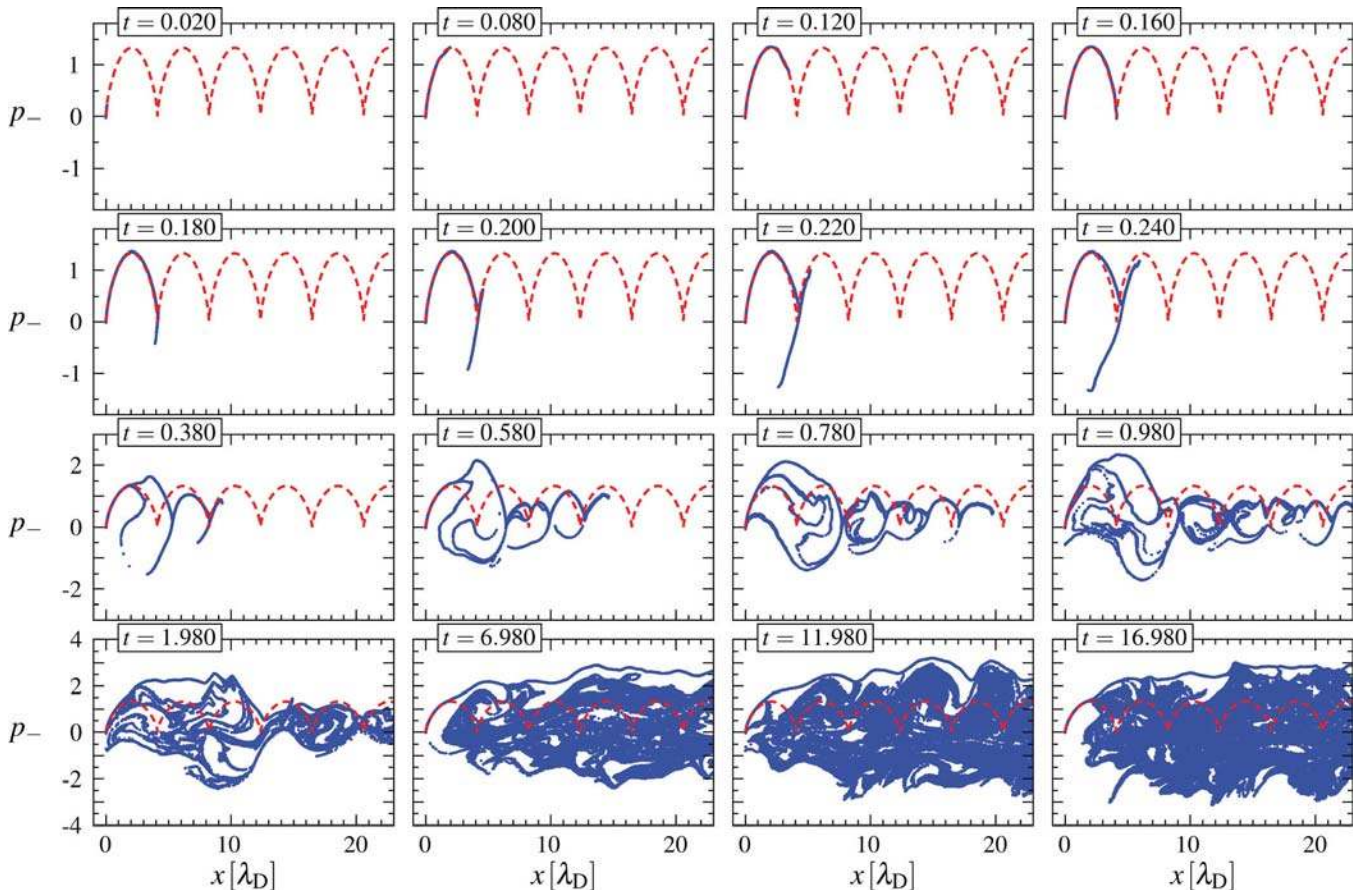

Figure 5. Development of 'trapped particle' flow when the space charge limited flow which starts into vacuum. Phase space portrait of particles are shown for 16 moments of time indicated in small boxes on the top of each plot. The current density $j_{\rm m} = 0.5 j_{\rm GJ}$. The distance x is measured in units of the Debye length. Red dashed lines show the analytical solution for stationary flow. Particle momenta p_- are normalized to $m_e c$. The total length of the computational domain $L = 50\lambda_{\rm D,\,GJ}$, only part of it ($x < 50\lambda_{\rm D,\,GJ}$) is shown here. Time is measured in fly-by time (L/c) of the whole domain. Snapshots in the same row have the same time interval between them, but these time intervals are different for different rows; they increase towards the bottom row.

the standing non-linear wave structure breaks quickly – particles at the velocity zeros of the cold flow go both up and down.

A good example of this inherent instability is shown in Fig. 5. We start from a vacuum configuration – when there are no particles in the domain – and let the system evolve. In Fig. 5 we show snapshots of the phase space portraits of the flow with $j_{\rm m} = 0.5 j_{\rm GJ}$; the distance from the NS, normalized to $\lambda_{\rm D,\,GJ}$, is along x-axis, and particle momenta, normalized to $m_e c$, are along y-axis. The whole domain has the length $L = 50\lambda_{\rm D,\,GJ}$ and we show only a part of it here. Time t is measured in fly-by time of the whole domain L/c. With the dashed red line we show phase space trajectories of particles from stationary solution. Particles coming from the surface at first follow the trajectories of the stationary solution. However, after coming to the first stagnation points some of the particles are turned back and the flow starts to randomize. After several tens of plasma periods $\lambda_{\rm D,\,GJ}/c$ the flow reaches its final configuration.

Examples of final configurations for space charge limited flow with different current densities are shown in Fig. 6, where we plot phase space portrait of particles in the whole computation domain. The flow has two components: a warm beam of particles with highest momentum which produce the required current density and a cloud of charged particles circulating in the domain – these compose an electrically trapped, 'thermal' component. In the cloud component there is roughly equal number of particles moving in opposite directions; these particles do not contribute to the current but contribute $\eta_{\rm GJ} - j_{\rm m}/c$ to the charge density keeping $\eta_{\rm total}$ equal to the GJ charge density. The distinction between these components is not absolute as some particles from the beam go into the cloud and vice versa, although the fraction of mixing particles is small. Some of the particles in the cloud have very low momenta and so they can adjust to any given charge density. Hence, in sub-GJ space charge limited flow, $0 \le j_{\rm m}/j_{\rm GJ} < 1$, the electric field is not sensitive to variation in the GJ charge density[3] – in contrast to the large importance of variation in the GJ charge density for relativistic acceleration of space charge limited cold beams in the polar cap cascade models of Arons & Scharlemann (1979) and Muslimov & Tsygan (1992).

Plasma flow in the sub-GJ regime can be described as a beam of mildly relativistic particles propagating through a cloud of trapped particles with near-thermal distribution. In Fig. 7 we plot particle distribution functions. The beam component is visible as a bump on the distribution function at the high momentum side. The cloud component has a near-thermal (Maxwell–Juttner) momentum distribution (at least in its low-energy part) $\partial n/\partial p \propto$ const – such quasi-thermalization is a common consequence of the phase mixing between the particles and fields built into the wave breaking process.

[3] We performed simulations for $j_{\rm m}/j_{\rm GJ} < 1$ with variable GJ charge density, and, as expected, saw the electric field to be just as screened as in the uniform GJ density case.

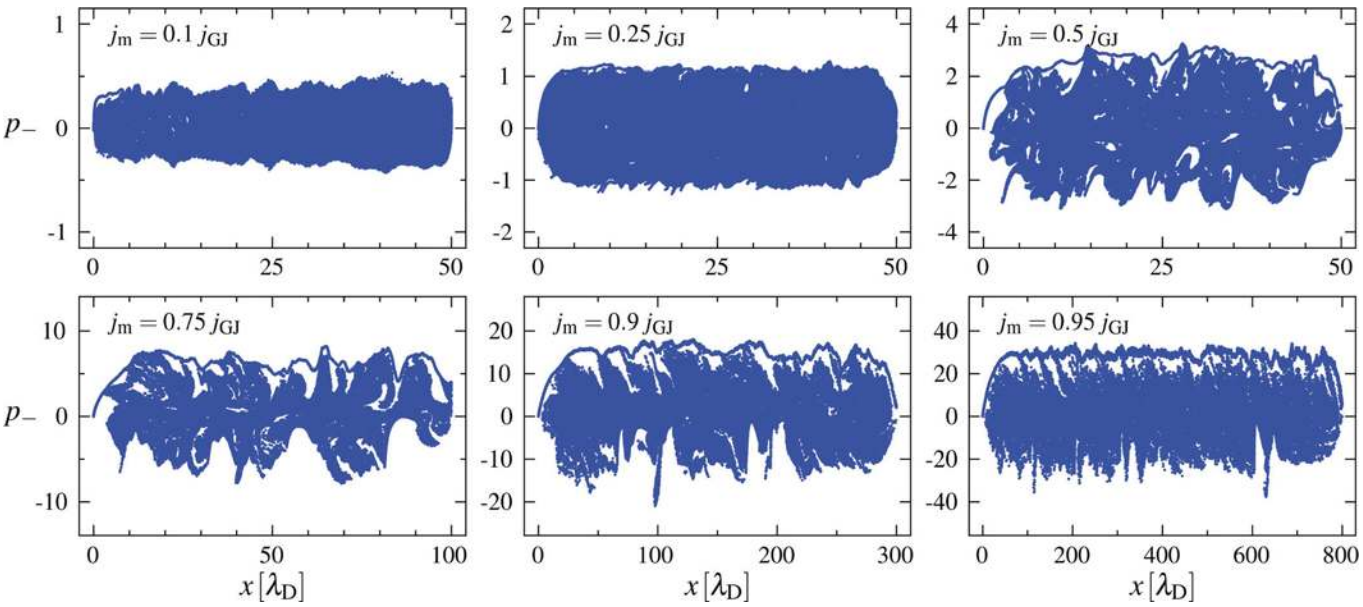

Figure 6. Phase space portraits of well-developed space charge limited flows for six different current densities: $j_m/j_{GJ} = 0.1, 0.25, 0.5, 0.75, 0.9, 0.95$. Current density j_m is indicated in the left upper part on each plot. Distance is measured in units of λ_D, and particle momenta p_- are normalized to $m_e c$. Note that the lengths of the computation domain differ between these plots.

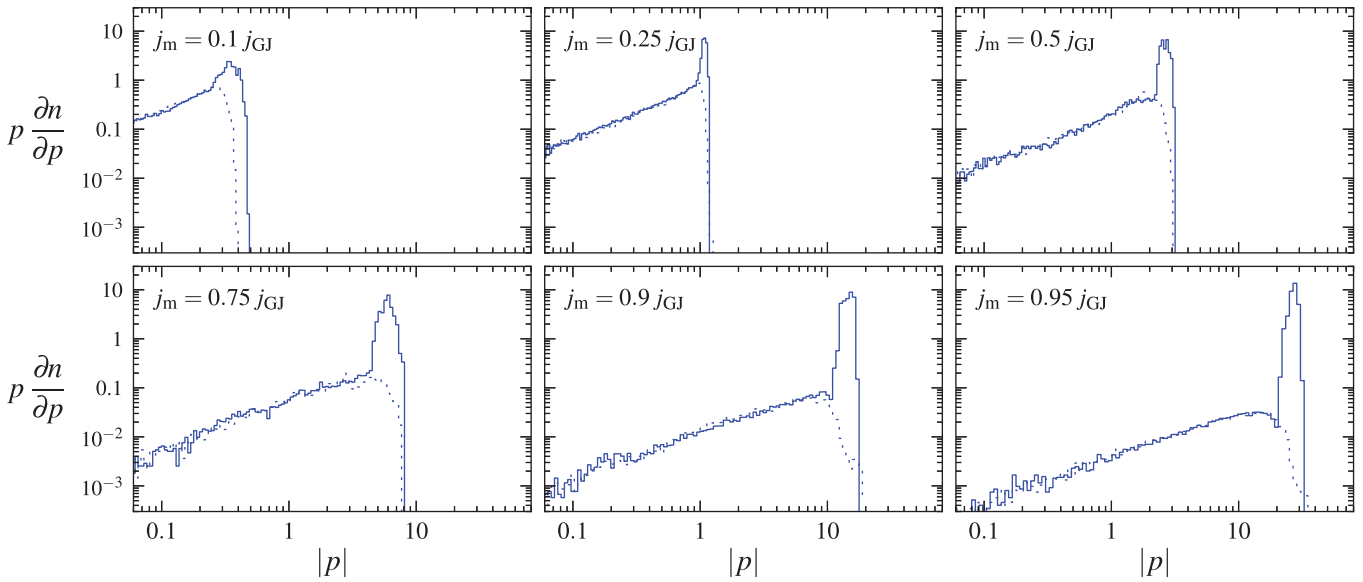

Figure 7. Particle distribution functions $p\,(\partial n/\partial p)$ for well-developed space charge limited flows from Fig. 6. Distribution functions of particles with positive momenta (moving towards the magnetosphere) are shown by solid lines, and distribution functions of particles with negative momenta (moving towards the NS) by dashed lines.

When particles leave the NS they are non-relativistic and their charge density $\eta = j_m/v = \xi j_{GJ}/v$ is larger than the GJ charge density and so they form a charge sheet near the surface generating accelerating electric field, just as in the idealized stationary case (see Fig. 4). When particles reach the velocity such that $|j_m|/v < |\eta_{GJ}|$ the electric field derivative dE/ds changes sign and after some distance the electric field can start decelerating particles. At the point where $E = 0$ particles reach their maximum momentum. Above the gap particles from the cloud component add additional charge and so the change density there is equal to η_{GJ} and the electric field is screened. The length of this gap is of the order of $s_{max} = s_0/2$ (half the spatial period of cold flow oscillations) and so the maximum momentum particles gain in this gap is comparable to p_{max} (both s_{max} and p_{max} depend on j_m). In Fig. 9 we plot momenta of particles in the beam component as functions of $\xi = j_m/j_{GJ}$ superimposed on the theoretical dependence of p_{max} given by equation (10); the agreement is pretty good. The current density in the final configuration is close to j_m throughout the domain, with small fluctuations around this value $\delta j \ll j_m$.

In Fig. 8 we plot the electric field in the calculation domain at the same moments of time as the phase space portraits shown in Fig. 6. The electric field at any given point fluctuates, but the relative fluctuation at the beginning and at the end of the domain (accelerating and decelerating regions; see below) are much smaller than those in the centre of the domain (the region of the charge cloud). The electric field in the gap near the NS launches the beam component. The

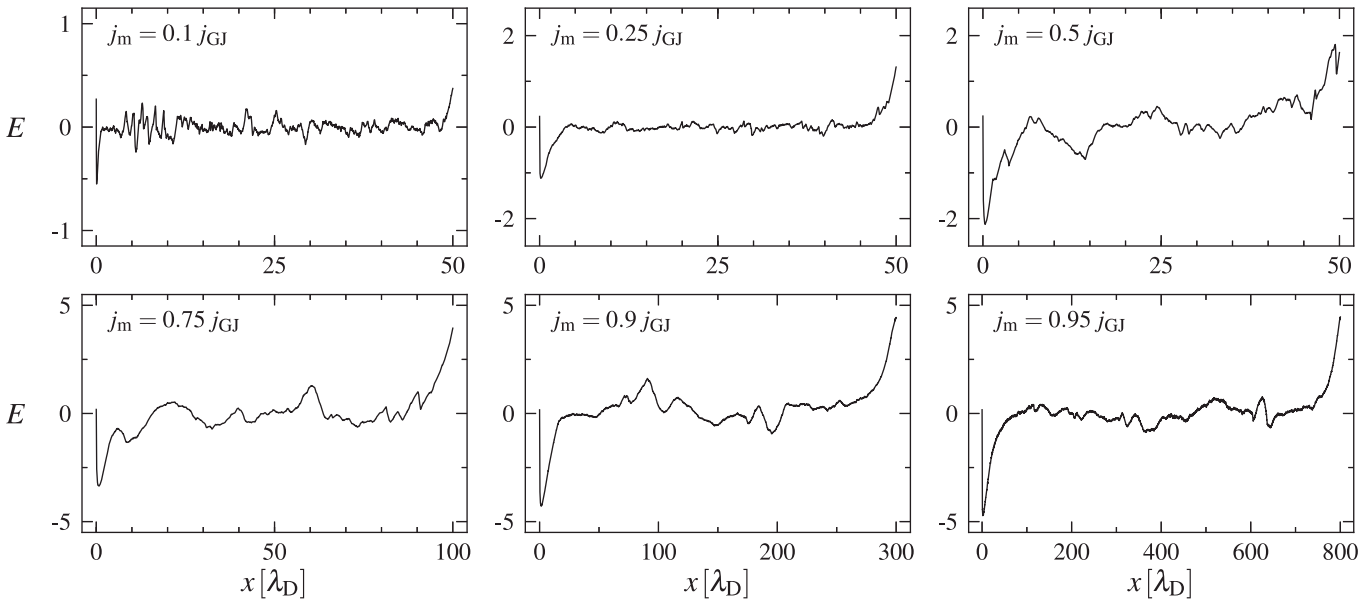

Figure 8. Snapshots of the electric field E for well-developed space charge limited flows taken at the same moment as the phase space portraits from Fig. 6. E is normalized to $\pi\eta_{GJ}\lambda_{D,GJ}$.

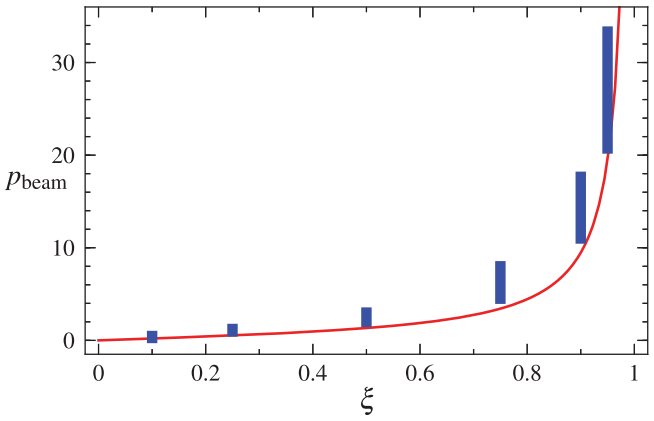

Figure 9. Momenta of the current currying particle beam. The widths of the peaks at Fig. 7 as the function of $\xi = j_m/j_{GJ}$ are shown by the blue bars. The solid red line is the maximum achieved momentum for the stationary SCLF solution.

electric field at the other end of the computation domain supports the cloud components by reversing the momenta of most of the particles in the cloud moving away from the NS, sending them back. This electric field is not strong enough to reflect most of the beam particles. The mixing between the beam and cloud components is the strongest here. This electric field appears self-consistently when the flow reaches its steady configuration,[4] because it is needed to sustain the cloud component necessary to match both the charge and the current density in the domain. In our small-scale 1D simulations we impose the current density on the domain, which finally gives rise to the electric field at the right end of the domain. In reality, it is the magnetosphere which sets the current density by twisting the magnetic field lines and generating electric field reversing some of the particles. This second region with an unscreened electric field at the magnetosphere end of the domain in our model may be a 'compressed' version of some parts of the outer magnetosphere. For example, on field lines that pass through the null surface where $\boldsymbol{\Omega} \cdot \boldsymbol{B} = 0$, the plasma cloud and beam, composed of only one sign of charge, cannot freely enter the outer magnetosphere (Scharlemann, Arons & Fawley 1978) in the absence of other sources of electric field in other parts of the magnetosphere (Goldreich & Julian's 'hanging charge clouds'), offering the possibility of opening a vacuum gap within the otherwise force-free structure. On the other hand, on polar field lines that never cross the null surface – most of them, in the aligned rotator – the charge-separated beam and cloud can extend outwards 'forever', in principle. Multi-dimensional particle simulations, analogous to those of Spitkovsky & Arons (2002), are required to see if indeed this speculation is true (as well as determine how this essentially 1D model might fit together with the other, more 'lively' aspects of the polar flow outlined in Section 6).

In Fig. 10 we show power spectra of the fluctuating electric field in the central parts of the calculation domain, outside of the acceleration zones. $I_k = |E_k|^2$, where E_k is the spatial Fourier amplitude of the electric field and the wave vector k is normalized to the $\lambda_{D,GJ}^{-1}$. These spectra can be fitted with the power law $I_k \propto k^{-\alpha}$ with α between 2 and 3 for all current densities.

Thus, along magnetic field lines where the current density is sub-GJ there is no pair formation, so long as strong electric fields in neighbouring, more active flow zones do not leak into the cloud. In an aligned rotator, for example, no pairs are forming above most of the polar cap area. Plasma flowing along such magnetic field lines is mildly relativistic, consists of particles of only one sign (electrons) and its density is low, equal to the GJ number density. However, observational evidence for ongoing pair formation in pulsars is very strong and, hence, there must be regions in the pulsar magnetosphere where electron–positron plasma is created.

6 PLASMA FLOW WITH PAIR FORMATION – SUPER-GJ AND RETURN CURRENT REGIONS

Let us now consider what happens along magnetic field lines where the current density has either (i) the opposite sign to the GJ current density, $j/j_{GJ} < 0$, anti-GJ flow, or (ii) the same sign and absolute

[4] The *formation* of the cloud component is not linked to the appearance of the electric field at the end of the domain (see e.g. Fig. 5).

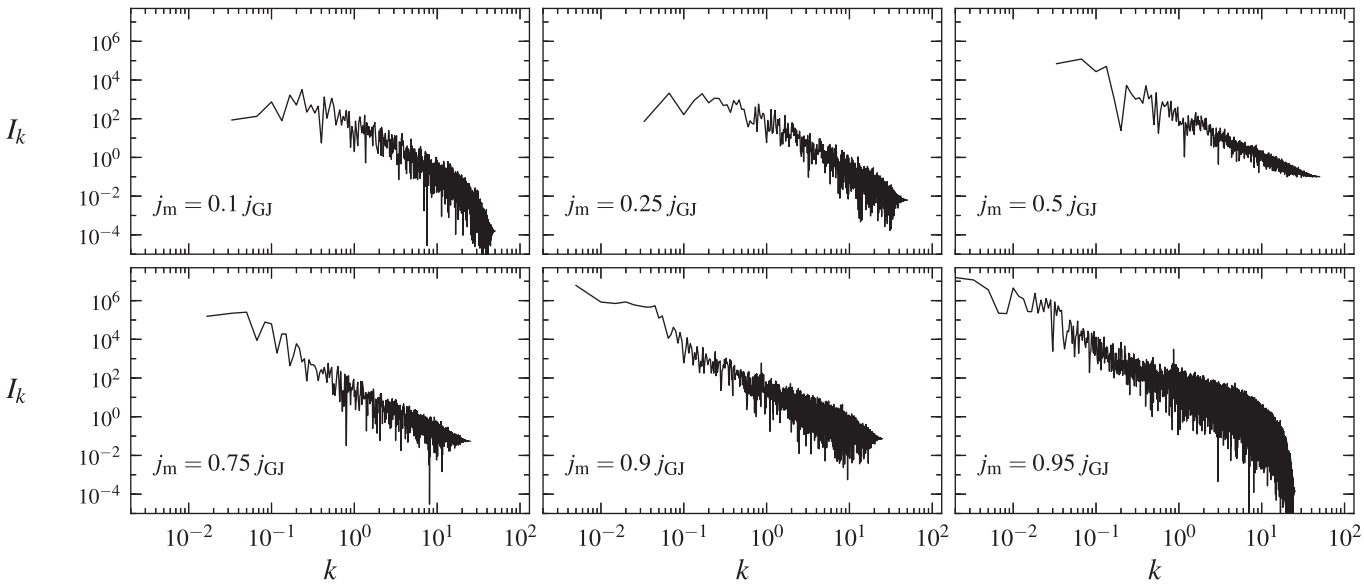

Figure 10. Power spectra of the electric field $I_k = |E_k|^2$ for well developed space charge limited flows from Fig. 6. k is normalized to the corresponding $1/\lambda_{D,\,GJ}$.

value larger than the GJ current density, $j/j_{GJ} > 1$, super-GJ flow. Case (i) includes the regions of return current, including the current sheet, while case (ii) is relevant for most of the magnetic field lines in a nearly orthogonal rotator. As we show in this section, in both of these cases a strong accelerating electric field is generated. When the resulting potential drop is sufficient to accelerate particles up to the energies such that they can emit photons that convert to pairs within the accelerator, the plasma flow will be highly non-stationary with intermittent pair creation.

In a real pulsar the magnetic field strength falls with the distance ($\propto r^{-3}$ for a dipole field) and pair creation is possible only at sufficiently low altitude (if gamma-ray interaction with thermal low energy photons is neglected). In order to imitate the effect of pair creation attenuation with the distance we set the magnetic field strength to zero starting at distance x_B from the NS – the magnetic field is given by

$$B(x) = \begin{cases} B_0, & \text{if } x \le x_B \\ 0, & \text{if } x > x_B. \end{cases} \tag{15}$$

If the charge density were formed from steadily flowing relativistic beams, it would vary with the height as $\eta(x) \propto B(x)$. The GJ charge density changes in a slightly different way, $\eta(x) \propto B(x) f(x)$ due to inertial frame dragging (Muslimov & Tsygan 1992; Beskin 1990) or/and field line curvature (Scharlemann et al. 1978). If one neglects the latter effects, scaling $\propto B(x)$ can be incorporated into the spatial (for equation 13) or temporal (for equation 12) coordinates. The electrodynamics of the cascade zone can be modelled in a 1D problem with constant GJ charge density; the only effect of the GJ charge density variation will be in changing the spatial (and temporal) scales. The same scaled 1D model can also be used to study the effects on the electrodynamics of the cascade zone of deviation of the GJ charge density scaling from being $\propto B(x)$ by considering a problem where η_{GJ} depends on the distance; the variation of the GJ charge density will be given by $f(x)$ as the dependence on $B(x)$ is already incorporated in the model. First, in Sections 6.1 and 6.2, we consider the case when the GJ charge density is constant, i.e. this case corresponds to a model where variation of η_{GJ}/B is neglected. Then in Section 6.3 we address the influence of the GJ charge density variation on the physics of the cascade zone.

While simulations of space charge limited flow with sub-GJ current densities described in Section 5 can be considered as directly related to more complete pulsar models – the distance over which wave breaking and trapping control the flow is much smaller than the width of the polar cap, and the 1D approximation is well motivated – the pair creation models presented in this section can be considered only as illustrative of the physics but not fully applicable to pulsars. The spatial scales over which pair creating photons are absorbed, even when they are emitted at very low altitude (e.g. the attenuation length of the magnetic field), are much larger than the width of the polar cap, making transverse structure essential for modelling the pulsar environment – such effects are necessary for a full evaluation of the pair yield, since much of the pair creation occurs in regions beyond the acceleration zone. Nevertheless, from our 1D models we obtain insight into the basic cascades physics in a regime never modelled previously. Multi-dimensional models will be considered elsewhere.

Within the context of the 1D model, the domain length, L, and the value of x_B (the height above which the magnetic field is too weak to support pair creation) are the parameters having the largest departure from what would appear in multi-dimensional context. These lengths in our simulations are much smaller than in real pulsars, but that choice allowed us to construct models utilizing reasonable amounts of CPU time and to explore a broad parameter space. L and x_B were chosen in such a way that the minimum size of the accelerating region necessary to start pair creation is at least two to three times less than x_B.

We performed numerous simulations for different initial conditions and physical parameters in order to study the qualitative behaviour of cascades. We performed simulations with different values of the numerical parameters (spatial resolution, time-steps, particle injection rate, number of particles per cell) in order to check the numerical convergence. In all physical cases presented in this section plasma flow is quasi-periodic, and this behaviour does not depend on initial conditions – after a short relaxation time, comparable to the fly-by time of a relativistic particle through the

computational domain, the system settles down to a limit cycle sort of behaviour. We describe here a particular set of simulations which is representative of all other models. Simulations described in Sections 6.1 and 6.2 have the following physical parameters: the length of the domain $L = 2.4 \times 10^4$ cm, the potential drop in vacuum across the domain $\Delta V = 10^{14}$ V,[5] the radius of curvature of the magnetic field lines with respect to a photon orbit $\rho_c = 10^6$ cm $\sim$ the stellar radius (small compared to the pure star centred dipole value $\sqrt{R_* R_{\rm LC}} \sim 10^{7.8} P^{1/2}$ cm but easily attained in offset dipole geometry (Arons 1998; Harding & Muslimov 2011; Arons, in preparation); magnetic field strength $B_0 = 10^{12}$ G. The distance $x_{\rm B}$ marking the transition to the outer magnetosphere with a small magnetic field is set to $x_{\rm B} = 0.7L$. The particular simulations described in these two sections differ only in the imposed current density $j_{\rm m}$.

We illustrate the flow dynamics with a series of snapshots for different physical quantities shown in Figs 11–16 and 20–22. In these figures, each column gives detailed information about physical conditions in the computation domain at a given moment of time: the number densities of electrons and positrons $n_\pm$ (shown as charge densities of electrons and positrons $\eta_\pm$, $n_\pm = |\eta_\pm|$), total charge density η, current density j, the accelerating electric field E, phase portraits of electrons, positrons and pair producing photons, and, in Figs 14–16, protons. Particles with positive values of the four-velocity p are those which move away from the NS (towards higher altitude), and particles with negative p move towards the NS. These plots are similar to ones in Timokhin (2010), with the only difference that now we use semi-logarithmic scale for particle momenta (linear for $-5 < p < 5$ and logarithmic everywhere else) on phase space portraits that show dynamics of high and low energy particles on the same plot.

The number density, charge density and the current density are normalized to the corresponding GJ values: $\eta_\pm$ and η are normalized to $|\eta^0_{\rm GJ}|$, j to $|\eta^0_{\rm GJ}|c$, where $\eta^0_{\rm GJ}$ is the GJ charge density at the NS surface (the distinction between $\eta_{\rm GJ}$ and $\eta^0_{\rm GJ}$ will be important for models described in Sections 6.3 and 6.4). The electric field is normalized to $E_0 \equiv |\eta^0_{\rm GJ}|\pi L$. The distance x on these plots is normalized to L, much larger than the Debye length $\lambda_{\rm D,\,GJ}$. The time t is normalized to the relativistic fly-by time of the computational domain $L/c = 0.8\,\mu$s for the chosen parameters. The time is counted from the start of a particular simulation, so only time intervals between the snapshots have a physical meaning.

In all cases, plasma flow and pair formation have limit cycle behaviour. In each case we illustrate this behaviour by three series of snapshots taken within one typical cycle. These three series show three phases of plasma flow: cascade ignition (Figs 11, 14 and 20), development of the cascade (Figs 12, 15 and 21) and filling the domain with dense pair plasma (Figs 13, 16 and 22). In each figure time intervals between snapshots are equal, but these intervals are different in different figures.

[5] Such vacuum potential drops over the domains of this size are realistic in young, high magnetospheric voltage pulsars, $\Phi_{\rm m} > 10^{15}$ V. This choice allows studying pair formation over distances smaller compared to the polar flux time diameter. In more common pulsars with $\Phi_{\rm m} < 10^{13}$ V, pair formation happens over (much) larger distances. However, as we mentioned before, our simulations represent a toy model addressing the general behaviour of the polar cap acceleration zone and our choice of parameters is motivated by convenience of simulations, rather than by attempt to model a real pulsar.

6.1 Flow with $j_{\rm m}/j_{\rm GJ} < 0$

In this section we describe cascade development for two cases when the imposed current density is anti-GJ (i.e. has the opposite sign to the GJ current density), for $j_{\rm m} = -0.5 j_{\rm GJ}$ and $j_{\rm m} = -1.5 j_{\rm GJ}$. To support such current electrons on average must move towards smaller x, down towards the NS, positrons towards larger x, up into the magnetosphere. Electrons could be freely emitted from the NS surface, but because the imposed current causes the growing electric field to point away from the surface, electrons at the surface are accelerated downwards and none is extracted from the star.[6] This situation resembles the case of the Ruderman & Sutherland (1975) cascades studied in Timokhin (2010) in the sense that all the particles are produced during the burst of pair formation. Hence, the physics of pair cascades with anti-GJ imposed current density discussed in this section are also applicable to Ruderman & Sutherland cascades as well.

Particles leave the domain and some time after the burst of pair formation the domain becomes depleted of electrons. This process starts at the right end of the domain – at the 'magnetosphere' end – as electrons are moving down towards the NS. In the region depleted of electrons, the positrons support the current density $j < j_{\rm m}$ with charge density $\eta > \eta_{\rm GJ}$. This gives rise to the electric field which accelerates positrons towards the magnetosphere – see the phase portraits of positrons in Figs 11 and 14. The electric field in this region at any given point is growing with time and the size of the region with unscreened electric field is getting bigger as the remaining electrons are moving towards the NS. The electric field grows linearly with the distance because positrons are relativistic and so their charge density remains constant (see plots for E in Figs 11 and 14).

As the region with the unscreened electric field grows, positrons are being accelerated up to higher and higher energies and begin emitting pair producing gamma-rays. Positrons remaining from the previous burst of pair formation are the particles which ignite the next burst. As positrons are moving up (and so do the first pair producing photons), the first pairs are produced at the largest distance from the NS where pair formation is still possible, in our case near $x = x_{\rm B} = 0.7L$. The injected pairs are picked up by a very strong electric field and are accelerated to high energies in less time than the first generation positrons. They emit pair-producing capable gamma-rays, but now both secondary electrons and positrons are emitting pairs. As electrons and positrons move in opposite directions so do the gamma-rays – see snapshots for gamma-rays phase space at $t > 8.100$ in Fig. 11 and $t > 6.390$ in Fig. 14.

Secondary electrons and positrons are moving in opposite directions and the plasma gets polarized – see plots for $\eta_\pm$ and η at $t = 8.260$ in Fig. 11 and at $t = 6.430$ in Fig. 14. When their number density becomes comparable to the GJ number density, these particles start screening the electric field (see plots for E at $t = 8.260$ and 8.270 in Figs 11 and 12 and at $t = 6.430$ and 6.440 in Figs 14 and 15). The screening starts in the region where the first pairs were injected because pairs have been injected here for the longest time and their number density is larger.

The rate at which particles left from the previous burst of pair formation are leaving the domain depends on the imposed current density. The average bulk motion of electrons for $j_{\rm m} = -0.5 j_{\rm GJ}$ is

[6] Due to numerical noise the electric field fluctuates and sometimes electrons 'from the NS surface' enter the domain; however, the number of such electrons is well below the fluctuation of electron number density due to numerical noise.

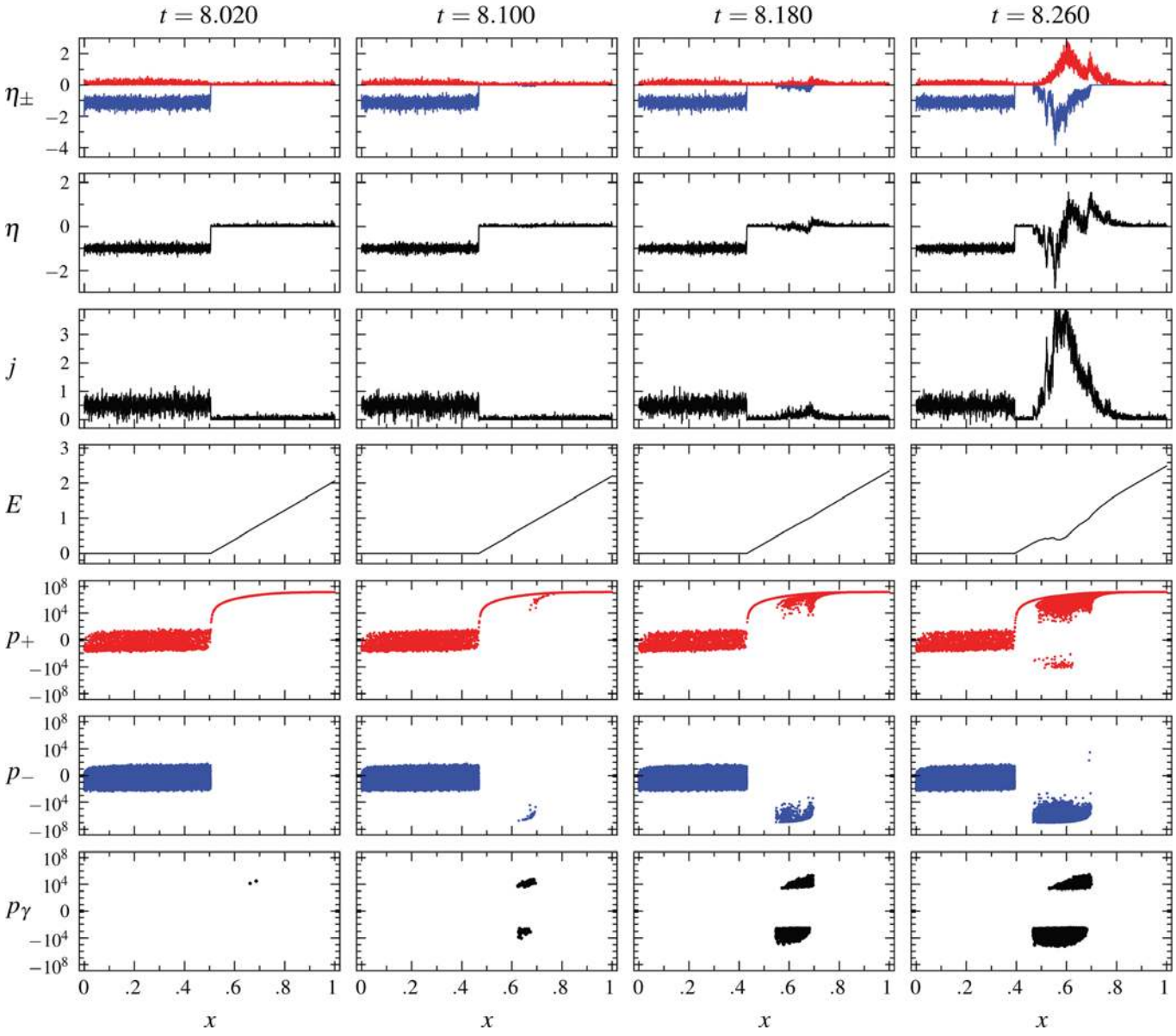

Figure 11. Ignition of pair formation in anti-GJ flow with $j_m = -0.5j_{GJ}$. Several physical quantities are shown as functions of the distance x from the NS; x is normalized to the domain size L. Plots in each column (for the same time t) are aligned – they share the same values of x. The following quantities are plotted: first row: $\eta_\pm$ – charge density of electrons (negative values, blue line) and positrons (positive values, red line); $\eta_\pm$ is normalized to the absolute value of the Goldreich–Julian charge density $|\eta_{GJ}|$. Second row: the total charge density η normalized to the absolute value of the Goldreich–Julian charge density $|\eta_{GJ}|$. Third row: current density j normalized to the absolute value of the Goldreich–Julian current density $|j_{GJ}| \equiv |\eta_{GJ}c|$. Fourth row: accelerating electric field E normalized to the 'vacuum' electric field $E_0 \equiv |\eta_{GJ}|\pi L$. Fifth row: phase space portrait of positrons (horizontal axis – positron position x, vertical axis – positron momentum p_+ normalized to $m_e c$). The vertical axis is logarithmic except for the region around zero momentum ($-5 < p_+ < 5$), where the scale is linear. Sixth row: phase space portrait of electrons (horizontal axis – electron position x, vertical axis – electron momentum p_- normalized to $m_e c$). Seventh row: phase space portrait of pair-producing photons (horizontal axis – photon position x, vertical axis – photon momentum p_γ normalized to $m_e c$).

less than $0.5c$, while for $j_m = -1.5j_{GJ}$ it is close to c,[7] and the size of the electron-depleted region grows slower in the first case than in the second one. Second generation electrons, which mark the upper boundary of the gap, move with ultrarelativistic velocity towards the NS. Because of this in the case of $j_m = -0.5j_{GJ}$ the gap with the accelerating electric field quickly disappears – at $t = 8.430$ in Fig. 12 secondary particles have already caught up with the particles from the previous burst of pair formation and the electric field is screened everywhere where pair formation is possible. In the case of $j_m = -1.5j_{GJ}$ the gap moves towards the NS approximately retaining its size (see Figs 15 and 16). This behaviour is generic. Namely, for imposed current densities with less-than-GJ absolute values, $|j_m| < |j_{GJ}|$, the average bulk motion of particles from the previous burst of pair formation is non-relativistic, which leads to quick closure of the accelerating gap. If the absolute value of the imposed current density is larger-than-GJ, $|j_m| > |j_{GJ}|$, the average bulk motion of

[7] Note that the time intervals between the snapshots in Fig. 11 is two times larger than that in Fig. 14.

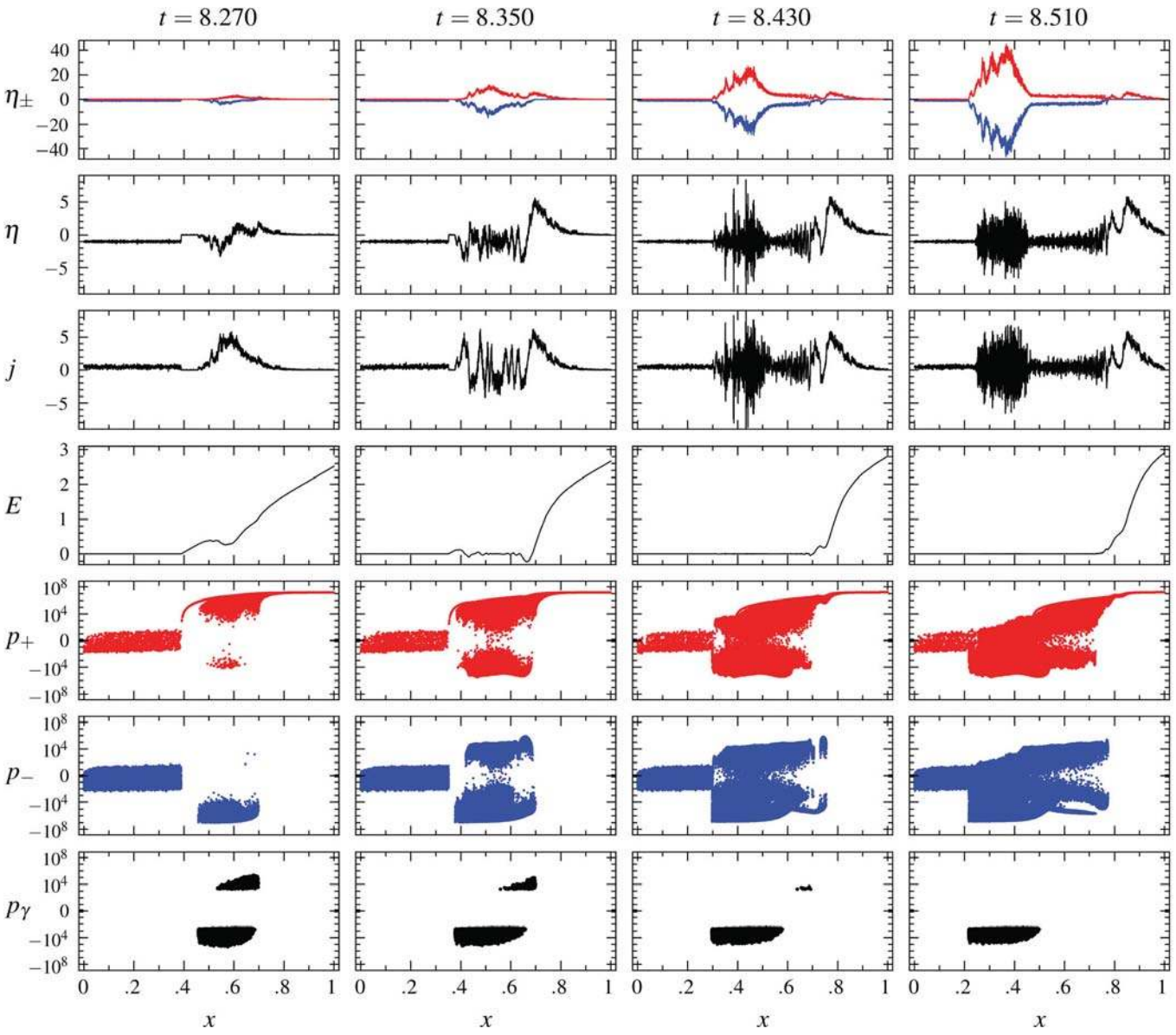

Figure 12. Screening of the electric field in anti-GJ flow with $j_m = -0.5 j_{GJ}$. The same quantities are plotted as in Fig. 11.

particles from the previous burst of pair formation is relativistic and the gap propagates in the direction of this bulk motion. The same behaviour was observed also in the case of Ruderman–Sutherland cascades studied in Timokhin (2010).

In the case of $j_m = -0.5 j_{GJ}$ the gap with the accelerating electric field closes and particles in the region where pair formation is possible are not accelerated anymore. The pair formation continues only due to particles being accelerated before the gap disappeared. There are comparable numbers of particles accelerated in both directions, but electrons moving towards the NS propagate in the region where pair formation is possible and so after screening of the electric field most of the pairs are created with the initial momenta directed towards the NS (see phase portraits for pair producing gamma-rays for $t > 8.180$ in Figs 11–13 and particle distribution functions in Fig. 17). In the case of $j_m = -1.5 j_{GJ}$ the gap propagates down to the NS surface. While the gap is moving, positrons left from the previous bursts of pair formation, which are still present at the NS side of the domain, enter the gap, are picked up by the electric field, and emit pair producing gamma-rays. In this case the pair production is sustained not only by electrons accelerated in the initial screening event but also by positrons continuously accelerated in the moving gap towards the magnetosphere. Phase portraits of gamma-rays in Figs 14–16 clearly show the presence of gamma-rays moving towards the magnetosphere during all stages of cascade development (see also the plot for particle distribution functions in Fig. 18). Gamma-rays with positive momenta occupy a larger fraction of the space over time, as the gap propagates towards the NS.

Regions far from the NS surface experience charge starvation first. The pair formation is possible only in the regions with a strong magnetic field and until the starved region extends into the strong field domain the electric field remains unscreened. After the start of pair formation, the dense plasma propagates also in the direction of the magnetosphere screening the accelerating electric field there. In our simulations the region with $x > 0.7L$ represents the rest of the magnetosphere, and in snapshots with $t = 8.430$–8.990, in Figs 12

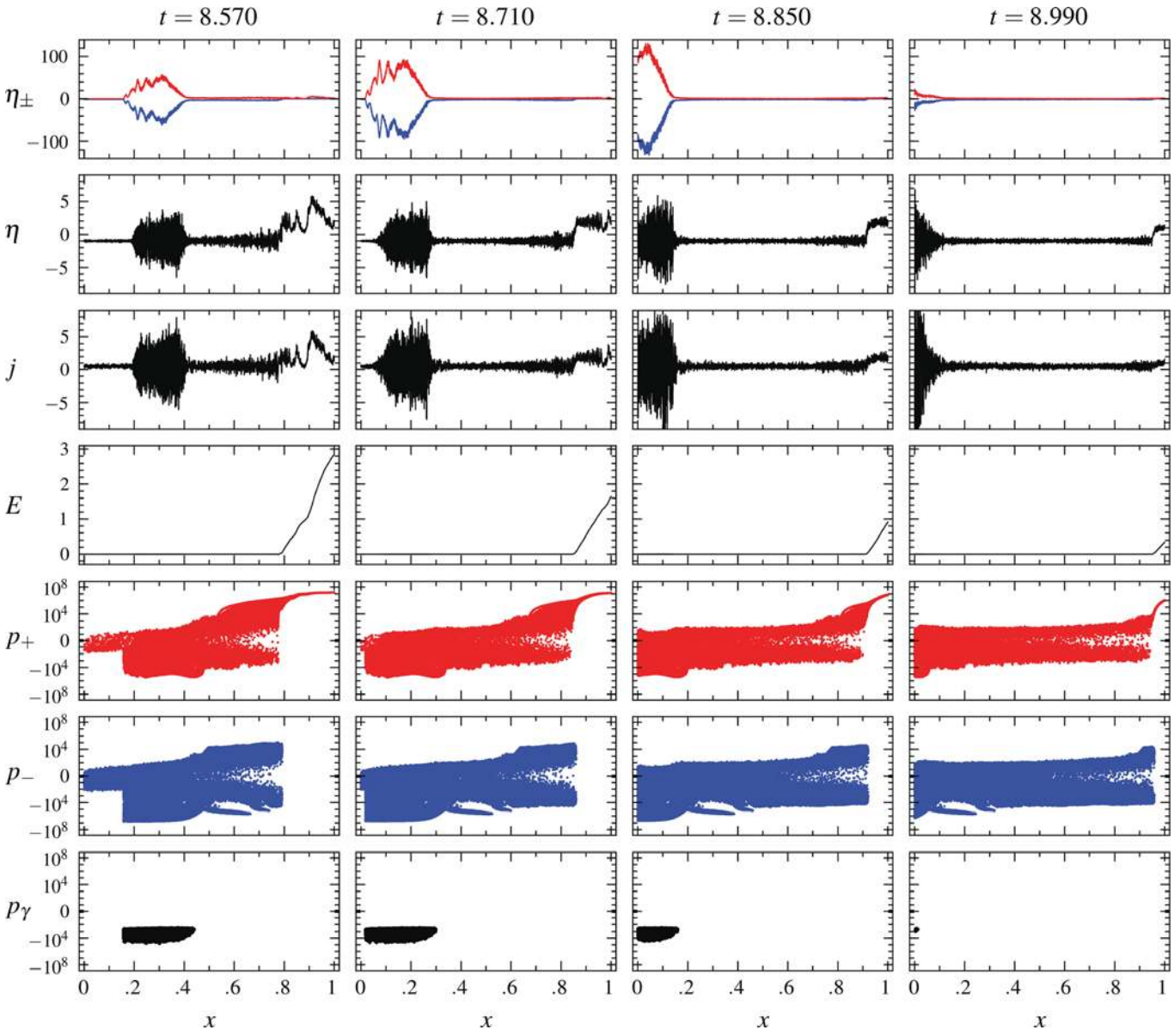

Figure 13. Filling of computation domain with dense pair plasma in anti-GJ flow with $j_m = -0.5 j_{GJ}$. The same quantities are plotted as in Fig. 11.

and 13, and $t = 6.560$–6.930, in Figs 15 and 16, one can clearly see how the dense pair plasma fills the domain with $x > 0.7L$. Filling of that domain with plasma is forced by a small electric field induced in the dense pair plasma by the imposed current. The rate at which these regions are filled with the dense plasma depends on the imposed current – in the case of $j_m = -0.5 j_{GJ}$ the average bulk motion of the pair plasma is about $0.5c$, while for $j_m = -1.5 j_{GJ}$ it is relativistic.

The accelerating electric field is very strong in the domain where pairs cannot be produced until electrons generated in the discharge arrive, and positrons (either primary or secondary ones) entering this domain before electron arrival are accelerated up to high energies. In our model pairs are created only by single photon absorption in a strong magnetic field, which automatically restricts pair formation to the polar cap region. However, electron–positron creation via γ–γ absorption can be possible at much higher distances from the polar cap, similar to the outer gap scenario (Cheng et al. 1986). In our model between the bursts of polar cap pair formation in the magnetospheric region above the low-altitude pair producing zone, at $x > x_B$, particles can be accelerated up to radiation-reaction limited energies and emit very high energy gamma-rays. In a more realistic model, when γ–γ absorption is taken into account, this should give rise to cascades in the outer magnetosphere resembling to some extent the outer gap scenario, except that the accelerating zone would not be limited to the region around the null surface, where the GJ charge density changes sign. Due to the intermittency of plasma flow in the return current region *both* polar cap and the outer gaps like cascades might exist along the same magnetic field lines. However, without higher dimensional simulations it is not clear how the interaction between two such cascade zones would play out.

Screening of the accelerating electric field during each burst of pair formation gives rise to a superluminal electrostatic wave. In Fig. 19 we show screening of the electric field in the gap for the

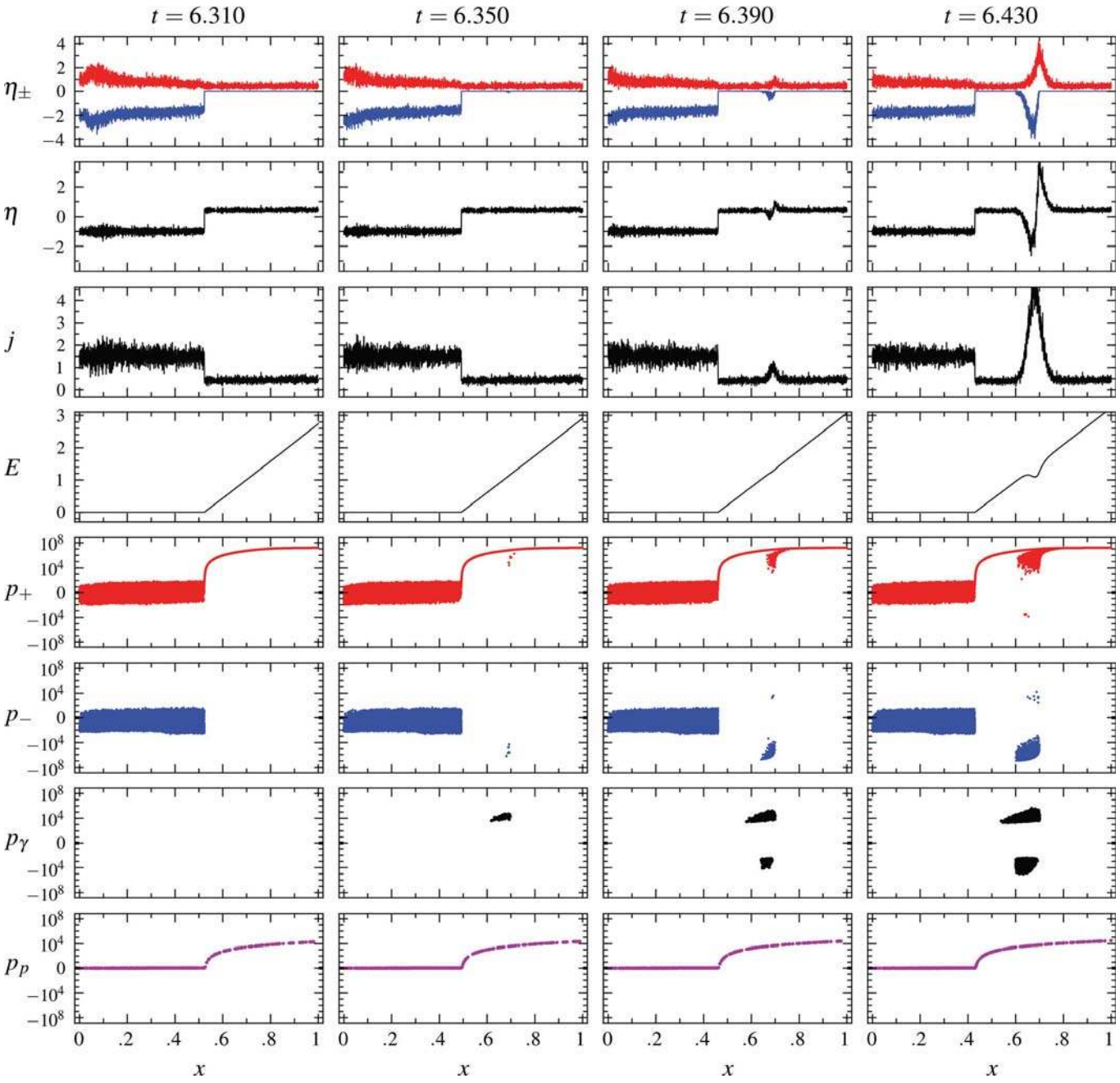

Figure 14. Ignition of pair formation in anti-GJ flow with $j_m = -1.5 j_{GJ}$. The same quantities are plotted as in Fig. 11 with the addition of the phase space portraits for protons in eighth row: (horizontal axis – proton position x, vertical axis – proton momentum p_p normalized to $m_p c$).

flow with $j_m = -0.5 j_{GJ}$, for flow with $j_m = -1.5 j_{GJ}$ the situation is very similar. Plots in Fig. 19 show in more detail than in Fig. 12 how the accelerating electric field is being screened by newly created pair plasma about $t = 8.350$. Screening of the electric field starts in the middle of the blob of newly created plasma and spreads to its edges. This spreading occurs in the form of an electrostatic wave the phase velocity of which is larger than c. This process is almost identical to what was observed for cascades described in Timokhin (2010) where more detailed discussion of the screening process can be found in section 4.2 [cf. our Fig. 19 with fig. 5 in Timokhin (2010)].

As in the simulations described in Timokhin (2010), second generation particle momentum distributions are very broad, extending towards non-relativistic energies. At least one of the reasons for momentum broadening of the particle spectra is trapping of particles in the strong electrostatic wave excited at the beginning of each burst of pair formation. The dynamics of these discharges are very similar to what is seen in simulations of the Ruderman & Sutherland cascade; more details on momentum spreading can be found in section 4.3 of Timokhin (2010). The appearance of the low energy component in the pair plasma is visible in the electron and positron phase portraits – initially at distances where pairs are injected, there are no particles in the phase space with low momenta, but later particles fill in the low momentum regions (see plots at $t \geq 8.350$ in Figs 12 and 13 and for $t \geq 6.500$ in Figs 15 and 16). In Figs 17 and

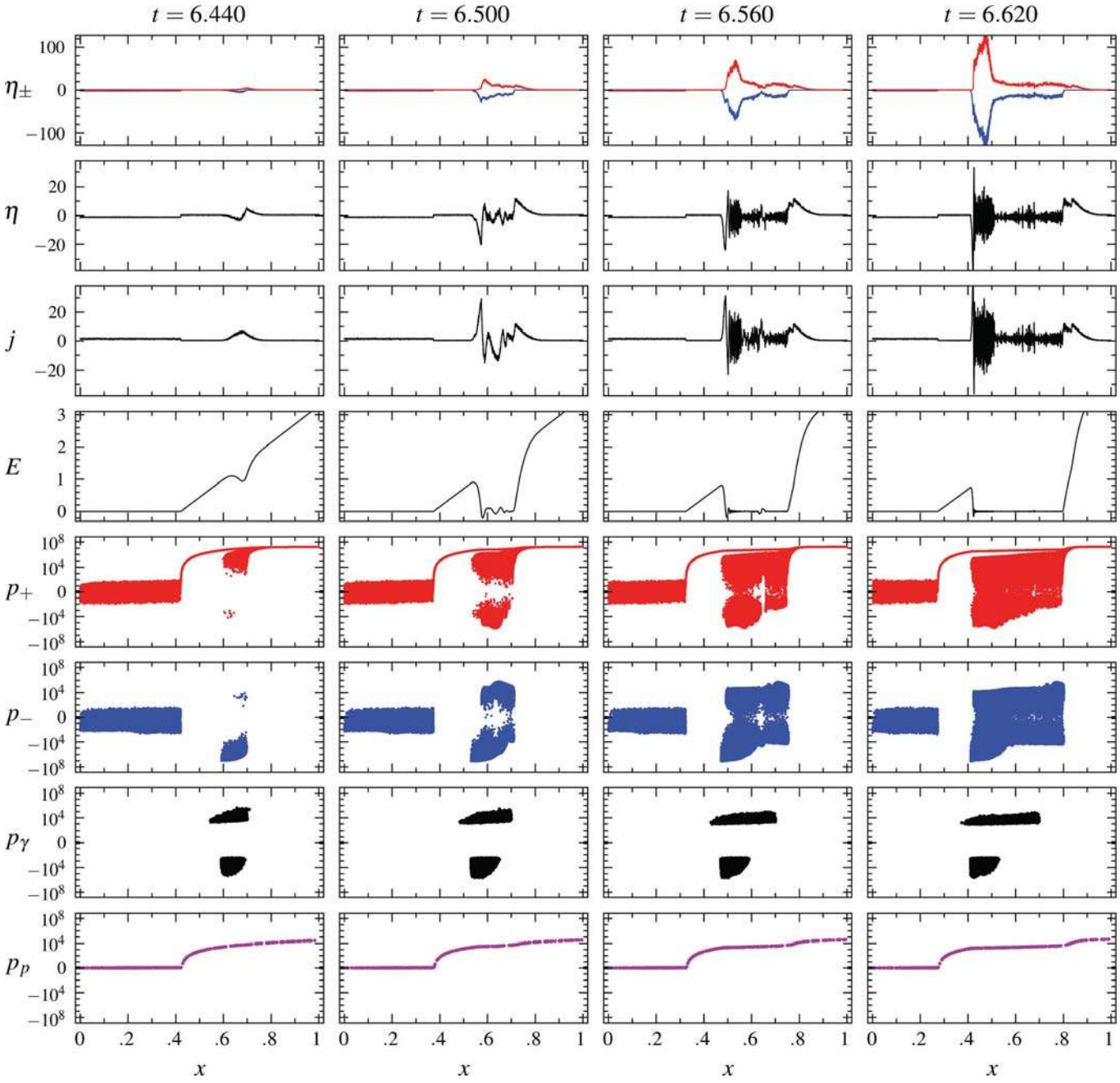

Figure 15. Screening of the electric field in anti-GJ flow with $j_{\rm m} = -1.5 j_{\rm GJ}$. The same quantities are plotted as in Fig. 14.

18 we plot the particle momentum distribution p ($\partial n/\partial p$) for three different moments of time. In the upper panel we plot the momentum distribution of particles moving towards the magnetosphere, p is positive; in the lower panel – the momentum distribution of particles moving towards the NS, p is negative. These distributions are averages for regions where the electric field at the magnetosphere end is screened. On these plots one can see that the low energy plasma component is present at all stages of cascade development.

There is a physical effect specific to cascades along field lines carrying return current – positive ions (in our model protons) can be pulled from the NS. Both electrons and protons can be extracted from the NS surface, and in our simulations we allow injection of both species. The imposed current density requires positively charged particles to move towards the magnetosphere, i.e. protons could be pulled from the NS. However, for less-than-GJ current densities ($|j_{\rm m}| < |j_{\rm GJ}|$) there are always electrons and positrons near the NS surface left from the previous burst of pair formation. The gap's accelerating electric field disappears before it reaches the NS, while pair plasma appears after every burst of pair formation keeping the electric field near NS screened. In our simulations of cascades with less-than-GJ current densities we did not see injection of protons. In the case of larger-than-GJ current density ($|j_{\rm m}| > |j_{\rm GJ}|$) protons are indeed pulled from the NS, at least at some stage of cascade development, and this cannot be attributed only to numerical effects. In this case we see some protons pulled from the NS at any time, even if pair plasma is present near the NS. The number density of

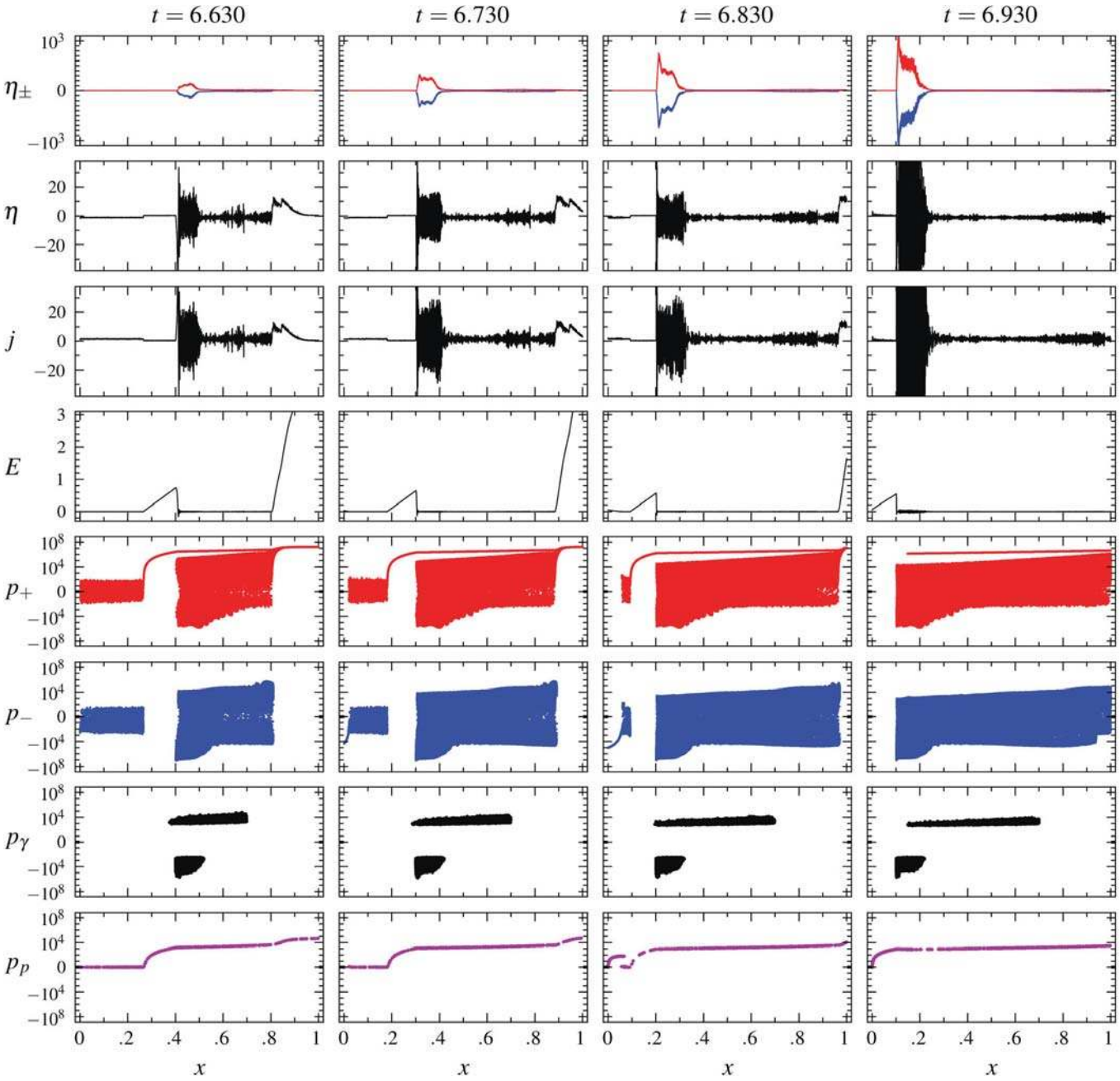

Figure 16. Filling of computation domain with dense pair plasma in anti-GJ flow with $j_m = -1.5 j_{GJ}$. The same quantities are plotted as in Fig. 14.

these protons never exceeds $\sim 0.2 n_{GJ}$, at least 10 times less than the number density of electrons and positrons; protons do not play a substantial role in the electrodynamics of discharges. The number density of protons pulled from the NS while electrons and positrons are still present near the NS surface depends on the numerical resolution and, hence, our simulations are inconclusive about whether this effect is real. However, there is a stage in cascade development when the region near the NS gets depleted of pair plasma; at those times proton extraction from the NS is certainly a real effect. The number of particles left from the previous burst of pair formation near the NS is not enough to support the imposed current density and screen the electric field until the new portion of the pair plasma arrives. A gap with the electric field appears at the NS surface – see snapshots at $t = 6.730, 6.830$ in Fig. 16. This gap is best visible on phase portraits of positrons as a second region (the one close to the NS) depleted of those particles. The electric field in the gap starts accelerating protons from the NS surface, as is clearly visible in phase space portrait for protons in Fig. 16. In our simulations this second gap does not become large enough to accelerate electrons to energies sufficient to start another burst of pair formation near the NS surface, but we cannot exclude this possibility in all cases. Finally, the main gap reaches the star and pulls out protons as well – see snapshot at $t = 6.930$ in Fig. 16.

6.2 Flow with $j_m/j_{GJ} > 1$

In this section we describe cascade development for the case when the imposed current density is super-GJ. As an example of such

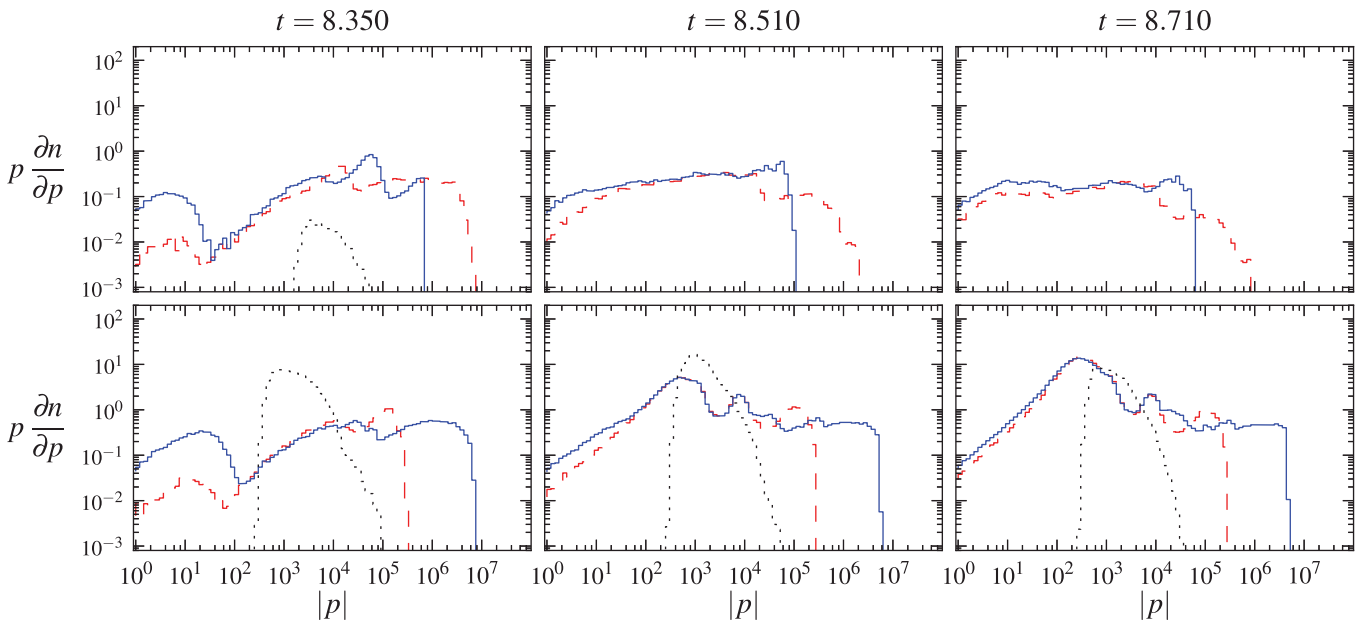

Figure 17. Momentum distributions of particles at three moments of time for cascade with anti-GJ current density $j_m = -0.5j_{GJ}$. Positron distributions are shown by solid blue lines, electron distributions by dashed red lines, distribution of pair producing photons by dotted black lines. Plots in the top row show distributions for particles moving towards the magnetosphere ($p > 0$) and plots in the bottom row show the distributions for particles moving towards the NS ($p < 0$). Each column corresponds to the same moment of time shown above the plots. Plots in each columns are aligned and share the same values of $|p|$. The following spacial regions were used for plotting the average distribution functions: $x \in [0, 0.7]$ for $t = 8.350$, $x \in [0, 0.75]$ for $t = 8.510$ and $x \in [0, 0.85]$ for $t = 8.710$.

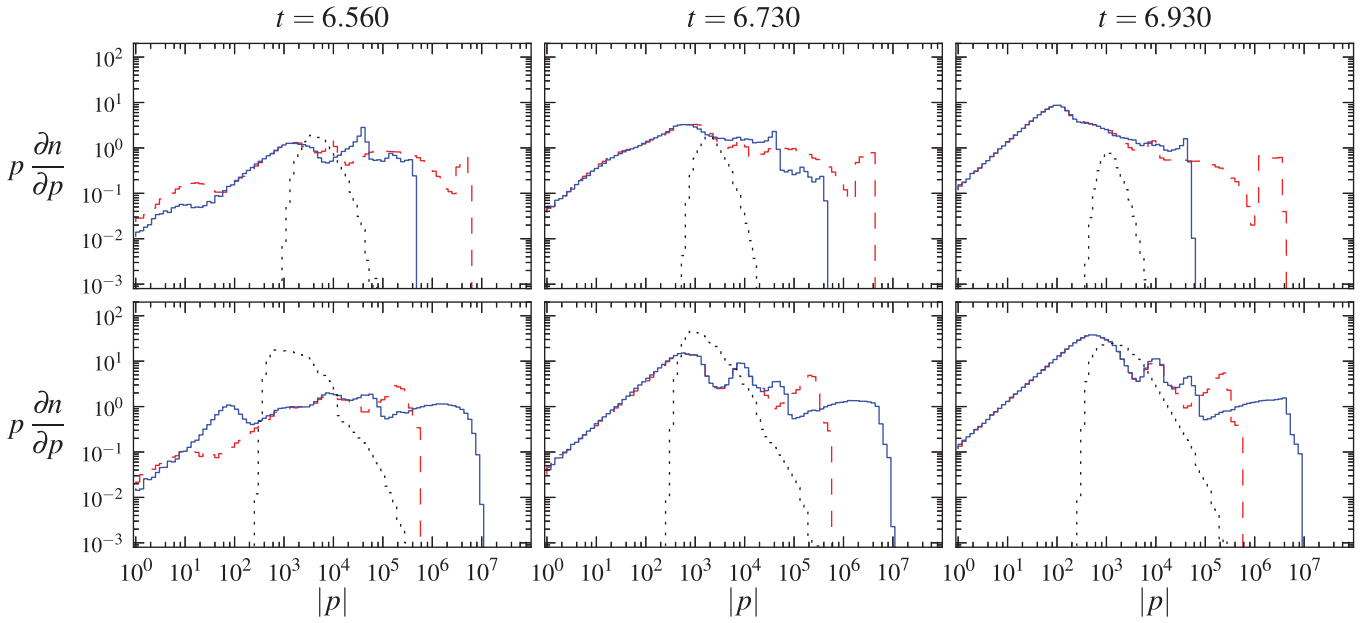

Figure 18. Momentum distributions of particles at three moments of time for cascade with anti-GJ current density $j_m = -1.5j_{GJ}$. Notations are the same as in Fig. 17. The following spacial regions were used for plotting the average distribution functions: $x \in [0, 0.75]$ for $t = 6.560$, $x \in [0, 0.88]$ for $t = 6.730$ and $x \in [0, 1]$ for $t = 6.930$.

flow we consider the case with $j_m = 1.5j_{GJ}$. To support this current density electrons must move up, towards the magnetosphere, and positrons down, towards the NS. There is a continuous source of electrons at the surface of the NS, $x = 0$. Positrons appear during the bursts of pair formation and there is no source of positrons during the quiet phase, between successive bursts of pair formation. To keep the electric field screened there *must* be both electrons and positrons present at each point – electrons with larger-than-GJ number density moving up and positrons moving down. Positrons compensate for the larger-than-GJ number density of electrons keeping the total charge density equal to the GJ charge density.

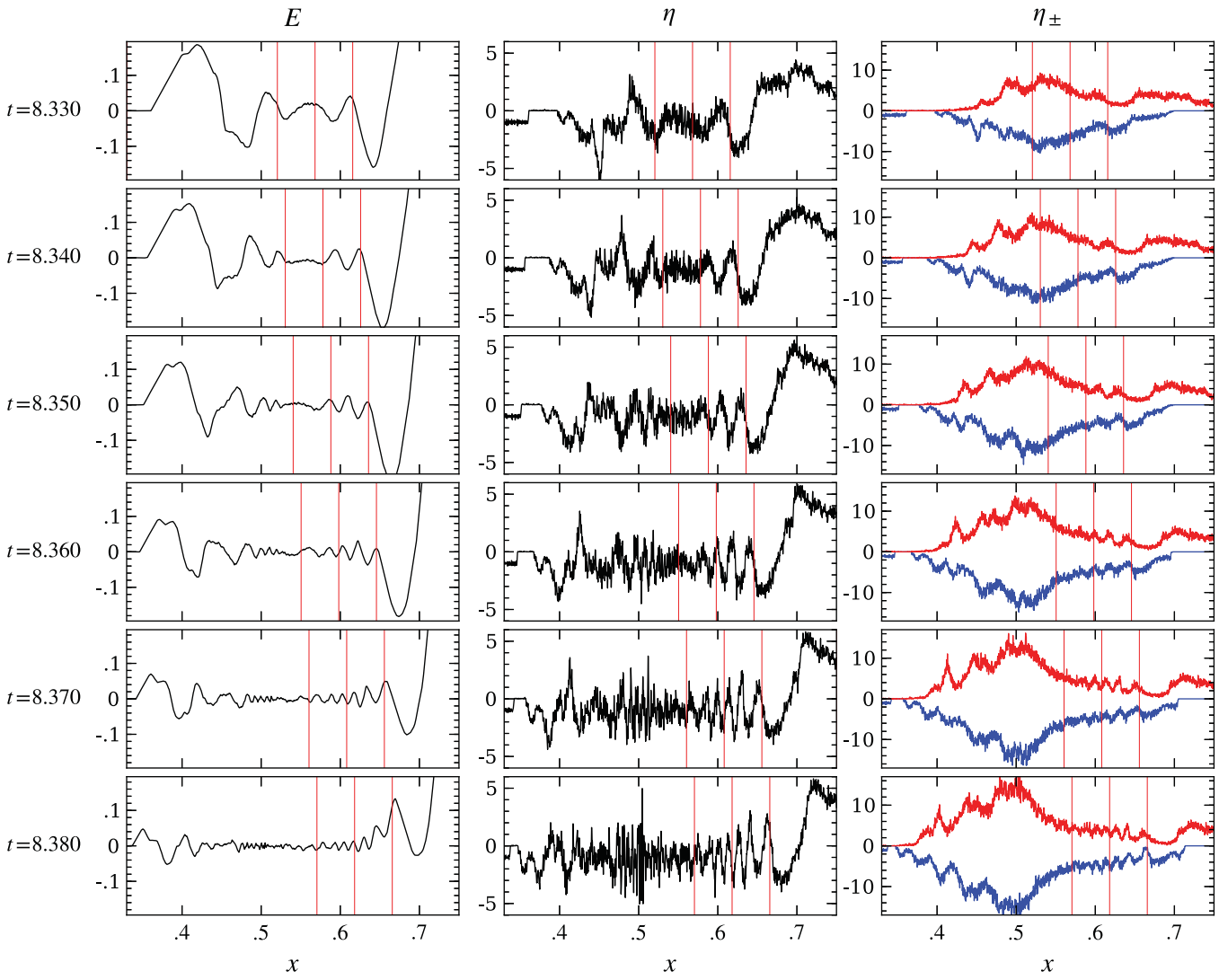

Figure 19. Screening of the electric field and formation of superluminal electrostatic wave for cascade with $j_{\rm m} = -0.5 j_{\rm GJ}$. There are six snapshots for the electric field E, the total change density η and the charge density of electrons (negative values, blue line) and positrons (positive values, red line) $\eta_{\pm}$. All quantities are plotted as functions of distance x for the part of the calculation domain with intense pair formation. Snapshots are taken at equally separated time intervals. Plots in each column are aligned and share the same values of x. The same normalizations for physical quantities are used as in Fig. 11. The three thin red vertical lines in each plot mark fiducial points moving with the speed of light towards the magnetosphere.

Positrons are leaving the domain and as there is no source of positrons, some time after the burst of pair formation the domain becomes depleted of positrons. This depletion starts at the upper end of the domain – at the 'magnetosphere' – as positrons are moving towards the NS. In the region depleted of positrons electrons produce current density $|j| < |j_{\rm m}|$ and the charge density $|\eta| > |\eta_{\rm GJ}|$, because their number density is set at regions closer to the NS where positrons are still present. This gives rise to the accelerating electric field which grows as the remaining positrons are moving towards the NS (see Fig. 20). For time shots at $t = 9.380$–9.500 on the plots for the charge density η and the current density j there are small jumps in both η and j at the point where the number density of positrons drops to zero. The electron number density remains the same, but positrons are leaving, enlarging the region depleted of positive charges.

As the gap grows, electrons are accelerated up to higher and higher energies and start emitting pair producing gamma-rays. In this case, electrons extracted from the NS surface, with the number density of the order of $|j_{\rm m}|/e$, are the particles which ignite the next burst of pair creation. As electrons are moving up (as do the first pair producing photons), the first pairs are produced at the farthest distance where pair formation starts to be possible, near $x = x_{\rm B} = 0.7L$ in our example. The injected pairs are picked up by the very strong electric field and are accelerated to high energies in less time than the primary electrons. Soon they start emitting pair producing capable gamma-rays which decay into pairs, see snapshots for $t \geq 9.420$ in Fig. 20. Electrons and positrons are moving in opposite directions; the pair plasma becomes polarized and starts screening the electric field, see plots for $\eta_{\pm}$, η and E at $t = 9.500, 9.520$ in Figs 20 and 21.

The screening of the electric field proceeds similarly to that in the case of anti-GJ flow with $j_{\rm m} = -1.5 j_{\rm GJ}$ described in Section 6.1. The electric field is being screened first near $x = x_{\rm B}$; this creates a finite size gap with accelerating electric field which moves towards the NS. The bulk motion of positrons left from the previous burst of pair formation is relativistic and the newly created pairs are

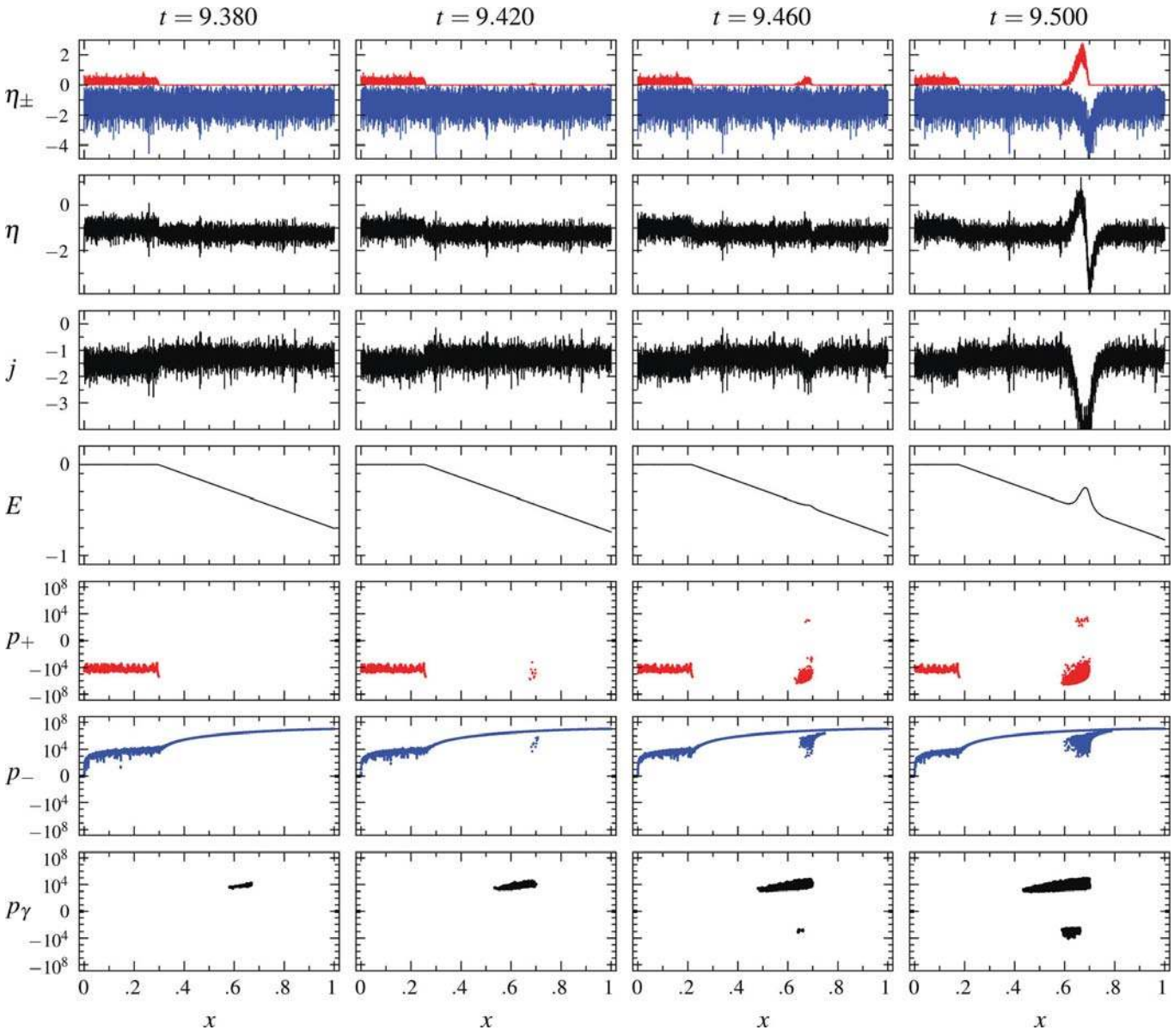

Figure 20. Ignition of pair formation in super-GJ flow with $j_m = 1.5j_{GJ}$. The same quantities are plotted as in Fig. 11.

relativistic too, so the boundaries of the regions where the electric field is screened are moving in the same direction (towards the NS) with the same speed. The region in between with a non-screened field – the gap – is therefore also moving, retaining its size. Electrons are continuously extracted from the NS to sustain the imposed current density. They enter the gap, are accelerated and emit pair producing gamma-rays. Pairs are produced by (i) primary electrons extracted from the NS surface accelerated by the moving gap and (ii) secondary positrons moving towards the NS accelerated in the initial screening event. The beam of primary electrons accelerated in the gap is clearly seen on plots for particle momentum distribution (Fig. 23) as a spike in the electron distribution function for positive values of p (the upper plots in Fig. 23). In contrast to the case with $j_m = -1.5j_{GJ}$, where the number of particles which were continuously accelerated in the gap was small and most of the pair were produced with momenta directed towards the NS, here more pairs are injected with momenta directed towards the magnetosphere – see Fig. 23 and plots for particle number density $\eta_\pm$ at $t > 9.640$ in Figs 21 and 22. As in the case of anti-GJ flow secondary particles have broad momentum spectra – the low energy plasma components are present at all stages of cascade development (Fig. 23).

The pair creation ends when the down flow component of the pairs reaches the stellar surface – the gap closes and the accelerating electric field is poisoned throughout the strong magnetic field region, while the beam component that emits the primary pair creating photons and its daughter pairs move up at the speed of light, into the magnetosphere, as can be seen in the e^+ and e^- phase portraits with advancing time in Figs 21 and 22. Positrons' bulk motion is towards the NS and some time after the plasma burst leaves – the wake of the departing burst being the source of positrons – the upper regions become deplete of positrons and the cycle starts again.

Both in the case of super-GJ flow with constant GJ charge density described here and in anti-GJ flow described in Section 6.1, the cascade starts at the upper boundary of the strong field region when the upper regions become depleted of positrons or electrons correspondingly, as the latter move down. The rate at which these

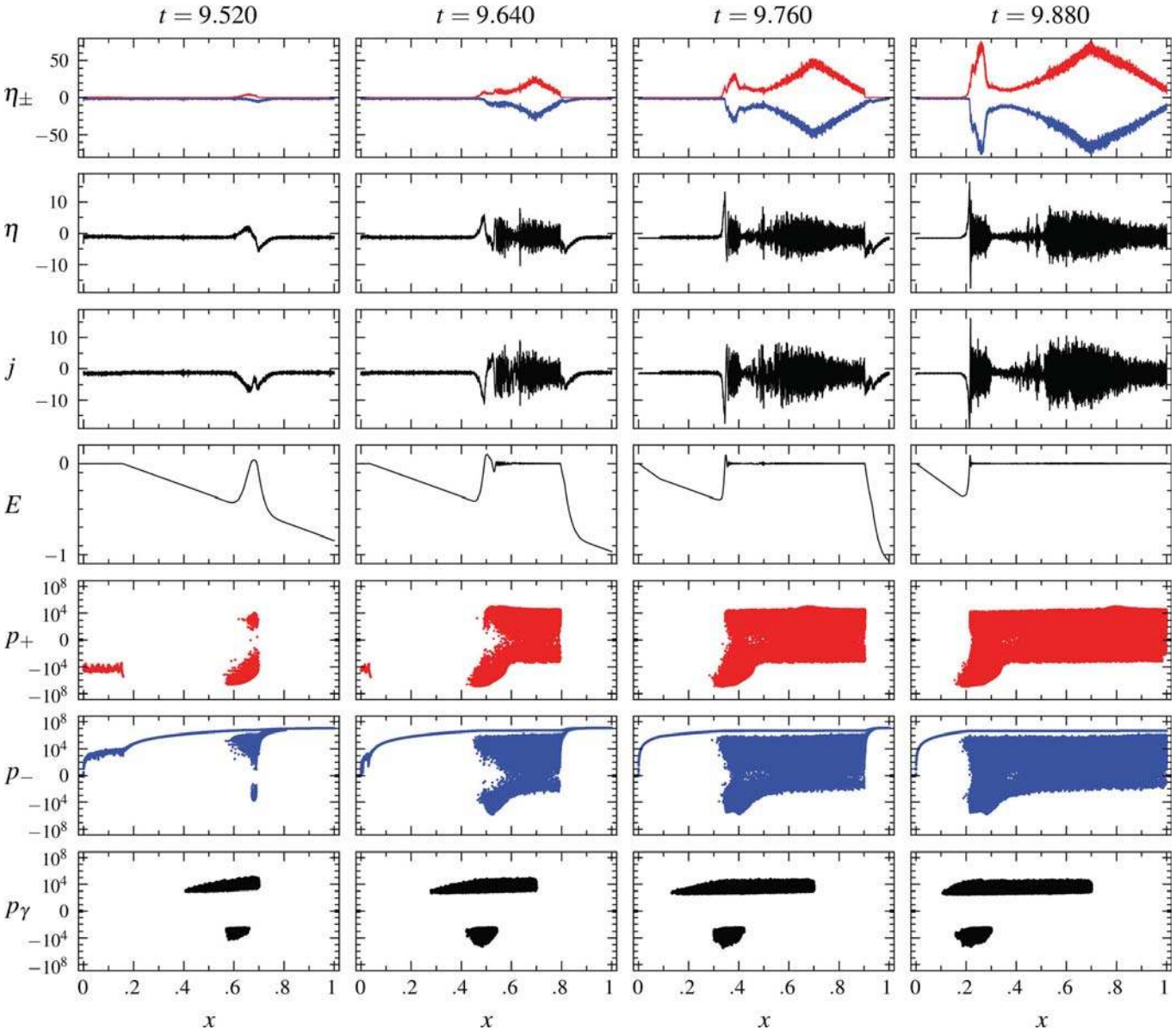

Figure 21. Screening of the electric field in super-GJ flow with $j_m = 1.5 j_{GJ}$. The same quantities are plotted as in Fig. 11.

regions become charge depleted depends on the imposed current density; the higher the absolute value of j_m the faster is the bulk motion of the charge component moving towards the NS. For $|j_m|$ comparable or larger than $|j_{GJ}|$ this bulk velocity is close to c. Thus the limit cycle period is larger than the relativistic fly-by time over the length of the strong field region. In our simulations, that region has size $0.7L = 168$ m, with fly by time 0.56 μs. However, in a real pulsar, the optical depth for pair creation by curvature photons emitted by the beam exceeds unity all the way out to heights comparable to the stellar radius. Then the fly-by and recurrence times might be as long ∼30 μs, with the intermittent plasma starved regions taking the form of long filaments. Assessing these structures and accounting for competition between neighbouring filamentary gaps are intrinsically 2D issues, and will be treated elsewhere.

Because the cascade starts far from the NS, at the largest distance where pair formation becomes possible, in our simulations the accelerating electric field is unscreened between bursts of pair formation above the pair formation zone. In this regard in the case of constant GJ charge density super-GJ flow is similar to the anti-GJ flow. Namely another cascade zone in the outer magnetosphere might coexist with the polar cap accelerating zone. However, as we will show in the next section variation of the GJ charge density with the distance can significantly change the behaviour of cascades in the super-GJ flow.

6.3 Effects of spatially varying Goldreich–Julian charge density

In this section we address the effect of the mismatch between the charge density of the space charge limited beam component and the local GJ charge density on the cascade development. In the widely adopted steady flow model of polar cap cascades (Arons & Scharlemann 1979; Muslimov & Tsygan 1992) this mismatch is the reason for the appearance of the accelerating electric field.

We performed simulations with different scaling of the GJ charge density, both in shape (linear, power law, exponential,

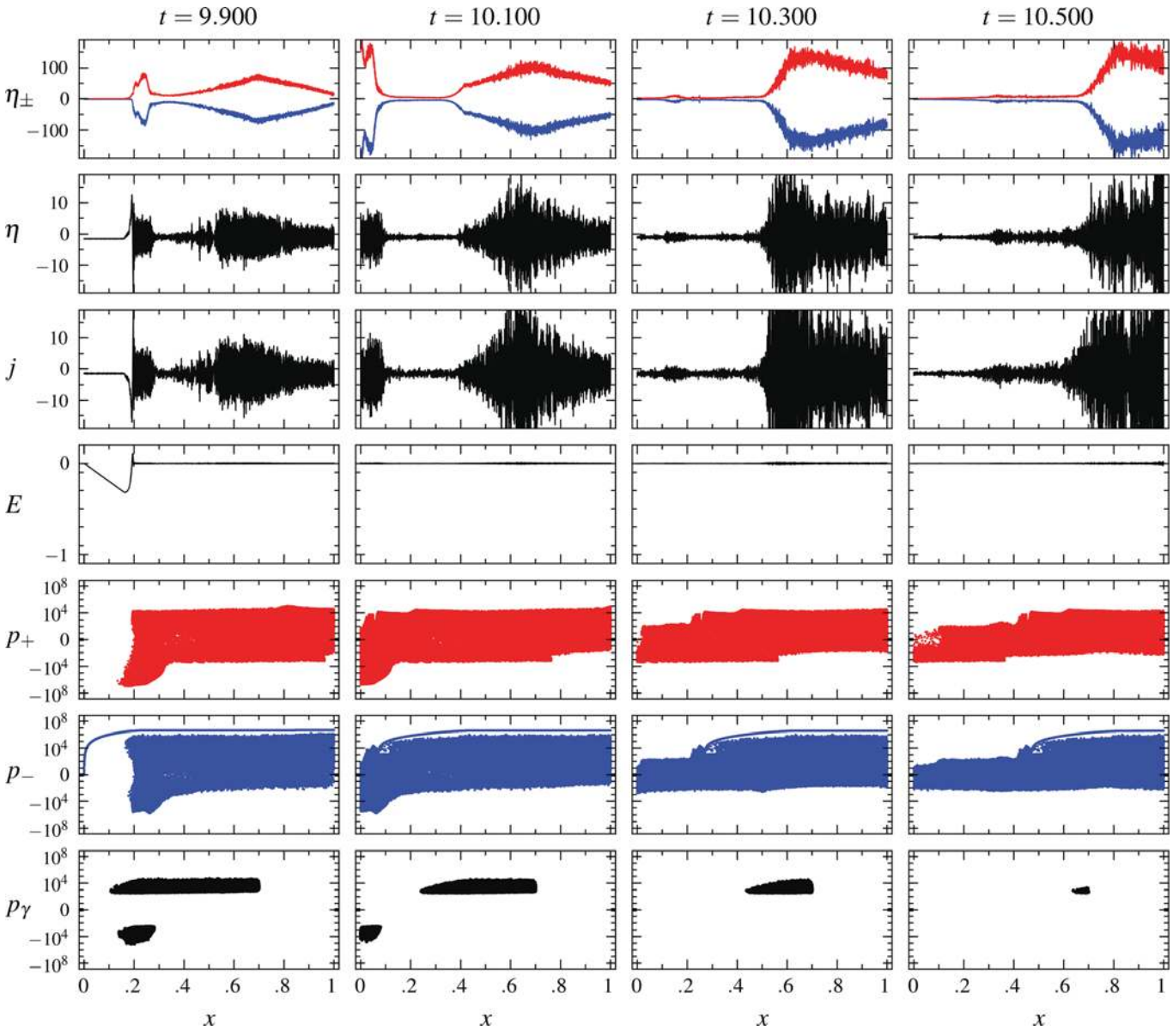

Figure 22. Filling of computation domain with dense pair plasma in super-GJ flow with $j_m = 1.5 j_{GJ}$. The same quantities are plotted as in Fig. 11.

decreasing/increasing with the distance) and in amplitude for all the cases considered in the previous sections. For the space charge limited flow with $0 < j_m/j_{GJ} < 1$ and $j_m/j_{GJ} < 0$ we found no qualitative difference in cascade behaviour due to variation of the GJ charge density. Namely, for anti-GJ flows, $j_m/j_{GJ} < 0$, the regions far from the NS became charge-depleted first and the cascade started at the largest distance where pair formation is possible, with the acceleration zone propagating towards the NS. Sub-GJ flows, with $0 < j_m/j_{GJ} < 1$, – if the imposed current density was less than the *local* value of the GJ current density $\eta_{GJ}(x)\, c$ everywhere – remained low energetic and had two components: a moderately relativistic beam propagating through a cloud of trapped particles. The main properties of space charge limited flow for these cases described in Sections 5 and 6.1 are not affected by variations of the GJ charge density with the distance.

The flow with super-GJ current density $j_m/j_{GJ} > 1$, however, can be strongly affected by variations of the GJ charge density – we observed different flow behaviour when the absolute value of the η_{GJ}/B increased with the distance from the NS. In that case the gap can appear close to the NS surface, in contrast to all other cases when it appeared at large distances. If such gaps can generate pairs, the regions above such gaps, far from the NS, remain filled with dense pair plasma at all times.

Below we describe in detail an example of such flow using simulations with exaggerated charge density contrast in order to clearly demonstrate the above mentioned effects. We assume that the GJ charge density changes with the distance x as

$$\eta(x) = \eta^0_{GJ}\left[1 + a\left(\frac{x}{L}\right)\right], \tag{16}$$

where η^0_{GJ} is the GJ charge density at the surface of the NS and a is a positive number.

Very close to the surface ($x \ll R_*$) all the sources of inhomogeneity of η_{GJ}/B can be approximated in this manner. For example, if variations of the GJ charge density are because of the field line curvature (Arons & Scharlemann 1979) the parameter a in equation

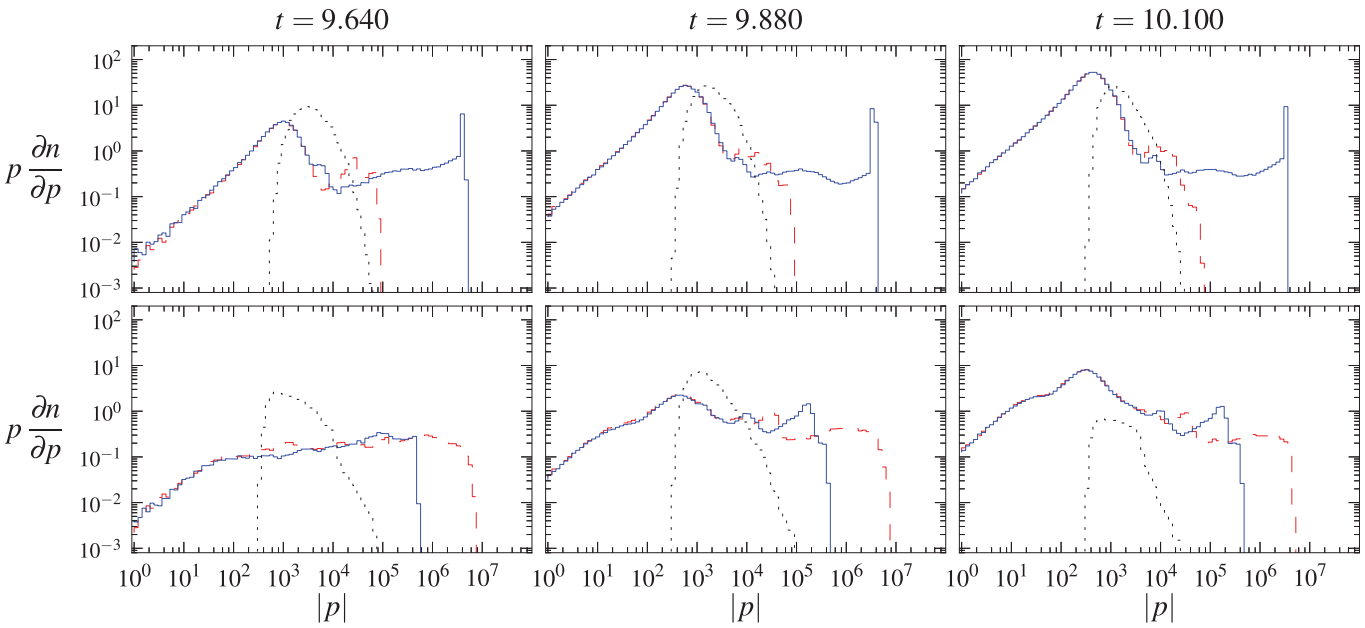

Figure 23. Momentum distributions of particles at three moments of time for cascade with super-GJ current density $j_m = 1.5 j_{GJ}$. Notations are the same as in Fig. 17. The following spatial regions were used for plotting the average distribution functions: $x \in [0, 0.795]$ for $t = 9.640$, $x \in [0, 1]$ for $t = 9.880$ and $x \in [0, 1]$ for $t = 10.100$.

(16) for the dipolar magnetic field would be given by the following expression

$$a_{AS} \approx -\frac{3}{4}\,\frac{\theta_* \cos\phi_* \sin\chi}{\cos\chi - (3/2)\,\theta_* \cos\phi_* \sin\chi}\,\frac{L}{R_*}\,, \qquad (17)$$

where θ_* and ϕ_* are colatitude and azimuth of the field line at the NS surface [cf. equation (12) in Arons & Scharlemann (1979)]. Note that for favourably curved magnetic field lines $\cos\phi_* < 0$ and so $a_{AS} > 0$. If GJ charge density variations are due to inertial frame dragging (Muslimov & Tsygan 1992) then

$$a_{MT} \approx 3\kappa_g \cos\chi\,\frac{L}{R_*}\,, \qquad (18)$$

$\kappa_g \equiv 2GI/R_*^3c^2 \sim 0.15$ and $I =$ NS's moment of inertia [cf. equation (32) in Muslimov & Tsygan (1992)].

Physical parameters of our simulations are chosen in such a way that the length of the accelerating gap is smaller than that of x_B. This setup differs from those described in Sections 6.1 and 6.2 in that the vacuum potential drop over the domain is larger – $\Delta V = 9 \times 10^{14}$ V.[8] The parameter in expression (16) for the GJ charge density is $a = 0.7$, so that the GJ charge density varies linearly from $-|\eta^0_{GJ}|$ to $-1.7|\eta^0_{GJ}|$ throughout the domain.[9] The imposed current density is $j_m = 2j^0_{GJ} \equiv 2\eta^0_{GJ}c$, so that everywhere in the domain the imposed current density is larger than the local value of the GJ current density, $j_m > \eta_{GJ}(x)\,c$. As the variation of the GJ charge density with the distance (after accounting for decrease in B; see the second paragraph of Section 6) is not larger than 15 per cent (Hibschman & Arons 2001), our setup can be considered as a toy model for cascades in young pulsars with $j_m > 1.15 j^0_{GJ}$. All other parameters of the model are the same as those of the models in Sections 6.1 and 6.2.

[8] See Footnote 5.

[9] This amount of variation is huge compared to what actually occurs – for example, if the variation is due to inertial frame dragging, for realistic parameters $a \sim 0.01$, if $L \sim r_{pc}$.

In contrast to all other cases considered in previous sections the dense pair plasma is always present at large distances from the NS – the intermittent temporal gaps separating periods when the domain is full of plasma disappear. So, we illustrate our example with two series of snapshots in Figs 24 and 25.

When the whole domain is filled with pair plasma the current density is constant, $j = j_m$. The number density of electrons is larger than $|\eta_{GJ}|/e$ and positrons (which are left from the previous burst of pair formation) are necessary to keep the charge density equal to the local value of the GJ charge density. The absolute value of the GJ charge density is smaller closer to the NS surface, η_{GJ} is negative and more positrons are necessary to screen the electric field there than at larger altitudes. Positrons, on average, move towards the NS, and, as they slam on the NS surface and leave the domain, positrons from higher altitudes should come closer to the NS in order to keep the electric field screened. At some altitude the required flux of positrons towards the NS becomes larger than the positron flux that can be extracted from an adjacent higher altitude region without making that region charge starved – the resulting charge starvation causes a starvation electric field to appear close to the NS (see snapshot at $t = 9.528$ in Fig. 24, the gap is best visible in the phase portraits on electrons and positrons). In the region above the gap, there are still enough positrons to screen the electric field – less positrons are needed here as the absolute value of the GJ charge density is higher there and so the mismatch in charge density $|j_m/c - \eta(x)|$ is smaller. At lower altitudes, after all positrons which had been there at an earlier time, before the gap appeared, leave the domain, the influx of positrons from above is unable to keep the electric field screened and so the gap extends up to the NS surface (snapshot at $t = 9.636$ in Fig. 24).

The upper end of the gap extends towards higher altitudes as positrons move towards the NS, depleting higher altitude regions of positive charge. While the gap develops, until the ignition of the new cascade, the current density remains close to the imposed current density – electrons are being extracted from the NS surface and provide the required current density (see plots for j in Fig. 24).

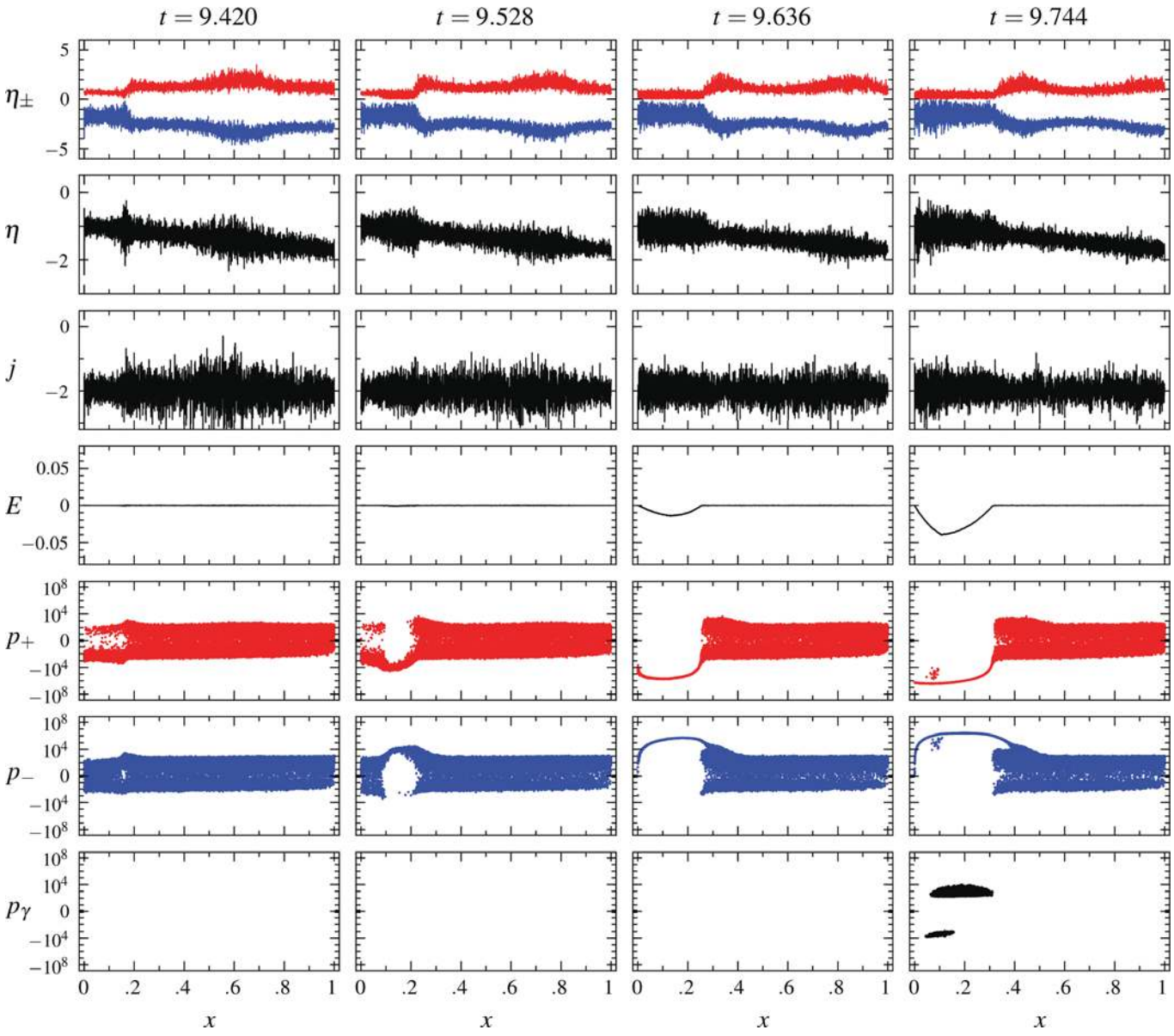

Figure 24. Ignition of pair formation in the flow with linearly varying GJ charge density and the imposed current density $j_m = 2j_{GJ}$. The same quantities are plotted as in Fig. 11.

The current density in the domain is super-GJ, $j > GJ_j$, and as there are too few positrons in the gap the charge density there becomes super-GJ, $|\eta| > |\eta_{GJ}|$; this gives rise to a strong accelerating electric field in the gap (see the plot for E at $t = 9.636$ in Fig. 24). Both electrons extracted from the NS surface and positrons flowing from higher altitudes are being accelerated in the gap and as the gap widens their maximum energies get higher and they become the primary particles igniting the new discharge cycle (snapshot at $t = 9.744$ in Fig. 24).

Filling of the gap with pair plasma proceeds quickly, as the pairs are injected throughout the whole length of the gap (time shots at $t = 9.780$ and 9.816 in Fig. 25). This happens because both electrons and positrons, moving in opposite directions, are emitting pair creation capable photons, and their number densities are comparable. The gap is filled with plasma before the particles created in the previous burst of pair formation leave the higher altitude region, and so, in contrast to the cases described in Sections 6.1 and 6.2 the higher altitude regions are always filled with dense pair plasma.

Screening of the accelerating electric field during each burst of pair formation proceeds slightly differently than in cases described in the previous sections. Particles are injected throughout the whole length of the gap and not at the gap's one end. Simulations shown in Fig. 25 have two 'centres' within the gap where screening starts. In Fig. 26 we show in more detail than in Fig. 25 how the accelerating electric field is being screened by newly created pair plasma about the time $t = 9.816$. Fluctuations of charge and particle number densities are significantly less pronounced than those in Fig. 19 because the accelerating field was due to mismatch of the charge density $|j_m/c - \eta| < |GJ\eta|$. The region of the screened electric field spreads from two centres towards the edges of the gap. In Fig. 26 we show spreading of the second zone with the centre around $x \simeq 0.2$; the first 'centre' was at $x \simeq 0.1$ where the screening started earlier and the electric field is now almost completely shorted out. This spreading occurs again in the form of an electrostatic wave phase velocity of which is larger than c and amplitude decreases with time.

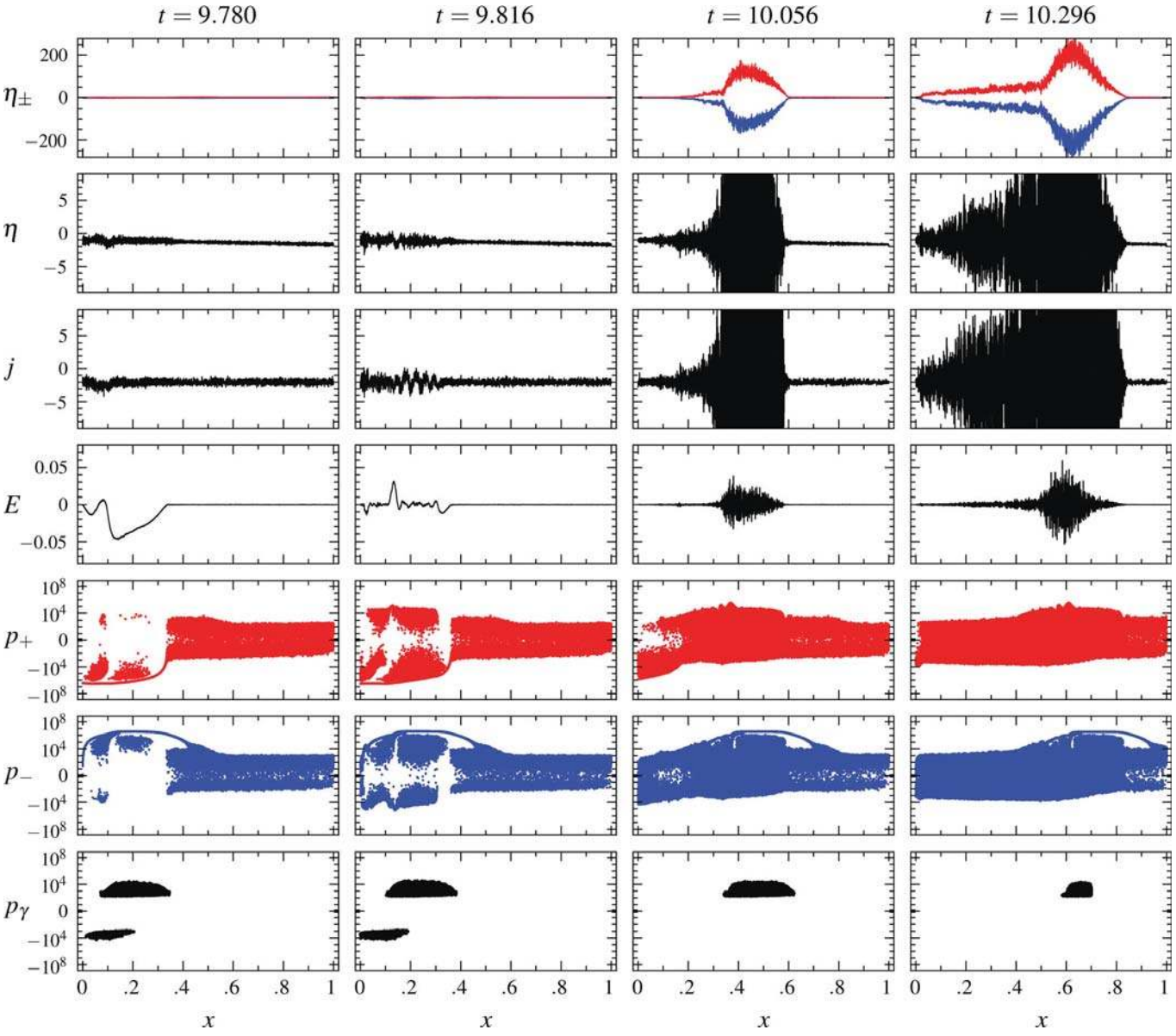

Figure 25. Screening of the electric field and final stages of pair formation in the flow with linearly varying GJ charge density and the imposed current density $j_m = 2j_{GJ}$. The same quantities are plotted as in Fig. 11. Note that the time interval between the first two snapshots is smaller than those between the rest of the plots.

The position where the gap appears depends on the imposed current density and on the variation of the GJ charge density – for higher j_m and/or stronger variation of $|\mathrm{GJ}\eta|$ the gap starts developing closer to the NS. The accelerating electric field in this gap is smaller than that in case with the constant GJ charge density from Section 6.2 because the number density of positrons is high and so not the whole charge density j_m/c is contributing to the electric field. If this electric field is not enough to produce pairs, then the gap grows up to high altitude until most positrons leave the domain; then a vacuum-like gap, with the charge density of the order of j_m/c, starts developing at the outer end of the domain as in the case of constant GJ charge density from Section 6.2.

The reason why variation of GJ charge density does not affect space charge limited flow with sub-GJ current density is the presence of the trapped particle 'cloud' component which can adjust to any charge density variation (assuming the current density remains sub-GJ), as was mentioned in Section 5. For flow with anti-GJ current density the accelerating electric field appears in the region depleted of electrons, which on average move towards the NS. In this case regions closer to the NS always have the larger number density of particles of the same sign as η_{GJ} and will become charge starved last, and so the gap develops at higher altitudes. For flows with the super-GJ current density when the absolute value of the GJ charge density *decreases* with altitude, $a < 0$, fewer positrons are necessary at lower altitudes to poison the electric field than at higher altitudes. Positrons are moving towards the NS and the low-altitude region becomes charge starved after all the others and the gap develops at higher altitudes as in the case of the flow with a constant GJ charge density.

Therefore, the regions with super-GJ flow can have two qualitatively different behaviours depending on the value of the imposed current density and the variation of the GJ charge density. The cascade either starts close to the NS and high altitude regions are always filled with dense pair plasma, or the cascade starts at high altitude

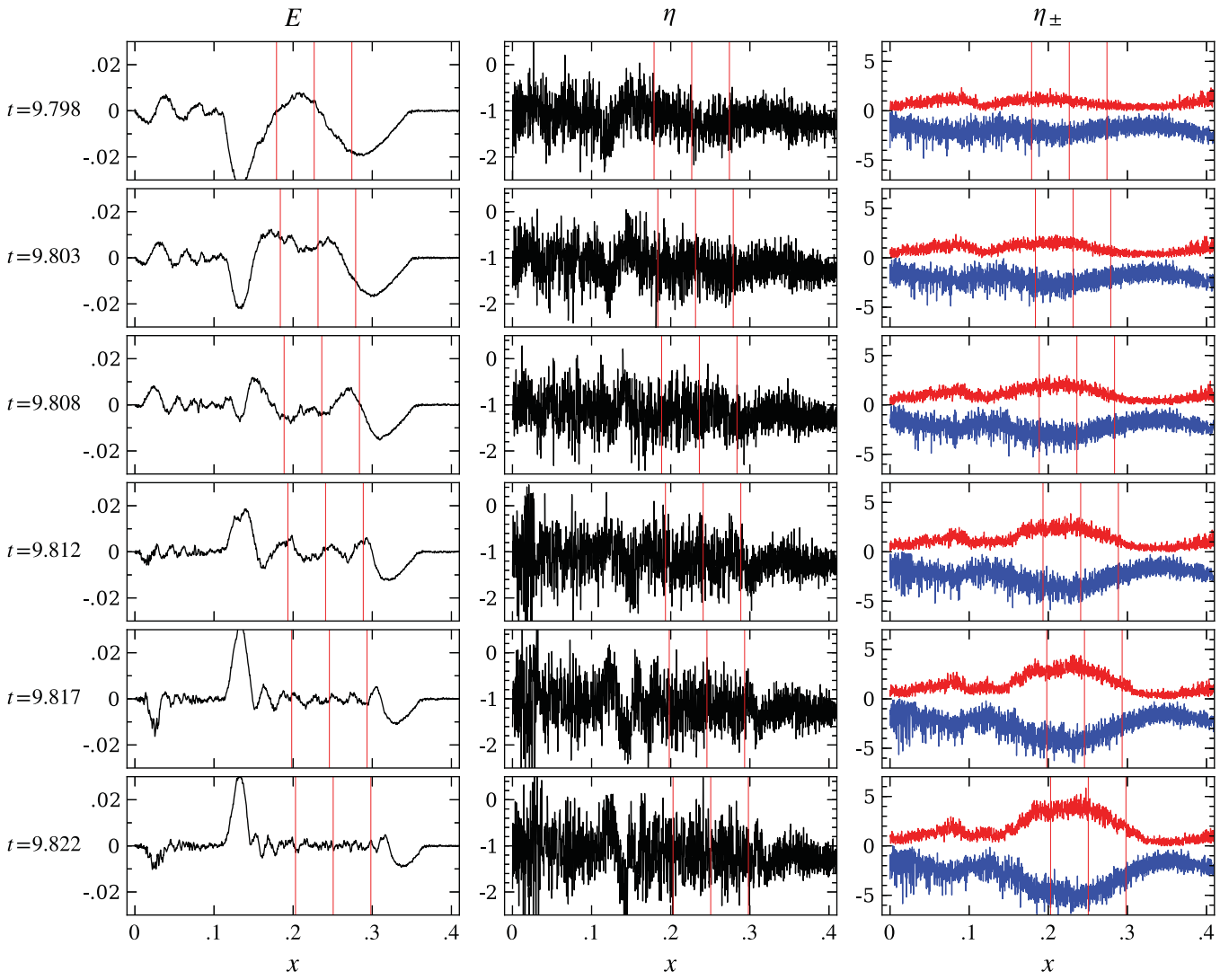

Figure 26. Screening of the electric field and the formation of superluminal electrostatic wave in the flow with linearly varying GJ charge density and the imposed current density $j_{\rm m} = 2j_{\rm GJ}$. The same quantities are plotted as in Fig. 19.

and between the bursts of pair formation the high altitude regions are charge starved with vacuum-like accelerating electric field – in the second case an additional cascade zone might appear in the outer magnetosphere. In the first case the period between successive bursts of pair formation should be of the order the gap's fly-by time and can be as short as $\sim r_{\rm pc}/c \sim$ fractions of microseconds; in the second case the repetition rate will be larger than the fly-by time of the strong field zone, $\sim R_*/c \sim$ tens of microseconds. From our toy model we cannot make quantitative prediction about the values of the imposed current density and magnitudes of the GJ charge density variations which separate those behaviours.

6.4 On stationary cascades

In all models previously considered in the literature, the size of the accelerating gap was limited by the opacity of the magnetosphere to the gamma-rays: pairs were injected when the optical depth to pair creation reached unity and those pairs screened the electric field. In our simulations with the constant GJ charge density, the electric field in the gap monotonically increases with distance, and the gap grows with time. That electric field could be screened only by the injection of particles with the charge sign opposite to the charge sign of primary particles, and those particles, when injected, were accelerated in the direction opposite to the direction of motion of the primary particles by a strong electric field. They start emitting pair producing gamma-rays after travelling a short distance, injecting pairs and so screening the electric field in their way. That led to the motion of the gap as a whole or to the gap closure, if the other end of the gap moved with subrelativistic velocity.

In the case of a flow with varying GJ charge density, described in Section 6.3, the initial field was not a monotonic function of the distance, but the gap was growing and, again, the only way to limit the gap and screen the electric field was by the injection of particles of the opposite sign. Once injected those particles ultimately destroyed the gap, since their flux exceeded that of the primary beam – stationary equilibria with counter streaming particles of the opposite sign exist only when the counter streaming flux is less than the primary flux, as in the Arons & Scharlemann (1979) model. Stationary particle acceleration and pair creation would be possible if pairs are injected (mostly) outside the gap, so that there will not be too many particles with charge sign opposite to that of primary particles within the gap.

For example, the stationary flow model of Arons & Scharlemann (1979) constructs a finite length acceleration zone bounded by the stellar surface below and the abrupt onset of pair creation above, which screens the electric field in a thin layer [the pair formation front (PFF)]. The space charge limited (electron) beam extracted from the surface provides the primary particles that radiate pair creating gamma-rays. Almost all of the pair creation occurs above the PFF. A small amount of trapping within the transitional PFF layer sends charges of sign opposite to the primary beam (positrons) back down towards the surface with flux small in comparison to that of the primary beam, while extra electrons are added to the beam, restoring the charge density to equality with the Goldreich–Julian density. This restoration causes the screening ('poisoning') of the accelerating field. In that model, $E \to 0$ at the PFF is imposed as a boundary condition, using the conclusion that dense pairs ($n_\pm \gg |\eta_{\rm GJ}/e|$) flash into existence at a rather well-defined height – a physically correct conclusion when curvature radiation dominates the gamma-ray emission and one photon absorption in the magnetic field is the major opacity source, since each primary beam particle emits many pair creating gamma-rays and opacity is a rapidly varying exponential function of the photon energy. The application of that boundary condition, along with the space charge limited flow condition at the NS, has the consequence that the charge density of the beam has a unique value $\eta_{\rm beam}$. Since $j = c\eta_{\rm beam}$, this model becomes discrepant with the magnetospheric current density $j_{\rm m}$, in general.

We tried to find an Arons–Scharlemann like solution with the acceleration gap limited by the PFF. For the linearly varying GJ charge density given by equation (16) and model parameters from Section 6.3 we explored the parameter space by running different simulations for different values of the imposed current density starting from $j_{\rm m} = 2j^0_{\rm GJ}$ and decreasing it up to $j_{\rm m} \simeq j^0_{\rm GJ}$ when pair production ceased. In each subsequent simulation with smaller $j_{\rm m}$ the position of the first pair injection moved further from the NS because the accelerating electric field was also smaller. In all cases when pair injection occurred inside the gap the gap boundary starts moving – we never saw a stationary PFF (nor did we see a stationary PFF in any other simulations). So, the conclusion implied by the simulations is that the time asymptotic state is not a steady flow similar to Arons & Scharlemann's. Even though acceleration in the charge starved gaps is limited by pair creation with thin boundaries between pairs and quasi-vacuum, reminiscent of Arons & Scharlemann's PFFs, the gaps move, either up into the magnetosphere or down towards the star – there is no truly stationary state, and fully developed limit cycles appear to be the answer, at least in one dimension.

We now exhibit a novel steady flow model, which takes advantage of the properties of non-neutral beam flow when $\eta_{\rm GJ}/B$ is non-uniform, that does not require poisoning by the pairs to produce $E = 0$ at the gap's top. This model exploits the variation of the charge density with distance, in the case when the current density is larger than the local GJ current density only up to some height h_s, then at distances larger than h_s – where the non-neutral flow becomes sub-GJ – the electric field will be screened on the scale of the local Debye length, as discussed in Section 5. In such a situation the accelerating electric field exists only up to the distance h_s, above which it is shorted out by a mixture of trapped electrons – those with two turning points in their orbits – and free pairs.

We assume the GJ charge density varies linearly with the distance, equation (16), as discussed in Section 6.3. By hypothesis, the flow is steady and the current density is equal to the imposed current density $j_{\rm m} = \xi j^0_{\rm GJ}$, $\xi > 1$ (see equation 12). If $\xi - 1 < a$, at some point the non-neutral beam flow becomes sub-GJ. From the Poisson equation for the electric field (6), in the absence of pairs we have

$$E_s = 4\pi\eta^0_{\rm GJ} L \left[(\xi - 1)\,\frac{x}{L} - \frac{a}{2}\left(\frac{x}{L}\right)^2\right]. \tag{19}$$

At the distance

$$h_s = 2\frac{\xi - 1}{a}L, \tag{20}$$

E_s changes sign as the flow becomes sub-GJ. Identifying h_s with the gap height yields the gap's potential drop to be

$$\Delta V_{s,\,\rm gap} = \frac{8}{3}\pi\eta^0_{\rm GJ} L^2 \frac{(\xi - 1)^3}{a^2}, \tag{21}$$

increasing in proportion to the imposed current density. If the resulting potential drop in the gap is large enough for particles to inject pairs within the gap with a number large enough to form a positron back flux larger than the primary electron flux, the flow will be non-stationary, like that described in Section 6.3. But if the potential drop is such that copious pairs will be injected at distances larger than h_s, positrons will be subjected only to a fluctuating, relatively small electric field, which sustain the cloud component at altitudes higher than h_s, where the flow is sub-GJ. Only a fraction of the positrons will be advected into the gap, and, if this fraction will be much smaller than the GJ charge density the flow in the gap will be not disturbed enough to make it non-stationary.

As an example of a flow with $E(h_s) = 0$ in the non-neutral current flow, pair creation *and* non-neutral trapping, we show snapshots in Fig. 27 of the flow with the same parameters as in Section 6.3, except with a carefully chosen current density which was set large enough to allow pair formation within the domain (at $x < x_{\rm B}$), but small enough so that the particle back flux does not destroy the gap. The imposed current density in this model is $j_{\rm m} = 1.059\,j^0_{\rm GJ}$. Above the altitude $x = h_s \approx 0.17L$ the flow is sub-GJ and clearly has beam-cloud structure qualitatively similar to that in sub-GJ flows from Section 5 (see phase portraits for electrons). The charged cloud of trapped electrons screens the electric field at $x > h_s$. Primary electrons, when accelerated up to high energies, emit gamma-rays which decay into electron–positron pairs *above* the gap.

Both secondary electrons and positrons mix with the cloud component and some positrons are advected towards the gap. The gap shrinks a bit and the resulting potential becomes smaller than a critical value necessary to sustain pair production. When the number density of positrons drops, the gap gets bigger and the pair formation starts again. The gap, however, never disappears and the cascade is close to a stationary configuration. This configuration is quite sensitive to the imposed current density; large gap fluctuations appear at imposed current densities only a few per cent larger than $j_{\rm m} = 1.059\,j^0_{\rm GJ}$. Our model, however, has an exaggerated charge density gradient and a very high voltage, and we expect that the mixing of positrons and their advection for real pulsar parameters would be less efficient and, hence, there might be a larger parameter range (i.e. an interval of the imposed current densities) where this gap plasma flow can sustain quasi-stationary cascades.

Such stationary configurations require the imposed current density to be larger that the local GJ current density at the NS surface but then becoming less than the local GJ current density at some distance from the NS. Variations of the GJ charge density (after accounting for the decreasing magnetic field) would not be larger than $\simeq$15 per cent (Muslimov & Tsygan 1992; Hibschman & Arons 2001) and, hence, the imposed current densities for stationary cascades are within the range $|j_{\rm m} - j^0_{\rm GJ}| \lesssim 0.15$, $j_{\rm m}/j_{\rm GJ} > 1$. Taking

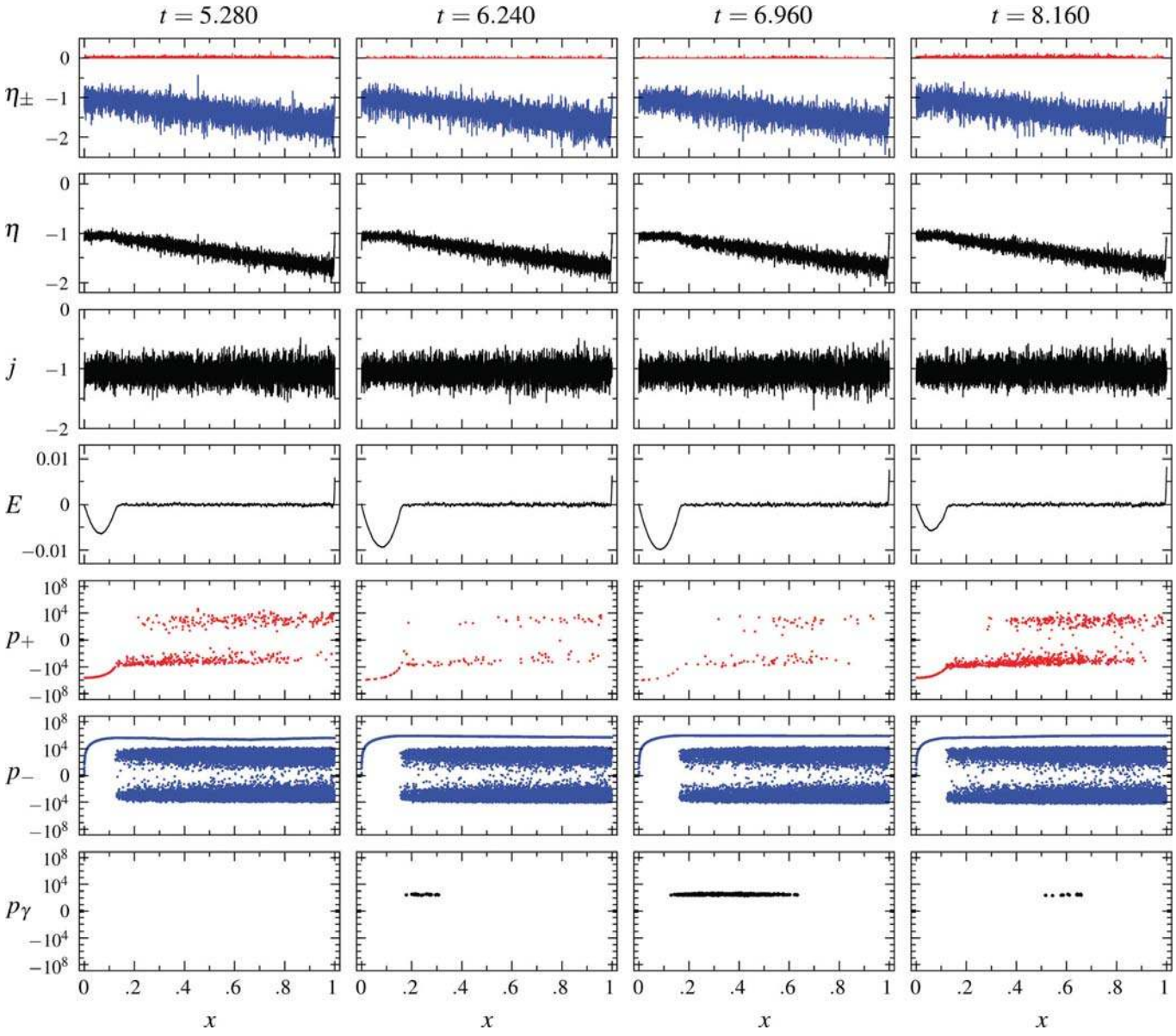

Figure 27. Plasma flow with quasi-stationary cascade. The imposed current density is $j_m = 1.059 j_{GJ}$; it is 'fine-tuned' in such way that the accelerating electric gap near the NS surface does not disappear. All other physical parameters are the same as in the case shown in Figs 20 and 21. The same quantities are plotted as in Fig. 11. Note that the time intervals between snapshots are not equal.

into account that the resulting gap should not be very large to prevent pair injection within the gap, that range is even smaller.

Fig. 1 makes clear that in the force-free theory, the current density does not mostly fall in this narrow range, lending support to the conclusion that limit cycle and trapping behaviour are the generic physics for polar flow, with and without pairs.

7 DISCUSSION

These calculations, and those reported in Timokhin (2010), were designed to investigate the theoretical issue of how the pulsar magnetosphere with current flow determined by the magnetosphere's global dynamics couples to the NS through the polar cap beam acceleration and pair creation zone. This problem was investigated 30–40 years ago, primarily using the order of magnitude estimates and analytical, steady flow models of charge-separated beams; the accelerator was modelled as having voltage fixed by pair creation and geometry. That led to a determination of the charge density in the accelerator with the current then simply being charge density times the speed of light.[10] No effort was made to show that the current density estimated actually matched that required by the global structure – the models yielded currents with the correct order of magnitude, and in the absence of actual solutions for the global structure of the magnetosphere, that answer was regarded as good enough, although scepticism was expressed that operating the accelerator model as having fixed voltage could actually produce the correct answer (see Mestel 1999 and references therein). The calculations reported here show that indeed when the accelerator is

[10] In differing degrees, the charge density was made up of counter streaming relativistic beams, leading to current density lying between $\eta_{GJ}c$ and $2\eta_{GJ}c$.

operated with current fixed rather than voltage, the polar cap accelerator does work, and works in a fully time-dependent manner, as first conjectured by Goldreich & Julian (1969) and Sturrock (1971), but with behaviour different from previously published models.[11]

Our results show that when the acceleration and cascades are one dimensional, acceleration and pair creation exhibit limit cycle behaviour, with cycle time somewhat larger than the relativistic fly-by time over the length of the accelerator. When the 1D approximation is realistic (very young pulsars), the length of the accelerator is less than the polar cap diameter $r_{\rm pc} \approx 144P^{-1/2}$ m, suggesting quasi-periodicity in the acceleration and pair creation on time-scales $\gtrsim 10^{-6}P^{-1/2}$ s. As was suggested long ago, such variations, if reflected in the radio emission, might be the origin of the microstructure in the radio emission (Ruderman & Sutherland 1975). If limit cycle behaviour is robust with respect to multi-dimensional considerations, this dynamical behaviour might turn out to be a useful model for microstructure (in contrast to non-linear optical phenomena in the transfer of radio waves through the pair plasma, for example).

When charges are fully bound to the surface (solid surface with high binding energy and no atmosphere; Medin & Lai 2010), current flow always adjusts to the magnetospheric load through pair creation discharges, as was shown in Timokhin (2010). The lowest energy particles in the pair discharge exhibit transient trapping in the fluctuating electric field. Those reversals of particle momenta allow both current and charge densities to adjust to the presumed force-free conditions, for any value of the magnetospherically imposed current density.

At long periods/weak B, pair creation becomes impossible, the magnetosphere is a vacuum with no conduction current flow and spin down occurs through the generation of strong vacuum waves (Pacini 1967). Pulsars enter this regime by crossing the pair creation 'death valley', theoretically expected for magnetospheric voltages $\Phi_{\rm m} = \sqrt{W_{\rm R}/c} \approx 10^{13}\,(\dot{P}/10^{-15})^{1/2}P^{-3/2}$ V $\lesssim 10^{12} \equiv \Phi_{\rm death}$ V [a restatement of the death line based on curvature gamma-ray emission and one photon magnetic conversion estimated by Sturrock (1971)]. The fact that this death line describes the disappearance boundary of radio pulsars in the P, $\dot{P}$ diagram reasonably well (see e.g. fig. 15.1 in Arons 2009) provides a strong hint that low-altitude, polar cap pair creation with high-energy beam acceleration and one-photon magnetic conversion of the curvature γ-rays has something to do with the pulsar activity.

A warm, quasi-neutral atmosphere plasma atmosphere overlying the magnetized ocean and solid crust, with no restrictions on charged particle motion along B, is the likely surface state of most pulsars, either because of the residual heat of the NS or because of polar cap heating by precipitating particles from the magnetosphere (from local pair discharges or from the return current flow). The upper atmosphere can then freely supply charge, in a manner very similar to a space charge limited current flow from the cathode of a classical vacuum tube. Our simulation results on space charge limited flow with (and without) pair creation reveal a variety of noteworthy new features.

We have made the first determination of the polar accelerator's behaviour under conditions where the current density, not the voltage, is held fixed. We found that space charge limited flow is not always high-energy. Emission of pair creating gamma-rays does not occur on all polar field lines, even when $\Phi_{\rm m} > \Phi_{\rm death}$. The force-free model of the magnetosphere suggests the polar current flow includes sub-GJ flow regions with $0 < j/j_{\rm GJ} < 1$, where the low energy current flows (with the Lorentz factor $\gamma_{\rm beam} \lesssim 3$) with no (curvature) gamma-ray emission and no pair creation (inverse Compton gamma-ray emission and γ–γ conversion to pairs are both negligible), with adjustment of the current density and charge density to the force-free values through formation of a trapped particle, non-neutral hanging charge cloud. This kind of quasi-stationary flow occupies most of the polar flux tube for the aligned and almost aligned rotator, but progressively disappears as the obliquity increases. The force-free model also requires regions of distributed return current flow, $j/j_{\rm GJ} < 0$, and, as the obliquity increases, regions of super-GJ current flow, $j/j_{\rm GJ} > 1$, occupying most of the polar flux tube as the obliquity approaches 90°. Both the return current and super-GJ regimes exhibit unsteady, high-energy current flow (an unsteady beam), driving discharges copiously creating pairs whose character is similar to that encountered when the atmosphere is absent and the surface is a strongly bound solid. These regions, as projected on to the polar cap, are shown in Fig. 1. In the special case of $j_{\rm m}/j^0_{\rm GJ}$ being slightly larger than unity, the plasma flow can sustain quasi-stationary cascades, and a new class of such models was described in Section 6.4. But generally speaking, such stationary regimes represent a singular case, rarely if ever achievable by magnetospheres described by the force-free model.

The only previous quantitative study of time-dependent cascades in space charge limited flow is that of Levinson et al. (2005). They used a two-fluid model and concluded that chaotic pair formation takes place throughout the whole zone where pair formation is possible. Our simulations do not support their conclusions. Particle trapping plays a significant role in adjusting of the plasma flow to the required current density and, hence, the plasma cannot be adequately represented as two fluids (electrons and positrons) each with its own unidirectional velocity. These two-fluid representations introduced additional rigidity into the system and this, in our opinion, led to the formation of a strong chaotic electric field everywhere in the domain.

The most recent analytical treatment of the problem was presented in Beloborodov (2008). Our results support Beloborodov's (2008) general conjecture about the character of plasma flow in the force-free regime, that the sub-GJ flow is low-energetic and pair formation is possible only in super-GJ or anti-GJ current flow. The simulations differ from his qualitative picture of what would happen in several respects: (a) the low energy flow with trapped particles does not retain the spatial oscillations of the cold flow, replacing those by the two-component beam/cloud structure – the warm beam has non-oscillatory velocity, while the trapped particles, not included in his picture, are those with two turning points in their orbits; (b) bursts of pair cascades repeat after longer time than h/c, h being the gap height; and (c) in most cases the gap is not destroyed but moves as a whole, usually relativistically.

The discharges were given a novel treatment. After the seminal efforts of Ruderman & Sutherland (1975) but prior to our work, models universally incorporated their assumption that when pair creation is copious (many convertible gamma-rays per primary high-energy particle, as is the case in the curvature radiation cascades typical of young, high voltage pulsars), at and above the height where pairs start appearing, $E_\parallel$ drops to zero and stays that way at all greater altitudes. Arons & Scharlemann (1979) formalized this into the dynamics of a PFF, showing that when pair creation

[11] Following Shibata (1991), when the pulsar is not near 'death valley' in $P - \dot{P}$ space, the load inserted into the magnetospheric circuit by the pair creation discharges creates a small perturbation of the magnetospheric current $j_{\rm m}$, thus justifying our treatment of $j_{\rm m}$ as an external parameter in the description of the discharges.

is copious, the transition between a charged starved region where $E_\parallel \neq 0$ and the pair-dominated region where $E_\parallel$ can be set equal to zero is thin – that structure necessarily involves one sided particle trapping, under pulsar conditions, thus causing the formation of counter streaming components in the current flow. Our solutions exhibit this transition between the dense plasma and the quasi-vacuum regions outside. But, since $E_\parallel$ was obtained from a dynamical field equation, we nowhere assumed $E_\parallel$ had to be zero everywhere outside (above or below) a pair discharge. Instead, the pair creation itself creates the polarizable plasma that dynamically resets $E_\parallel$ to zero inside the discharge, while outside the electric field was allowed to float to whatever is dynamically required. The resulting models thus exhibit macroscopic intermittency – a pair discharge shorts out $E_\parallel$, and then as the cloud of pair plasma moves out into the magnetosphere or towards the surface, a gap reforms in which residual particles accelerate, radiate gamma-rays and form a new discharge. The fact that pair creation opacity declines with distance from the NS was modelled by setting the magnetic field equal to zero in the upper part (typically the upper 30 per cent) of the simulation domain. That *Ansatz* forces the one photon pair creation opacity to be zero in the upper part of the domain.

It must be said, however, that the resulting model of the intermittency is very simplified – probably oversimplified. The representation of the 'magnetosphere' as a region of negligible pair creation optical depth to gamma-rays emitted from just above the polar cap is the right general idea, but the 1D character of our simulations almost certainly leads to an overemphasis on the coherence of the intermittent discharges – they form coherent slabs of pair plasma, separated by coherent slabs of quasi-vacuum. In reality, the low opacity region where discharges must end appears at heights $\sim R_* \gg r_{\rm pc}$ = polar cap and polar flux tube transverse radius. Then, the acceleration zone left behind a discharge created plasma cloud is long and skinny, with the narrow 'wave-guide' geometry (and the physics of the polar flux tube's boundary) playing an essential role in the nature of the quasi-vacuum field. Under these circumstances, it is unclear and unknown whether the discharges would preserve anything like the coherence exhibited in the results reported here – the formation of multiple 'lightning bolts' is perhaps more likely, simultaneously coexisting within the polar flux tube, the electric fields of the discharges affecting the dynamics of their neighbours, causing the discharges to influence each other – a complex dynamical system quite likely to be chaotic.

In addition, the extent of the gaps formed between discharges requires consideration of all the sources of pair conversion opacity, not only one photon conversion in the B field. Even when magnetic conversion drops to zero, γ–γ conversion with gamma-rays colliding with soft photons from the atmosphere (either heated polar cap or overall warm surface, if the star is young enough) can provide discharge initiating pairs within quasi-vacuum gaps, limiting the extent of such gaps to less than what occurs when the opacity is set equal to zero. These issues require multi-dimensional modelling of the accelerator and the photon transfer, as well as extending the radiation transfer model, improvements required before the possible direct consequences of low-altitude discharges for observations can be addressed. Those consequences are the pair multiplicity of the outflow, the heating of the polar caps by the discharge components that move towards the NS, and the possible direct collective emission of photons by the time-dependent currents in the discharges.

The multiplicity ($\kappa_\pm \equiv n_{\rm pair}/n_{\rm GJ}$) within individual pair creation bursts show the traditional results – when a discharge occurs, $\kappa_\pm \approx \gamma_{\rm beam} m_\pm c^2/\varepsilon_{\rm curvature} \sim 10^3$ ($\varepsilon_{\rm curvature}$ = energy of pair producing curvature photons), somewhat enhanced by the conversion of the synchrotron photons in the cascade – thus, multiplicities within individual bursts up to $\sim 10^4$ are observed. Intermittency reduces the overall multiplicity of the outflow – the magnitude of this reduction is hard to judge without a multi-dimensional model. The intermittency reduction is offset by continued pair creation as the plasma clouds and their high energy leading edges drift out to heights of the order of the stellar radius and more, emphasizing again the need for a multi-dimensional treatment. However, the multiplicity is unlikely to be as high as is inferred from PWNe (Bucciantini et al. 2011), so long as the simple, star centred dipole B field model is retained. More general B fields, with smaller radii of curvature of photon orbits with respect to B, can lead to enhanced pair creating opacity and pair yield – the offset dipole model (Arons 1998; Harding & Muslimov 2011) is the most plausible magnetic anomaly model that can be consistent with the dipolar character of the polar flux tube revealed by radio observations (Rankin 1990; Kramer et al. 1998). Whether sufficiently large multiplicities can be obtained within the geometric constraints obtained from the radio polarimetry is under investigation.

Polar cap heating and consequent soft X-ray emission provide another possible observable that can constrain the model. In common with all discharge models, roughly half the energy in each discharge is deposited in the crust below the atmosphere and ocean. If intermittency is neglected, existing observations provide strong challenges to all polar cap discharge models, including ours. Intermittency reduces the average energy flux. Whether that effect allows this polar discharge model to survive confrontation with observations (or, better, prove useful in modelling such observations) remains to be studied. Simulating the particle back flux from a discharge is a particular challenge, requiring resolving the Debye length in the pairs, which rapidly decreases as the pair density grows.

Our results imply that discharges occur on some of the polar field lines for all inclinations. These discharges incorporate time-dependent, quasi-coherent currents on microsecond and shorter time-scales. It has not escaped our attention that such fluctuations might be a direct source of radio emission from the low-altitude polar flux tube, a region strongly suggested as the site of the radio emission by the radio astronomical phenomenology. Although the electric fields in our one-dimensional model are wholly electrostatic, therefore cannot leave the plasma, in a more general multi-dimensional setting which has substantial spatial inhomogeneity transverse to B, the field components parallel to B have accompanying components $E_\perp$ perpendicular to B which make the fluctuations fully electromagnetic. Therefore, these electrostatic spectra *may* be representative of electromagnetic fluctuations which can leave the plasma, and the pulsar. From the point of view of simulations, a multi-dimensional, electromagnetic treatment is required in order to investigate this possibility.[12]

In the frame of our model we can provide only estimates of the energy available for such directly excited waves. If the electrostatic oscillations could form an electromagnetic wave which leaves the plasma then the energy carried by the wave would be of the order of

$$W_{\rm r} \sim \frac{\langle E^2 \rangle}{8\pi}\, c\pi r_{\rm pc}^2 \,. \tag{22}$$

[12] Fawley (1978) used a linear response analysis to study this possibility in an analytic model of discharges when strong surface binding suppresses fee emission. The work described in this paper is the first to study fully nonlinear discharges in the free emission regime. Whether this idea for radio emission will lead to a useful model remains to be studied.

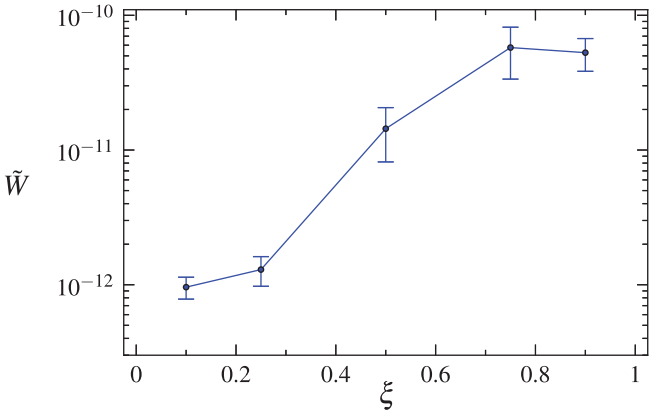

Figure 28. Estimated energy flux $\tilde{W}$ in plasma waves for sub-GJ flows as a function of $\xi = j_{\rm m}/j_{\rm GJ}$. $\tilde{W}$ is normalized to $W_{\rm md} B_{12}^{-1} P^2$.

Both kinds of flow, with or without pair formation, cause fluctuating electric field. Fluctuating electric field in the sub-GJ flow turns out to be too low to provide the energy even for the radio emission. The electric field for the sub-GJ flow shown in Fig. 8 is normalized to $E_0 = |\eta_{\rm GJ}|\pi\lambda_{\rm D,\,GJ}$; in this normalization the estimates for $W_{\rm r}$ is given by

$$W_{\rm r} \sim 4.8 \times 10^{-9}\,\langle\tilde{E}^2\rangle\, W_{\rm md} B_{12}^{-1} P^2\,, \tag{23}$$

where $\tilde{E}$ is the normalized electric field and $W_{\rm md}$ is magnetodipolar energy losses

$$W_{\rm md} = \frac{B_0^2 R_*^6 \Omega^4}{4c^3}\,. \tag{24}$$

In Fig. 28, we plot the estimated values of $\tilde{W}_{\rm r} = W_{\rm r}/B_{12}^{-1} P^2 W_{\rm md}$ as a function of $\xi = j_{\rm m}/j_{\rm GJ}$. It is evident that even for the Crab pulsar, known for its very low radio efficiency in terms of spin down energy losses $\sim 10^{-8}$, the energy in electrostatic oscillations of the cold flow cannot power the radio emission. For plasma flows with pair formation, screening of the electric field proceeds similarly to cascades in the Ruderman–Sutherland model studied in Timokhin (2010). We observed the formation of superluminal plasma waves during discharges in space charge limited flows, similar to what was found for strongly bound surfaces. The range of plasma oscillation wavelengths was rather broad, similar to what was observed in discharges discussed in Timokhin (2010). The electric field for plasma flows with pair formation discussed in Section 6 is normalized to $E_0 = |\eta_{\rm GJ}|\pi r_{\rm pc}$; in this normalization the estimates for $W_{\rm r}$ are given by

$$W_{\rm r} \sim \frac{1}{4}\langle\tilde{E}^2\rangle\, W_{\rm md}\,. \tag{25}$$

The amplitude of the (normalized) oscillating electric field during the screening phase of cascade development shown in Figs 19 and 26 is $\sim$0.1–0.01 and the energy in such oscillations is more than enough to power the radio emission. So, from the energetics point of view, it seems that the plasma flows with pair formation studied here are candidates for powering the pulsar radio emission through direct radiation by the discharge currents.

Finally, our work may have implications for the formation of the particle accelerators in the outer magnetosphere required to account for the gamma-ray pulsars. Low voltage, sub-GJ current flow may have a Holloway (1973) 'problem'; in that the non-neutral cloud and low energy, non-neutral current-carrying beam cannot cross the null surface where $\boldsymbol{\Omega}\cdot\boldsymbol{B} = 0$ – in contrast, field lines populated with dense plasma from discharges have no difficulty with plasma flowing across the null surface, the pair plasma clouds are quasi-neutral and easily adjust to the locally required charge density. Field lines passing from the low-altitude trapped cloud to the outer magnetosphere that go through the null surface might form a physically self-consistent gap reminiscent of the earliest proposals for 'outer gaps', with the potential for outer magnetosphere discharges that could provide a model for the observed gamma-ray emission. This issue also requires multi-dimensional modelling. The caustic formation exhibited by models for gamma-ray pulses suggests that if such gaps can form, they are localized (by pair creation?) to regions close to the flux bundles where return currents flow.

Another possibility for particle accelerators in the outer magnetosphere exists in the regions carrying the return current. At some time between the bursts of pair formation in the polar cap the electric field at large latitudes cannot be screened by pairs created in the polar cap. This field can accelerate particles and give rise to pair creation via γ–γ process. As we pointed out at the end of Section 6.1, an outer magnetosphere cascade zone might exist along the magnetic field lines carrying the return current. This might be a very intriguing possibility in view of the observational evidence that the spectrum of pulsar gamma-ray emission does not have a super-exponential cut-off, which should be present if there were absorption of gamma-rays in the magnetic field. Moreover, modelling of pulsar gamma-ray light curves suggests that the gamma-ray emission originates from the regions close to the boundary between the open and closed magnetic filed lines (e.g. Bai & Spitkovsky 2010). The return current regions for a broad range of pulsar inclination angles are close to that boundary or/and are within it, e.g. in Fig. 1 the return current is flowing in and around the current sheet for pulsar inclination angles $\alpha \lesssim 30^\circ$.

8 CONCLUSIONS

Our principal conclusion is simple – pair creation can occur at pulsar polar caps, but (almost) always in the form of fully time-dependent current flow (microsecond time-scales for the variability). That time dependence with pair creation allows the current to adjust to any magnetospheric load, while simultaneously allowing the charge density to adjust to the requirements of the force-free magnetosphere. We have also shown that a substantial fraction of the open field lines (fraction decreasing with increasing obliquity) solve the current flow problem with a low-energy, non-neutral beam carrying the current co-existing with a non-neutral, electrically trapped particle cloud. This is an essentially time-independent local solution. Exploring the consequences of these new results for global theory and observations requires extending the calculations to multi-dimensional, electromagnetic models for the accelerating electric field, and perhaps to background magnetic field models more general that the star centred dipole geometry (used here in the choice of the magnetic radius of curvature that enters into the pair conversion opacity).

ACKNOWLEDGMENTS

We wish to thank Xuening Bai for making the plot shown in our Fig. 1. This work was supported by NSF grant AST-0507813; NASA grants NNG06GJI08G, NNX09AU05G; and DOE grant DE-FC02-06ER41453. AT was also supported by an appointment to the NASA Postdoctoral program at NASA Goddard Space Flight centre, administered by ORAU.

REFERENCES

Abdo A. A. et al., 2010, ApJS, 187, 460
Akhiezer A. I., Polovin R., 1956, Zh. Eksp. Teor. Fiz., 30, 915
Aliu E. et al., 2011, Sci, 334, 69
Arons J., 1983, ApJ, 266, 215
Arons J., 1998, in Shibazaki N., ed., Neutron Stars and Pulsars: Thirty Years after the Discovery General Relativistic Polar Particle Acceleration and Pulsar Death, Proceedings of the International Conference on Neutron Stars and Pulsars held on November 17-20, 1997, at Tachikawa Hall, Rikkyo University, Tokyo, Japan. Universal Academy Press, Tokyo, p. 339
Arons J., 2009, in Becker W., ed., Pulsar Emission: Where to Go. Astrophysics and Space Science Library, Vol. 357. Springer, Berlin, p. 373
Arons J., Scharlemann E. T., 1979, ApJ, 231, 854
Bai X., Spitkovsky A., 2010, ApJ, 715, 1282
Beloborodov A. M., 2008, ApJ, 683, L41
Beskin V. S., 1990, Sov. Astron. Lett., 16, 286
Birdsall C., Langdon A., 1985, Plasma Physics via Computer Simulation. McGraw-Hill, New York
Bogdanov S., Rybicki G. B., Grindlay J. E., 2007, ApJ, 670, 668
Bucciantini N., Arons J., Amato E., 2011, MNRAS, 410, 381
Cheng K. S., Ho C., Ruderman M., 1986, ApJ, 300, 500
Contopoulos I., Kazanas D., Fendt C., 1999, ApJ, 511, 351
Erber T., 1966, Rev. Modern Phys., 38, 626
Fawley W. M., 1978, PhD thesis, AA (California Univ., Berkeley.)
Fawley W. M., Arons J., Scharlemann E. T., 1977, ApJ, 217, 227
Goldreich P., Julian W. H., 1969, ApJ, 157, 869
Harding A. K., Muslimov A. G., 2011, ApJ, 743, 181
Hibschman J. A., Arons J., 2001, ApJ, 554, 624
Holloway N. J., 1973, Nat, 246, 6
Kalapotharakos C., Contopoulos I., 2009, A&A, 496, 495
Kramer M., Xilouris K. M., Lorimer D. R., Doroshenko O., Jessner A., Wielebinski R., Wolszczan A., Camilo F., 1998, ApJ, 501, 270
Levinson A., Melrose D., Judge A., Luo Q., 2005, ApJ, 631, 456
Medin Z., Lai D., 2010, MNRAS, 406, 1379
Mestel L., 1999, Stellar Magnetism. International Series of Monographs on Physics, Vol. 99. Clarendon, Oxford
Mestel L., Robertson J. A., Wang Y.-M., Westfold K. C., 1985, MNRAS, 217, 443
Michel F. C., 1974, ApJ, 192, 713
Muslimov A. G., Tsygan A. I., 1992, MNRAS, 255, 61
Pacini F., 1967, Nat, 216, 567
Rankin J. M., 1990, ApJ, 352, 247
Ruderman M. A., Sutherland P. G., 1975, ApJ, 196, 51
Scharlemann E. T., Arons J., Fawley W. M., 1978, ApJ, 222, 297
Shibata S., 1991, ApJ, 378, 239
Shibata S., 1997, MNRAS, 287, 262
Spitkovsky A., 2006, ApJ, 648, L51
Spitkovsky A., Arons J., 2002, in Slane P. O., Gaensler B. M., eds, ASP Conf. Ser. Vol. 271. Neutron Stars in Supernova Remnants. Simulations of Pulsar Wind Formation. Astron. Soc. Pac., San Francisco, p. 81
Sturrock P. A., 1971, ApJ, 164, 529
Tademaru E., 1973, ApJ, 183, 625
Tajima T., Dawson J. M., 1979, Phys. Rev. Lett., 43, 267
Timokhin A. N., 2006, MNRAS, 368, 1055
Timokhin A. N., 2010, MNRAS, 408, 2092
Villasenor J., Buneman O., 1992, Comput. Phys. Commun., 69, 306

APPENDIX A: ONE-DIMENSIONAL ELECTRODYNAMICS OF THE POLAR CAP

Let us decompose the magnetic field in the acceleration zone into two terms $\boldsymbol{B} = \boldsymbol{B}_0 + \delta\boldsymbol{B}$, where $\boldsymbol{B}_0$ is the global time-averaged field (the 'external' field for our local problem; $= \boldsymbol{B}_{\rm magnetosphere}$) and $\delta\boldsymbol{B}$ is the fluctuating magnetic field due to local currents in the system caused by charge motion in the acceleration zone.

In our 1D approximation the characteristic size of the acceleration zone in longitudinal direction, along magnetic field lines, l is much smaller than its characteristic width w (the latter being of the order of $r_{\rm pc}$). The characteristic time-scale of electromagnetic field variations due to relativistic charge motion is $\tau \sim l/c$, as charges move along magnetic field lines. The characteristic scale of the global magnetic field variation in longitudinal direction $l_{\rm mag}$ is much larger than both l and w. The relation between these scales is $l \ll w \ll l_{\rm mag}$.

Electromagnetic field can be determined from Ampere's and Faraday's laws

$$\nabla \times \boldsymbol{B}_0 + \nabla \times \delta\boldsymbol{B} = \frac{4\pi}{c}\boldsymbol{j} + \frac{1}{c}\frac{\partial \boldsymbol{E}}{\partial t} \tag{A1}$$

$$\nabla \times \boldsymbol{E} = -\frac{1}{c}\frac{\partial\, \delta\boldsymbol{B}}{\partial t}\,. \tag{A2}$$

Combining Ampere's (A1) and Faraday's (A2) laws by eliminating the electric field we get an equation for the magnetic field $\delta\boldsymbol{B}$:

$$\frac{1}{c^2}\frac{\partial^2 \delta\boldsymbol{B}}{\partial t^2} - \nabla^2\delta\boldsymbol{B} = \frac{4\pi}{c}\nabla \times \boldsymbol{j} + \nabla^2\boldsymbol{B}_0\,. \tag{A3}$$

Only the perpendicular components of the magnetic field $\boldsymbol{B}_{0,\perp}$, $\delta\boldsymbol{B}_\perp$ affect the accelerating electric field $\boldsymbol{E}_\parallel$. Now using the perpendicular component of equation (A3) we estimate $\delta\boldsymbol{B}_\perp$.

The estimates of each of the terms in equation (A3) are as follows. For terms with $\delta\boldsymbol{B}_\perp$ we have

$$\left(\nabla^2\delta\boldsymbol{B}\right)_\perp \sim \frac{\delta B_\perp}{l^2} + \frac{\delta B_\perp}{w^2} \sim \frac{\delta B_\perp}{l^2} \tag{A4}$$

and

$$\left(\frac{1}{c^2}\frac{\partial^2 \delta\boldsymbol{B}}{\partial t^2}\right)_\perp \sim \frac{\delta B_\perp}{(c\tau)^2} \sim \frac{\delta B_\perp}{l^2}\,. \tag{A5}$$

The perpendicular component of the global magnetic field changes in the longitudinal direction on the scale $l_{\rm mag}$, in the lateral direction it changes on the scale w and, hence,

$$\left(\nabla^2\boldsymbol{B}_0\right)_\perp \sim \frac{B_{0,\perp}}{l_{\rm mag}^2} + \frac{B_{0,\perp}}{w^2} \sim \frac{B_{0,\perp}}{w^2}\,. \tag{A6}$$

Current flows along magnetic field lines and its perpendicular component is of the order of $(B_{0,\perp}/B_0)j \sim (l/\rho_c)j$, and as the radius of curvature of magnetic field lines ρ_c is much larger than any of the scales in our problem we have

$$(\nabla \times \boldsymbol{j})_\perp \sim \frac{j}{w} - \frac{j_\perp}{l} \sim \frac{j}{w} - \frac{l}{\rho_c}\frac{j}{l} \sim \frac{j}{w}\,. \tag{A7}$$

Combining estimates (A4)–(A7) from equation (A3) we have

$$\frac{\delta B_\perp}{w} \sim \left(\frac{l}{w}\right)^2\left(\frac{4\pi}{c}j + \frac{B_{0,\perp}}{w}\right)\,. \tag{A8}$$

The order-of-magnitude version of Ampere's law (A1) is

$$\frac{B_{0,\perp}}{w} + \frac{\delta B_\perp}{w} \sim \frac{4\pi}{c}j + \frac{E_\parallel}{c\tau}\,, \tag{A9}$$

and from equation (A8) it follows that the fluctuating magnetic field due to charge motion introduces only a second order term in l/w and it can be neglected. So, the Ampere law in one dimension has the form

$$\frac{\partial E_\parallel}{\partial t} = -4\pi\left(j - \frac{c}{4\pi}(\nabla \times \boldsymbol{B}_0)_\parallel\right) \equiv -4\pi(j - j_{\rm m})\,. \tag{A10}$$

The same expression for the accelerating electric field through the current density as in equation (A10) can be obtained from the Gauss

law and charge conservation [see e.g. Timokhin (2010), Appendix A]; in that case $j_{\rm m}$ emerges as an integration constant corresponding to the time-average current density flowing trough the system. In one dimension the system is essentially electrostatic; charges create only electric field, and naturally both Ampere's law and Gauss' law reduce to the same equation. The magnetic field perpendicular to the background stellar B field is negligible, both due to the background magnetospheric current and due to the rapidly variable currents within the acceleration zone considered in this study – in particular, to the lowest order in $(l/\rho_c)^2$, the particle orbits are determined by the stellar field B_0 and consideration of the full electromagnetism of the discharges is not required to characterize the discharge dynamics.

APPENDIX B: STATIONARY ONE-DIMENSIONAL SPACE CHARGE LIMITED FLOW

B1 General equations

Let us consider a stationary one-dimensional beam of equal particles with mass m and charge q having the same sign as the GJ charge density $\eta_{\rm GJ}$ flowing from the surface of the NS at $x = 0$ into the magnetosphere at $x > 0$. The current density of the beam is a fraction ξ of the GJ charge density,

$$j = \xi\, j_{\rm GJ}\,. \tag{B1}$$

For the energy of particles in the beam we have

$$mc^2\gamma + q\phi = mc^2\gamma_0 + q\phi_0\,, \tag{B2}$$

where $\gamma = (1 - v^2/c^2)^{-1/2}$ is particle's Lorentz factor, v is particle's velocity, ϕ is the electric potential; quantities with the subscript 0 refer to their values at NS surface, at $x = 0$. The electric potential ϕ is given by the Gauss law

$$\frac{{\rm d}^2\phi}{{\rm d}x^2} = -4\pi(\eta - \eta_{\rm GJ})\,, \tag{B3}$$

where $\eta = j/v$ is the charge density of the beam. We consider the case when v, γ, η and ϕ are functions of distance x, while $\eta_{\rm GJ}$ is constant.

Expressing ϕ through γ from equation (B2) and η through $j = v\eta$ we get an equation for the beam's Lorentz factor

$$\frac{{\rm d}^2\gamma}{{\rm d}x^2} = \frac{4\pi\eta_{\rm GJ}q}{mc^2}\left(\xi\,\frac{\gamma}{\sqrt{\gamma^2-1}} - 1\right)\,. \tag{B4}$$

The plasma frequency for a mildly relativistic plasma with the GJ charge density consisting of particles with charge q and mass m is

$$\omega_{\rm p,GJ} = \left(\frac{4\pi\eta_{\rm GJ}q}{m}\right)^{1/2}\,, \tag{B5}$$

and the Debye length (also the skin depth, since the characteristic velocity is c) of such a plasma is

$$\lambda_{\rm D,GJ} = \frac{c}{\omega_{\rm p,GJ}}\,. \tag{B6}$$

Introducing normalized distance $s \equiv x/\lambda_{\rm D,\,GJ}$ equation (B4) becomes

$$\frac{{\rm d}^2\gamma}{{\rm d}s^2} = \xi\,\frac{\gamma}{\sqrt{\gamma^2-1}} - 1\,. \tag{B7}$$

The first integral of this equation is easily obtained by multiplying both part by ${\rm d}\gamma/{\rm d}s$

$$\left(\frac{{\rm d}\gamma}{{\rm d}s}\right)^2 = 2\left[\xi\left(\sqrt{\gamma^2-1} - \sqrt{\gamma_0^2-1}\right) - (\gamma-\gamma_0)\right] + \left(\frac{{\rm d}\gamma}{{\rm d}s}\right)_0^2\,. \tag{B8}$$

Under the conventional assumptions the space charge limited flow starts at the surface with zero velocity and the electric field is completely screened, so $\gamma_0 = 1$ and $({\rm d}\gamma/{\rm d}s)_0 = 0$; with these assumptions equation (B8) becomes

$$\left(\frac{{\rm d}\gamma}{{\rm d}s}\right)^2 = 2\left(\xi\sqrt{\gamma^2-1} - \gamma + 1\right)\,. \tag{B9}$$

It is more convenient to analyse the properties of the flow in terms of the spatial component of the four-velocity (the normalized momentum $p \equiv \gamma v/c$). In terms of p equation (B9) becomes

$$\left(\frac{{\rm d}p}{{\rm d}s}\right)^2 = 2\,\frac{p^2+1}{p^2}\left(1 + \xi\,p - \sqrt{p^2+1}\right)\,. \tag{B10}$$

The right-hand site of equation (B10) is positive if either $\xi \geq 1$ or $0 \leq \xi < 1$ *and* $p < p_{\rm max}$, where

$$p_{\rm max} = \frac{2\xi}{1-\xi^2}\,. \tag{B11}$$

So, for $\xi \geq 1$ flow will accelerate monotonically, while for $0 \leq \xi < 1$ the momentum will oscillate in the range $[0, p_{\rm max}]$.

According to equation (B10) ${\rm d}p/{\rm d}s$ does not depend explicitly on the distance s and so its absolute value is the same for the same value of p; therefore for $0 \leq \xi < 1$ the function $p(s)$ is symmetric around its maxima and minima and is periodic.

B2 Ultra-relativistic flow

For $p \gg 1$ we can neglect terms of the order $O(1/p)$ and higher. Then equation (B10) takes the form

$$\left(\frac{{\rm d}p}{{\rm d}s}\right)^2 = 2\left[1 + p\,(\xi - 1)\right]\,; \tag{B12}$$

the solution of equation (B12) is (cf. equation B3 in Fawley et al. 1977)

$$p = \sqrt{2}s + \frac{\xi-1}{2}s^2\,. \tag{B13}$$

If $\xi \geq 1$ the flow is continuously accelerating and its momentum at large s will grow as

$$p = \frac{\xi-1}{2}s^2\,. \tag{B14}$$

For $\xi < 1$ the flow is oscillatory and its momentum periodically reaches $p_{\rm max}$ (see equation B11). If $1 - \xi \ll 1$ and $p_{\rm max} \gg 1$ the flow is relativistic almost everywhere. The wavelength of such spatial oscillations is twice the distance between the points where $p = 0$ and p reaches its maximum value. From equation (B13) the distance where p reaches it maximum is $\sqrt{2}(1-\xi)^{-1}$ and so the period of spatial oscillation is (Beloborodov 2008)

$$s_0 = 2\sqrt{2}(1-\xi)^{-1}\,. \tag{B15}$$

B3 Non-relativistic flow

Stationary space charge limited flow is non-relativistic at the beginning, close to the NS surface; it can remain non-relativistic if $\xi \ll 1$ (see equation B11).

For $p \ll 1$ we can neglect terms of the order $O(p^3)$ and higher and equation (B10) becomes the Cycloid equation

$$\left(\frac{\mathrm{d}p}{\mathrm{d}s}\right)^2 = \frac{2\xi - p}{p}\,. \tag{B16}$$

The solution of this equation in parametric form is (Beloborodov 2008)

$$p = \xi(1 - \cos\omega_{\mathrm{p,GJ}}t) \tag{B17}$$

$$s = \xi(\omega_{\mathrm{p,GJ}}t - \sin\omega_{\mathrm{p,GJ}}t)\,, \tag{B18}$$

where the time t is measured in seconds. The period of spatial oscillations is then

$$s_0 = 2\pi\xi\,. \tag{B19}$$

For small ξ the flow is always non-relativistic and equations (B17) and (B18) describe it accurately everywhere. For large ξ equations (B17) and (B18) are good approximation near the starting point of the flow for all ξ and for $\xi < 1$ also near periodically repeating stagnation points, with small values of p.

For small s, near the flow's starting point, the time t can be eliminated from (B17) and (B18) and we get (cf. equation 13 in Fawley et al. 1977)

$$p \simeq \left(\frac{9}{2}\right)^{1/3} \xi^{1/3} s^{2/3}. \tag{B20}$$

APPENDIX C: BOUNDARY CONDITIONS FOR MODELLING OF SPACE CHARGE LIMITED FLOW

For modelling of the space charge limited flow in the polar cap one needs to make an adequate numerical model for an infinitely large pool of particles available at the NS surface in order to correctly simulate the space charge limitation condition. This is not a trivial task. We found the following procedure works well.

The calculation domain of the length L is divided in M_x equal numerical cells (a typical value of M_x in our simulations is $\sim$ a few thousand). The electric field E and current j are set at cell boundaries $i = 0, \ldots, M_x$. For the calculation of the current density we use a 1D version of the charge conservative algorithm proposed by Villasenor & Buneman (1992), when charged particles are represented by uniformly charged sheets with the width equal to the cell size Δx and the position of a particle is the position of the sheet's centre. The fraction of the sheet passed through the cell boundary i during a time-step determines the contribution of the particle into the current j_i at that point.

At each end of the calculation domain we have one 'ghost' cell. The outside boundaries of the ghost shells are 'ghost' points with indexes $i = -1$ and $i = M_x + 1$. Equation (12) for the electric field is solved for points $0 \ldots M_x$. Particles can move into the ghost cells but when their positions are outside of the domain $[-\Delta x/2; L + \Delta x/2]$ and they are moving outwards they do not contribute to the current density in the domain anymore and such particles are deleted at the end of each time-step.

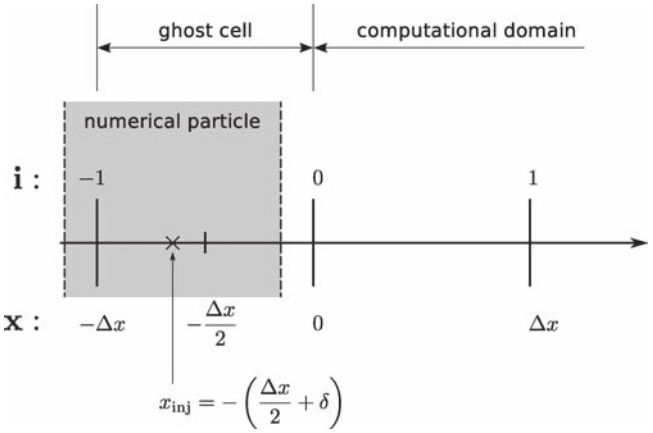

Figure C1. Numerical implementation of boundary conditions for space charge limited flow. Injection of one numerical particle is shown; particle's centre is marked by a cross. See text for explanations.

The electric field at the ghost points is set to zero. We solve a 1D *initial* value problem – the electric field in the domain is calculated from the values of the electric field at the same points at the previous time-step and is not coupled to the electric field at the 'ghost' points. The electric field inside the ghost cells, at the particles' position, is obtained by quadratic interpolation using values E_{-1}, E_0, E_1 (and $E_{M_x-1}, E_{M_x}, E_{M_x+1}$) and, therefore, setting E at the ghost point to zero ($E_{-1} = E_{M_x+1} = 0$) smoothly reduces the electric field inside 'ghost' cells towards their outer ends. Setting the electric field at ghost points at each time-step to the values obtained as extrapolation of electric field values near the domain boundaries (e.g. using quadratic extrapolation from points 0, 1, 2 and $M_x - 2, M_x - 1, M_x$) or to some non-zero values resulted only in higher numerical noise and did not change the system behaviour.

At the beginning of each time-step we inject certain amount of electrons N_{inj} and equal number of heavy positive charged particles ('ions') in the first 'ghost' cell of our computation domain at the position slightly outside the centre of the fist cell $x_{\mathrm{inj}} = -(\Delta x/2 + \delta)$ (see Fig. C1). The momentum of each injected particle is sampled from a uniform distribution in the interval $[-p_{\mathrm{inj}}, p_{\mathrm{inj}}]$. In this way, we can model finite temperature of the particles on one hand and populate the domain with particles more uniformly on the other hand, as each injected particle after the first time-step will have a slightly different position. If during this time-step the electric field inside the 'ghost' cell cannot move particles into the interval $[-\Delta x/2; L + \Delta x/2]$, they do not contribute to the current density and will be deleted at the end of the time-step. Depending on the value of the electric field either positive or negative particles will be 'sucked' into the domain.

We experimented with different values for N_{inj} and found that usually after N_{inj} exceeds the critical value $N_{\mathrm{inj}}^{\mathrm{cr}} \equiv 2(j_{\mathrm{m}}/Qc)(c\Delta t/\Delta x)$ by $\sim$20–30 per cent computational results stop depending on N_{inj}; further increase in N_{inj} results in higher numerical noise. $N_{\mathrm{inj}}^{\mathrm{cr}}$ is twice the number density of particles with relativistic velocities which must be injected at every time-step in order to provide the required current density j_{m}; Q is the charge of a numerical particle and c is the speed of light. The factor of 2 accounts for injected particles having negative initial momentum – most of them do not reach computational domain and are deleted. Having some injected particles with negative momenta results in slightly lower numerical noise as well as more realistically represents the finite temperature

of the NS atmosphere (the equivalent of the warm cathode in the analogous vacuum tube and high current beam technologies). The computational overhead caused by such particles is negligible, as $N_{\rm inj}$ is orders of magnitude less than the total number of particles. We also experimented with different values for the time-step and found that values of Δt such that $\Delta x/c\Delta t \sim 5$ results in relatively low level of numerical noise due to discrete events of particle injection; smaller Δt leads to larger numerical overhead, as the stability of the leapfrog scheme requires only that $\Delta t < 0.5\Delta x/c$.

This paper has been typeset from a TEX/LATEX file prepared by the author.